TUNABLE DIODE LASER DIAGNOSTICS

IN PHOTOCHEMISTRY

TUNABLE DIODE LASER DIAGNOSTICS IN PHOTOCHEMISTRY

By

PAUL HENRY BECKWITH, B. Eng.

A Thesis

Submitted to the School of Graduate Studies

in Partial Fulfilment of the Requirements

for the Degree

Master of Science

McMaster University

September 1986

MASTER OF SCIENCE (1986) McMASTER UNIVERSITY

(Physics) Hamilton, Ontario

TITLE: Tunable diode laser diagnostics in photochemistry.

AUTHOR: PAUL HENRY BECKWITH, B. Eng. (McMASTER UNIVERSITY)

SUPERVISOR: Professor J. Reid

NUMBER OF PAGES: xx, 101

ABSTRACT

A detailed experimental and theoretical study has been performed on several different photochemical systems. Lead-salt tunable diode lasers operating in the infrared region have been used as diagnostic tools to probe the molecules in these gaseous systems. Knowledge of these systems is expected to be useful in evaluating future schemes of laser isotope separation.

In the course of this work a computerized digital technique has been developed that allows molecular parameters such as linestrength and linewidth to be obtained by measuring the infrared absorption on vibrational-rotational transitions of the molecule. Molecular concentrations can then be determined enabling one to gain valuable insight into the chemical processes occurring in the system.

The digital technique was first tested on CO_2 gas in a multi-pass White cell to verify the validity of the measurements. Subsequently, measurements were performed on mixtures of NH_3/N_2, NH_3/Ar, HTO/H_2O, and HTO/air. Those NH_3 measurements that could be compared to previous measurements were found to be very accurate. For the HTO system, no previous measurements on linestrength and linewidth for the transitions examined have been performed.

Described next is the application of the tunable diode laser diagnostic system to the investigation of infrared multiphoton dissociation of deuterated chloroform immersed in a chloroform bath. The sensitivity of the technique allowed for the measurement of the few

parts per million of DCl formed by the photolysis of natural abundance $CDCl_3$ in $CHCl_3$.

In addition, the feasibility of transient detection with tunable diode lasers was examined. High fluence CO_2 laser pulses were used to dissociate C_3F_6 or C_2F_3Cl and create CF_2 radicals. Current-modulation of the tunable diode laser made it possible to monitor the transient CF_2 radicals as they were formed, and as they subsequently decayed. The sensitivity of the transient detection technique was found to be limited by detector noise.

ACKNOWLEDGEMENTS

I would like to take this opportunity to express my sincere appreciation to my supervisor, Dr. J. Reid, for his guidance and support in this endeavor.

Also, I would like to thank Dr. D. R. Smith, J. J. Orlando, C. E. Brown, P. P. Cherrier, and D. J. Danagher for their collaboration in various sections of this work.

In addition, I wish to extend my warm appreciation to my friends and colleagues, especially in the Optics group. Also, I give special thanks to my family for their support in my stay at McMaster.

Finally, I would like to thank my wife Elizabeth for her help and encouragement during the course of this project.

This work was supported, in part, by the Natural Sciences and Engineering Research Council of Canada.

TABLE OF CONTENTS

		Page
CHAPTER 1	INTRODUCTION	1
CHAPTER 2	INFRARED SPECTROSCOPY THEORY	6
	2.1 Introduction	6
	2.2 Direct Detection Lineshapes	7
	2.3 Linestrength and Linewidth Measurements	11
	2.4 Second Harmonic Detection	15
	2.5 Summary	16
CHAPTER 3	DIAGNOSTICS IN CO_2, NH_3, AND HTO SYSTEMS	17
	3.1 Introduction	17
	3.2 System Calibration	17
	3.3 Linewidths and Linestrengths in NH_3	19
	3.3.1 Introduction	19
	3.3.2 Experimental Apparatus	20
	3.3.3 Results	25
	3.3.4 Discussion and Conclusions	30
	3.4 Linewidths and Linestrengths in HTO	32
	3.5 Summary	39
CHAPTER 4	DIAGNOSTICS IN $CDCl_3$ DISSOCIATION	40
	4.1 Introduction	40
	4.2 Experimental Apparatus and Calibration Procedure	41
	4.3 Dissociation of $CDCl_3$ at Natural Abundance	55
	4.4 Summary	59
CHAPTER 5	TRANSIENT DETECTION OF CF_2 RADICALS	62

Page

5.1 Introduction 62

5.2 Detection of CF_2 Radicals 64

5.2.1 Apparatus 64

5.2.2 cw Spectroscopy of CF_2 66

5.2.3 Transient Spectroscopy of CF_2 68

5.3 Sensitivity of the Modulation Technique 70

5.4 Direct detection of Transient Absorption 75

5.5 Summary 80

CHAPTER 6 CONCLUSIONS 82

REFERENCES 84

LIST OF FIGURES

Page

Fig. 2.1: Data analysis technique for direct scans. Curves of the background (A), the absorption line (B), the optical zero (C), and the etalon fringes (D) are obtained with the TDL and stored. Analysis of this data gives a preliminary curve (F) and the final result (E). 8

Fig. 2.2: TDL tuning rate calibration procedure using a Ge etalon. In the lower section an etalon scan (fringe spacing = 0.01627 cm^{-1}) with a finesse (peak to trough signal/average signal) of ~0.5 is given. From the etalon scan a tuning curve (wavenumber versus digitization sample number) can be derived and is shown in the upper section. The middle section shows the slope of the tuning curve and a linear regression fit which gives the calibration factor. 13

Fig. 3.1: Schematic diagram of the apparatus. Lens L_1 collimates the output of the TDL and lens L_2 focuses the TDL beam onto the detector. Pure NH_3 and mixtures with N_2 and Ar are flowed from a flask through cells varying in length from 0.57 cm 21

to 15 cm. A germanium etalon can be placed in the beam to calibrate the wavenumber scale. The lock-in amplifier signal is digitized and stored in a micro-computer for subsequent analysis.

Fig. 3.2: Typical TDL scans of an NH_3 absorption line in the 0.57 cm cell, and a calibration etalon scan. The analog signal from the output of the lock-in amplifier is sampled at a 12 Hz rate, digitized, and stored. Approximately 500 data points are recorded in each scan with a digitization error of < 1 %. The "smoothness" of the displayed data in this and other Figures is limited by the printer resolution. 23

Fig. 3.3: Measured and calculated lineshapes for the data of Fig. 3.2. The upper scan shows the residuals (measured - calculated) as a percentage of the linecentre absorption α_o. These residuals are minimized to optimize the fit. The calculated Voigt profile[20] gives a best fit with a linecentre absorption of 0.8044 cm^{-1} at 834.012 cm^{-1}, and a HWHM pressure broadening coefficient, γ, of 14.60 MHz/Torr. The Doppler width is fixed at its theoretical value ($\Delta\nu_D = 1.255 \times 10^{-3}$ cm^{-1}). 24

Page

Fig. 3.4: Effects of pressure broadening by N_2 on a transition in NH_3. The low pressure scan (19.84 Torr) is shown relative to 0 and 100 % transmission of the TDL, the other scans are offset for clarity. The etalon scan (fringe spacing = 0.01627 cm^{-1}) is used to calibrate the tuning rate of the TDL and thus allows determination of the linewidths. 27

Fig. 3.5: Plots of total linewidth (Doppler plus Lorentz), and Lorentz component only, as a function of pressure for a selected number of transitions. Shown in the upper trace are the linewidths and the theoretical fits as generated by Pade approximations.[21] The straight-line least square fits in the lower traces give the listed pressure broadening coefficients, with their respective standard deviations. 28

Fig. 3.6: Typical TDL scan of an HTO absorption line at 1384.694 cm^{-1}, together with a calibration etalon scan. Optical pathlength is 4 m through 7 Torr of an HTO/H_2O mixture with a nominal specific activity of 5 Ci/ml. The analog signal from the output of the lock-in amplifier is sampled at a 12 Hz rate, digitized, and stored. Approximately 34

500 data points are recorded in each scan with a digitization error of < 0.1 %. The "smoothness" of the displayed data in this and other Figures is limited by the printer resolution.

Fig. 3.7: Measured and calculated lineshapes for the data of Fig. 3.6. The upper scan shows the residuals (measured - calculated) as a percentage of the linecentre absorption α_0. The calculated Voigt profile gives a best fit with a linecentre absorption of 2.8×10^{-1} m^{-1} with a HWHM pressure broadening coefficient of 16.8 MHz/Torr. 35

Fig. 3.8: Effects of pressure broadening by H_2O on a transition in HTO. The low pressure scan (2.1 Torr) is shown relative to 0 and 100 % transmission of the TDL, the other scans are offset for clarity. 36

Fig. 3.9: Plots of the total linewidth (Doppler plus Lorentz), and the Lorentz component only, as a function of pressure for three HTO transitions. The HTO transitions are identified by their respective wavenumber.[71] The straight-line least square fits in the lower traces give the pressure broadening coefficients, with their respective 37

standard deviations. Page

Fig. 4.1: Schematic diagram of the apparatus. Lens L_1 collimates the output of the TDL, lens L_2 focuses both the TDL and the CO_2 beams into the photolysis cell, and lens L_3 focuses the TDL onto the detector. Mirror M_1 transmits ~75 % of the TEA CO_2 pulse, and reflects ~85 % of the TDL radiation. The LiF filter prevents any 11 μm radiation from reaching the detector. 42

Fig. 4.2: Infrared spectrum of the deuterium chloride fundamental (2240 cm^{-1} - 1890 cm^{-1}) as measured on an IR grating spectrometer. Shown are the $D^{35}Cl$ and $D^{37}Cl$ transitions for the P and R branches and the operating wavenumber range of the lead-salt TDL used in the DCl detection. The illustrated spectrum is based on scans of 1 Torr DCl for a 3 m path length.[75] 44

Fig. 4.3: TDL scans taken during optimization of operating temperature. The laser beam passes through a gas cell containing 3.5 Torr of DCl in $CDCl_3$ (50 Torr total pressure) and is scanned in frequency over the R(7) line in $D^{35}Cl$ at 2168.962 cm^{-1}. From the central scan it can be seen that > 91 % of the 46

laser energy is in the mode of interest. The two additional scans illustrate the effect of minor changes in operating temperature.

Fig. 4.4: Typical TDL scans showing the formation of DCl and CO after irradiation of 2 Torr pure $CDCl_3$ with 80 pulses of 0.4 J energy per pulse. The CO_2 laser transition was 10P(48) (916.76 cm^{-1}). The etalon fringes are used to calibrate the wavenumber scale, and additional cells containing pure DCl and CO were used to confirm the line identifications. Also shown at the bottom of the figure are the calculated positions of the R(7) line in DCl (2168.962 cm^{-1}) and the R(6) line in CO (2169.1984 cm^{-1}).[75,76] 47

Fig. 4.5: Second harmonic detection with a TDL. Scan (a) is taken with a chopper and conventional amplitude detection. The DCl absorption is 35 % in a 10 cm path. Scan (b) is taken with the chopper removed and a 2.5 kHz modulation applied to the TDL current. Lock-in amplifier detection is carried out at 5 kHz. Scans (a) and (b) are taken with identical gain settings. For trace (c), amplification is increased by a factor of 1150, and there is only a trace of CO and DCl in 5 Torr 49

$CDCl_3$ in the cell (noise is not minimized).

Fig. 4.6: Calibration plots for CO and $CO/CHCl_3$ mixtures. The measured absorption coefficients are shown to be linear with CO content for a dynamic range of ~4 orders of magnitude. The straight line through the pure CO data (line A), from the Doppler regime equation (2-3), yields a linestrength in agreement with the AFGL value, while line B is consistent with the intermediate pressure regime equation (2-5) (using the measured pressure broadening coefficient of 8.0×10^{-5} cm^{-1} $Torr^{-1}$). Both sets of data were measured on the R(8) transition of CO. The third set of data (line C) was measured on the R(6) transition and illustrates results with both direct and 2f detection. Very dilute mixtures of CO in $CHCl_3$ are measured with 2f detection, and are shown on expanded scales (x10 or x100) to demonstrate linearity. The insert defines the parameters used in the Beer-Lambert equation (2-1). 51

Fig. 4.7: Measured linewidths for the R(7) line of $D^{35}Cl$ buffered by $CHCl_3$ or $CDCl_3$. The solid line drawn through the data points is the calculated linewidth for $\gamma_m = 9.7 \times 10^{-5}$ cm^{-1} $Torr^{-1}$ (best 54

fit value). The calculated linewidth is from Pade approximants of the Voigt profile as outlined by Minguzzi et al.[21]

Fig. 4.8: Formation of DCl as a function of the number of CO_2 irradiation pulses. Each pulse irradiates approximately 1 % of the total cell volume. Linearity in the upper section occurs with a small number of laser pulses, saturation in the lower section is due to DCl exchange reactions with the cell walls (with a larger number of laser pulses). 57

Fig. 4.9: Effect of wall reactions on gas concentrations in a pyrex cell. DCl and CO concentrations are measured as a function of time after (A): irradiation of 5 Torr $CDCl_3$ in a "clean" glass cell and (B): filling of a previously "conditioned" glass cell with 5 Torr of pure $CHCl_3$. A Monel cell is used to reduce the effect of these adverse wall reactions. 58

Fig. 4.10: Successive 2f scans taken of a sample of natural abundance chloroform after irradiation with 100 pulses of 10P(38) and 10P(48) radiation (0.4 J/pulse). The increase in DCl concentration after irradiation with 10P(48) is attributed to 60

IRMPD of naturally occurring $CDCl_3$ in the sample. Gas pressure in the cell is 5 Torr. The noise level is equivalent to ~0.8 ppm DCl, or a fractional absorption of 2×10^{-5} in the 10 cm cell.

Fig. 5.1: Schematic diagram of the apparatus for detection of CF_2 transients. Lens L_1 collimates the output beam of the TDL, lens L_2 compensates for the divergence of the CO_2 beam, and lens L_3 focuses both beams into the capillary waveguide cell. Mirror M_1 transmits ~70 % of the TDL radiation and reflects ~80 % of the TEA CO_2 pulse. Cells C_1 and C_2 contain either ethylene or cyclopropane, and prevent any scattered radiation from reaching the TDL or the sensitive HgCdTe detector. 65

Fig. 5.2: TDL spectrum of CF_2 in the 1243 cm^{-1} region. The upper section section shows the absorption lines created in a microwave discharge by Davies *et al.*[108], and in the present work. The lower trace shows an expanded section of the spectrum. The optimum gas mixture in the 2450 MHz microwave discharge was C_2F_3Cl/Ar in a 4:1 ratio at 280 mTorr, and the strongest CF_2 absorption lines observed in the present work had linecentre 67

absorptions of ~10 % (4 passes, 2.4 m total pathlength).

Fig. 5.3: Schematic illustration of transient detection of CF_2 using a wavelength modulated TDL. The TDL scans past the CF_2 doublet twice every cycle, and the detector output consists of an AM sine wave plus the absorption doublet. 69

Fig. 5.4: Experimental results on detection of CF_2. The CF_2 doublet (absorptions at 1242.9453 cm^{-1} and 1242.9523 cm^{-1}) observed in the middle trace is produced by irradiating 0.5 Torr of C_2F_3Cl in the capillary waveguide cell with a 9P(14) CO_2 pulse of fluence 10 J/cm^2. Trace B is recorded with no gas in the cell, and both traces are averages performed by a digital storage oscilloscope of 32 successive scans. 71

Fig. 5.5: Concentration of CF_2 monitored as a function of time. The upper trace, an average of 256 scans, illustrates the growth of CF_2 following CO_2 irradiation of 1.5 Torr C_2F_3Cl. The lower section shows the CF_2 decay, each trace is an average of 50 scans. Trace B was obtained with gas in the cell and the CO_2 beam blocked to allow subtraction 72

of the steady-state C_2F_3Cl absorptions and enhancement of the transient CF_2 absorptions.

Fig. 5.6: TDL scans taken with the AM background reduced by analog subtraction. Modulation frequency is 2.5 kHz, and the modulation amplitude and DC current can be adjusted to sweep over one or both of the N_2O lines recorded in direct detection in the upper trace. For the lower trace, most of the N_2O is frozen out of the cell, and the remaining linecentre absorption is only 0.03 %. Each trace is the average of 256 scans. 74

Fig. 5.7: Results obtained with a modulation frequency of 100 kHz. The N_2O is frozen out of the cell after the first trace. Note the substantial reduction in the AM background after analog subtraction is employed. A further reduction in background is obtained by digitally subtracting successive traces, i.e., by subtracting the background from signal-plus-background. Residual noise is detector noise. Each trace is the average of 256 scans. 76

Fig. 5.8: Direct detection of transient absorption with the TDL fixed at linecentre. The relevant energy 77

levels are illustrated in the upper part of the Figure, along with a direct detection scan over the NH_3 aP(4,0) transition. The NH_3/N_2 mixture is pumped with a Q-switched CO_2 laser, shown in the lower traces are the CO_2 pump pulse and the transient probe signals.

Fig. 5.9: Sensitivity limits obtained with a cw CO_2 laser as a probe. The upper trace shows the probe signal at NH_3/N_2 mixture pressures of 100 Torr (large signal-to-noise ratio), and trace A is recorded at 1.2 Torr. The background trace is recorded with the gas cell evacuated. Subtraction of the background from the signal allows determination of the true induced absorption signal. The noise level corresponds to detector noise, and has been minimized by averaging over 4096 scans using the digital oscilloscope and the micro-computer. 79

LIST OF TABLES

		Page
Table 3.1:	Line intensities, self-broadened widths, nitrogen-broadened widths, and argon-broadened widths in the ν_2 band of NH_3 at 296 K. Theoretical linestrengths were computed using a band strength of 546 cm^{-2} atm^{-1}.	29
Table 3.2:	Line positions, line intensities, water-broadened widths, and air-broadened widths in the ν_2 band of HTO at 297 K.	38
Table 4.1:	Line positions in the fundamental band of DCl.	45

CHAPTER 1

INTRODUCTION

For the past decade lead-salt tunable diode lasers (TDLs) have been widely employed in both pure and applied spectroscopy.[1-2] They have, for example, been used extensively for the detection and monitoring of gases in the atmosphere. Characteristic absorption spectra are used to identify atmospheric constituents; in addition their concentration can be determined by knowledge on the strengths of these spectra. A variety of TDL systems for measuring trace gases in tropospheric air were recently reviewed by Schiff *et al.*,[2] while Webster *et al.* discuss stratospheric measurements.[3] In laboratory systems, TDLs routinely find application in high resolution measurements of infrared spectra[4] as the laser gives improved resolution and sensitivity with respect to grating and Fourier transform spectrometers. TDL spectrometers have been used often since the first measurements of Doppler limited spectra were performed in 1970 by Hinkley.[5] The narrow TDL linewidth[6] allows Doppler-broadened transitions to be measured with negligible instrumental broadening, in addition it enables closely spaced lines from different species to be easily resolved. The high power output per unit spectral range (brightness), and the ability to modulate the TDL wavelength in conjunction with lock-in amplifier signal processing result in very high sensitivity for detection. Fractional absorbance, either steady-state or transient, on the order of 10^{-5} can be measured in gases. In addition, the wavelength region covered by a

given TDL can be tailored by varying the molar fractions of the tertiary compounds making up the lead-salt laser, this allows for laser operation anywhere from 2 - 30 μm.[7] This wavelength region is very rich in rotational and vibrational transitions for a large variety of molecules. Thus TDLs combine excellent specificity (the ability to distinguish between different molecules, including different isotopic species of the same molecule) with very high sensitivity, a non-destructive measurement technique, and fast response time. High sensitivity is desirable as it allows one to detect weak signals from low concentrations. In short, TDLs are ideal devices for the investigation of chemical reactions in gases.

It is somewhat surprising that TDLs have rarely been used for this type of measurement. In a recent literature survey of over 500 papers involving the use of TDLs,[4] only a few papers discussed the use of TDLs to monitor simple chemical reactions. For example, TDLs have been used to measure dissociation constants of H_2SO_4,[8] reaction rates of $N_2F_4 \leftrightharpoons 2NF_2$[9] and $HNO_3 + NO/HNO_2 + O_3$,[10] and reactions of HO_2 created by flash photolysis.[11] There may be some reluctance on the part of experimentalists in photochemistry and related fields to become dependent on a device which has the reputation of being complex to operate. More specifically, the single versus multi-mode emission, and discontinuous tuning behaviour of the TDL requires careful attention,[1] and until recently, TDLs suffered degradation with thermal cycling. However with modern TDLs, and with experience and care in operation, the wealth of information available to the analyst using a TDL to probe a chemical reaction more than compensates for any difficulties in

operation. There is no doubt that the ability to carry out chemical and isotopic analysis with high specificity and at low concentrations is very important. High sensitivity analytical techniques allow one to work at low percent photolytic conversion and thus minimize secondary reactions that may occur with the products. Experiments in laser induced isotope enrichment can involve very high single-step enrichment factors, in fact values up to 15,000 - 20,000 have been cited for D/H enrichment.[12] In such situations, high sensitivity and selectivity will allow measurements of very low residual levels of a depleted isotope in the reactant. In many applications, it is desirable to obtain data from the system at natural isotopic abundance, which again requires extremely high sensitivity.

The intent of this thesis is to demonstrate the usefulness of tunable diode lasers as diagnostic tools in a photochemical environment. In order to measure concentrations of gaseous species of interest from the infrared absorptions, a knowledge of certain molecular parameters such as linestrength and linewidth is required. A computerized data recording technique has been developed to allow accurate determination of these parameters.

The purpose of Chapter 2 is to provide the background information on infrared spectroscopy that is required for an understanding of the subsequent sections of the thesis. Initially, the analysis on lineshapes obtained by direct detection is discussed, and methods to extract the linewidth and linestrength are explained. In a final section, the second harmonic detection technique used in the determination of low concentrations of gaseous species is examined.

The tunable diode laser diagnostics that have been developed are examined in Chapter 3 for a variety of gaseous molecules. In initial experiments, the digital data recording system was tested for accuracy in the determination of linestrength and linewidth for a transition in CO_2 that has been carefully measured by other workers. Next, accurate measurements were made on several vibration-rotation transitions in the ν_2 fundamental band of NH_3. These transitions are of importance to cw and pulsed NH_3 laser systems. The last section discusses novel measurements made on several transitions in the ν_2 band of HTO. These data are of importance in studies on the sensitivity limits for the detection of HTO with tunable diode lasers. Such studies are necessary as HTO, even in low concentrations, poses a health hazard.

In Chapter 3 the versatility and the accuracy of the TDL diagnostic system is established. These techniques were used in the diagnostics of the photochemical system of $CDCl_3/CHCl_3$ as described in Chapter 4. This photochemical system may be useful in laser isotope separation. The infrared multiphoton dissociation (IRMPD) of $CDCl_3$ produces the highly reactive DCl molecule, which is detected with the tunable diode laser probe. Previous studies of this system could not detect the DCl molecule by direct methods. Chapter 4 also describes the first reported dissociation of natural abundance $CDCl_3$ in $CHCl_3$, and the subsequent high sensitivity detection of the low concentrations of DCl formed.

In the work reported in the final part of this thesis TDL diagnostic techniques are carried one step further and applied to the detection of transient absorption. Transient absorption signals can be

generated by highly reactive, short-lived molecular species that are created by photolysis with laser pulses. Initial studies were performed on the DCl molecule and problems of gas heating and shock induced effects were encountered. Current-modulation of the TDL overcame these problems, and the refined technique was used to monitor CF_2 transients created by single CO_2 laser pulses. CF_2 was also created in a microwave discharge cavity on a cw basis allowing absorptions to be characterized with the TDL. This work is described in Chapter 5.

Chapter 6 summarizes the conclusions of this thesis and makes recommendations for further areas of investigation. The work presented in this thesis is described in a series of papers[13-16] with collaborators D. J. Danagher and P. P. Cherrier (sections of Chapter 3), J. J. Orlando and D. R. Smith (sections of Chapter 4), D. J. Danagher, C. E. Brown and D. R. Smith (sections of Chapter 5). J. Reid, as supervisor, has been at the forefront in all of these papers.

CHAPTER 2

INFRARED SPECTROSCOPY THEORY

2.1 Introduction

The infrared spectroscopy theory that is necessary for an understanding of the measurements made with the tunable diode laser is presented in this chapter. In order to extract information on concentrations of molecules from infrared absorption spectra it is necessary to understand the origins of the lineshapes that are observed. In the direct detection method a chopper and conventional amplitude detection are employed to scan over absorption lines. The predicted lineshape can be generated analytically by varying line broadening parameters, allowing for a linestrength determination from the best fit. The next two sections outline the theory and the methods used in the computer program that generates the fitted lineshapes. These sections are followed by a discussion of second harmonic detection. When the concentration of the absorbing species is very low such that linecentre absorptions are < 1 %, it is necessary to increase the signal-to-noise ratio. One way of achieving this is by using second harmonic detection. This method has the high sensitivity that is required, for example, in the detection of DCl created from the infrared multiphoton dissociation (IRMPD) of natural abundance $CDCl_3$ in $CHCl_3$. However, second harmonic detection is limited to time constants of ~1 ms or larger, and therefore cannot be used to detect short lived transients. Current-modulation of the TDL allows for the high sensitivity detection

of transients on rapid timescales.

2.2 Direct Detection Lineshapes

Direct detection lineshapes are generated by scanning the TDL across an absorption line. The TDL beam is chopped, and the power that is transmitted through the absorption cell is detected and sent to a lock-in amplifier. The output of the lock-in amplifier is sent to an analog-to-digital converter, which interfaces the lock-in amplifier to a micro-computer. To process the stored data and extract information on molecular parameters the theory of infrared lineshapes must first be understood.

The transmission of monochromatic radiation through a homogeneous gas sample is described by the Beer-Lambert law

$$I(\nu) = I_0(\nu)\exp(-\alpha(\nu)L) \qquad (2\text{-}1)$$

where $I_0(\nu)$ and $I(\nu)$ are the incident and transmitted intensity as defined in Fig. 2.1, and L is the length of the cell. The absorption coefficient as a function of frequency (ν) is given by[17].

$$\alpha(\nu) = S_J\Phi(\nu-\nu_o)\frac{P_A}{760} \quad cm^{-1} \qquad (2\text{-}2)$$

where S_J is the linestrength (cm^{-2} atm^{-1}) of the absorption line, and P_A is the partial pressure of the absorber gas in Torr. The lineshape factor is given by

$$\Phi(\nu-\nu_o) = \frac{1}{\Delta\nu_D}\left(\frac{\ln 2}{\pi}\right)^{\frac{1}{2}} V(a,x) \qquad (2\text{-}3)$$

where the Doppler half-width at half maximum intensity (HWHM) for a

Fig. 2.1: Data analysis technique for direct scans. Curves of the background (A), the absorption line (B), the optical zero (C), and the etalon fringes (D) are obtained with the TDL and stored. Analysis of this data gives a preliminary curve (F) and the final result (E).

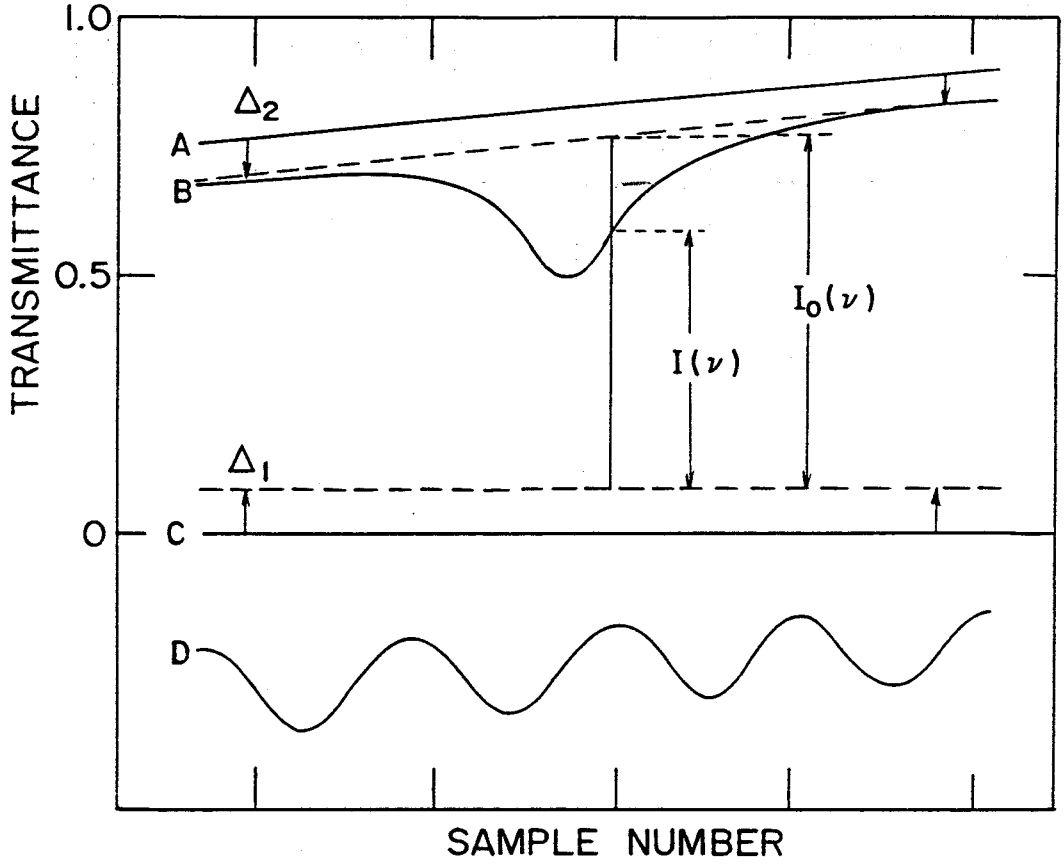
1.0
0.5
0
TRANSMITTANCE
Δ2
A
B
I(ν)
I0(ν)
Δ1
C
D
SAMPLE NUMBER

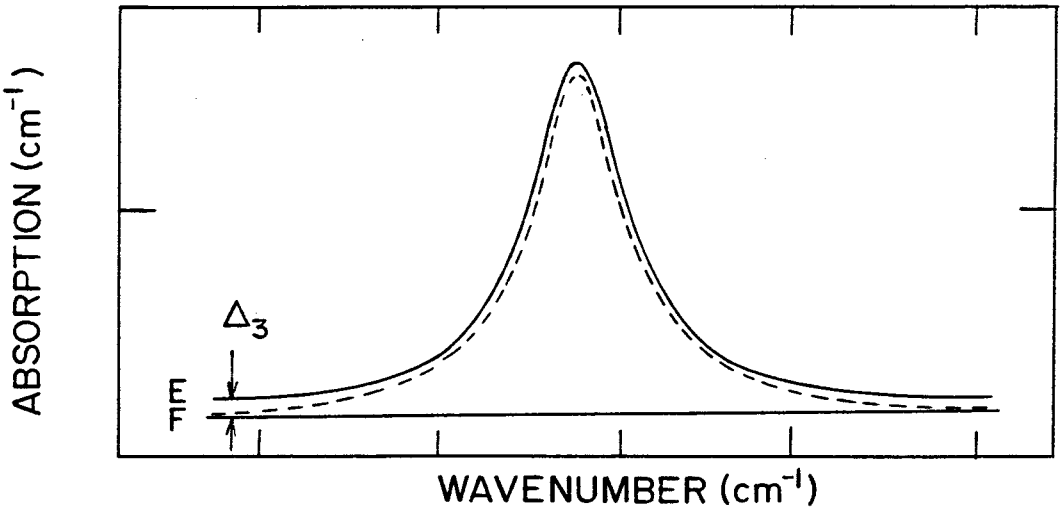
ABSORPTION (cm-1)
Δ3
E
F
WAVENUMBER (cm-1)

molecule of mass M at a temperature T (in K) is given by[18]

$$\Delta\nu_D = 3.581 \times 10^{-7} \nu_o \left(\frac{T}{M}\right)^{\frac{1}{2}} \tag{2-4}$$

where ν_0 is the frequency at linecentre. For most molecules of interest, the Doppler width is on the order of 10^{-3} cm^{-1} for transitions in the infrared. The Voigt profile is

$$V(a,x) = \frac{a}{\pi}\int_{-\infty}^{\infty} \frac{e^{-y^2}\, dy}{a^2 + (x-y)^2} \tag{2-5}$$

where

$$x = (\ln 2)^{\frac{1}{2}} \frac{(\nu - \nu_o)}{\Delta\nu_D} \tag{2-6}$$

is the offset from linecentre in normalized units and

$$a = (\ln 2)^{\frac{1}{2}} \frac{\Delta\nu_L}{\Delta\nu_D} \tag{2-7}$$

The pressure broadened linewidth (HWHM) is given by

$$\Delta\nu_L = \gamma_M P_T \tag{2-8}$$

where P_T is the total gas pressure in Torr, and γ_M is the pressure broadening parameter for the gas mixture. Typical values of γ_M range from 10^{-4} to 5×10^{-4} cm^{-1} $Torr^{-1}$. Thus, the parameter "a" is the ratio of the pressure broadening to Doppler broadening.

We shall now consider the more specific case of the absorption at linecentre (α_o) where x = 0. Experimentally α_o is the parameter that is most easily measured. The analysis will be performed for different regimes.

In the low pressure (< 1 Torr) or Doppler regime, $\Delta\nu_L \sim 0$ (thus

a = 0) and the lineshape is Gaussian. Thus, equations (2-2) and (2-3) can be simplified to give[13]

$$\alpha_o = \frac{S_J}{\Delta\nu_D}\left(\frac{\ln 2}{\pi}\right)^{\frac{1}{2}}\frac{P_A}{760} \quad cm^{-1} \qquad (2\text{-}9)$$

As the gas pressure is raised above 1 Torr, collisional broadening becomes significant. In the intermediate pressure region where $\Delta\nu_L \sim \Delta\nu_D$, simplification of the general equation gives[13]

$$\alpha_o = \frac{S_J}{\pi^{\frac{1}{2}}}\frac{a}{\Delta\nu_L}(1-\mathrm{erf}(a))\exp(a^2)\frac{P_A}{760} \quad cm^{-1} \qquad (2\text{-}10)$$

where erf(a) is the error function.[19] At high pressures (typically > 100 Torr) $\Delta\nu_L >> \Delta\nu_D$, and the general equations simplify to[13]

$$\alpha_o = \frac{S_J}{\pi\Delta\nu_L}\frac{P_A}{760} \quad cm^{-1} \qquad (2\text{-}11)$$

Note that for a fixed composition gas mixture both P_A and $\Delta\nu_L$ are proportional to P_T, and thus α_o is a constant independent of pressure when collisional broadening is dominant. Under these conditions the analytical sensitivity expressed as a ratio such as parts per million is independent of total pressure. This behaviour can be contrasted with the low pressure behaviour where α_o is proportional to total pressure (Eq. 2-9).

The three forms of the line shape function that are discussed at the beginning of this section are the Doppler, Voigt, and Lorentz profiles. These profiles are the ones that are most commonly encountered in laboratory, atmospheric, planetary or astronomical spectra. There are special conditions under which additional

collisional effects become apparent. More specifically, collisional narrowing has been observed, for example, when light absorber molecules undergo collisions with heavier buffer gas molecules. Under these conditions the Voigt profile, which is derived from a hard collision model, is replaced by the Galatry profile which is narrower and is derived from a soft collision model. These collisional narrowing effects are small for the molecules studied in this thesis and if accounted for would result in corrections to the fits of the order of a few percent.

2.3 Linestrength and Linewidth Measurements

In this section the procedures involved in the determination of linestrength and linewidth from the recorded spectrum of a single absorption line are discussed in detail. The analysis techniques are not necessarily limited to TDL spectra but could be applied to data obtained from a wide variety of high resolution spectrometers. The only requirement is that the instrumental broadening is small (10^{-4} cm^{-1}) compared to the Doppler width (10^{-3} cm^{-1}).

The experimental data obtained from the TDL spectrometer consists of transmitted intensities stored on the microcomputer as a function of the sample number of the digitization. This data is obtained while the laser diode is scanned in frequency across the absorption line. Four curves are required in the general case, namely the background (A), the absorption scan (B), the optical baseline (C), and the etalon calibration scan (D) as shown in Fig. 2.1. The first step in the computer analysis consists of the deconvolution of the

intensity data to obtain the absorption coefficient, α, as a function of sample number. Note that in most regions of operation, the TDL is multimode and a small fraction of the energy is not in the mode scanning the absorption line. This fraction is determined by placing a 100 % absorbing cell into the beam. This allows the baseline to be corrected by the amount Δ_1. Next the background I_0 must be found and its determination is dependent on the aquisition procedure in the experiment. If the absorption cell is left in the beam and evacuated then the background scan (A) can be used for I_0. However, if the entire cell is removed from the beam then the background scan (A) must be scaled down by Δ_2 to coincide with the extreme wings of the absorption scan (B). This is in the general case of a curving background. If the background is straight then a linear fit to points at extreme sides of the absorption line (B) can be used to determine I_0.

Next the horizontal scale (sample number) is calibrated to wavenumber (cm^{-1}). The sample numbers of the peaks of the etalon scan (D) are found, in some cases where there is noise or fringing in the scan it is necessary to average several points to smooth the data in order to arrive at the correct number of peaks in a given scan. From the known etalon fringe spacing in wavenumbers the calibration factor (cm^{-1}/sample number) is obtained. This method is shown in Fig. 2.2. The calibration factor then allows the absorption coefficient to be plotted as a function of wavenumber as is shown in Fig. 2.1 (curve F).

Finally, the theoretical Voigt profile is generated and matched to the experimental data to determine the parameters of importance. The

Fig. 2.2: TDL tuning rate calibration procedure using a Ge etalon. In the lower section an etalon scan (fringe spacing = 0.01627 cm^{-1}) with a finesse (peak to trough signal/average signal) of ~0.5 is given. From the etalon scan a tuning curve (wavenumber versus digitization sample number) can be derived and is shown in the upper section. The middle section shows the slope of the tuning curve and a linear regression fit which gives the calibration factor.

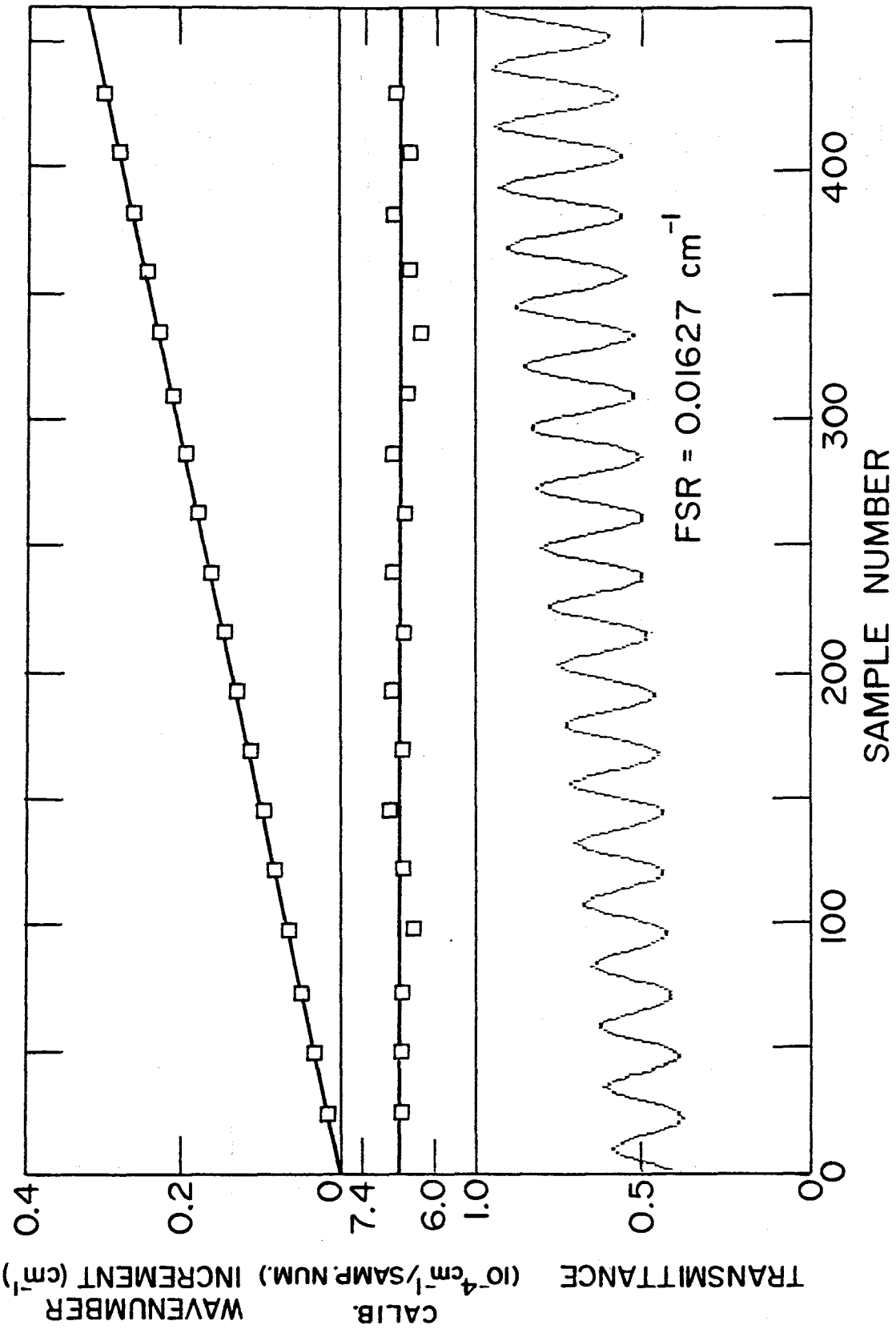
TRANSMITTANCE
CALIB. (10⁻⁴cm⁻¹/SAMP.NUM.)
WAVENUMBER INCREMENT (cm⁻¹)
0.5
1.0
6.0
7.4
0
0.2
0.4
0
100
200
300
400
SAMPLE NUMBER
FSR = 0.01627 cm⁻¹

equations used to generate the fit are given as Eq. (2.2), (2.3) and (2.5), the latter equation is calculated by numerical integration using the method of Drayson.[20] Parameters in the fit that are fixed include the total pressure P_T and the theoretical Doppler width $\Delta\nu_D$ which is calculated from Eq. (2-4). The linecentre frequency ν_0 and the linecentre absorption α_0 for the fit are obtained directly from the data. Thus, the only parameters that are varied to optimize the fit are the pressure broadening coefficient γ_M and an offset parameter Δ_3. The offset parameter matches the fit and the data at the extremes of the line while γ_M allows the width of the fit to match the data. The offset parameter is only necessary if the absorption line wings are nonzero at the edges of the stored data file, i.e., it is essentially a wing correction. Curve (E) as shown in Fig. 2.1 is the fitting curve that matches the data. The accuracy of the fit is determined by plotting the residuals (observed - calculated) expressed as a percentage of the linecentre absorption. In order to optimize the fit, the residuals are minimized, and the pressure broadening coefficient is determined. Then the factor $S_J P_A$ is obtained from Eq. (2-10), as the other terms in the equation are known. If either the linestrength S_J or the absorber pressure P_A are known, then the other parameter can be determined. In the case of transient absorptions, often neither parameter is known.

The analysis described above allows determination of S_J (or P_A) and γ_M from a single absorption scan at one pressure in a pure gas or mixture. An estimate of the accuracy of the determination of S_J (or P_A) can be obtained by repeating the measurements at various pressures. A more accurate γ_M can be found by plotting the total linewidth ($\Delta\nu$) as a

function of total pressure (P_T). The theoretical curve can be found from the following equations, known as simple Pade approximations:[21]

$$\frac{\Delta\nu}{\Delta\nu_D} = x + \frac{a_1+a_2x}{1+a_3x+a_4x^2}, \quad x = \frac{\gamma_M P_T}{\Delta\nu_D} \qquad \begin{aligned} a_1 &= 0.99957 \\ a_2 &= 0.24258 \\ a_3 &= 0.69923 \\ a_4 &= 0.25035 \end{aligned} \qquad (2\text{-}12)$$

The Doppler width is fixed at the theoretical value and γ_M is varied to optimize the fit. The accuracy of the approximation method in the theory is 0.1 %.

2.4 Second Harmonic Detection

When it is desirable to detect very low concentrations of the absorber molecule it is necessary to modulate the diode laser. The modulation technique as applied to transient detection is examined in detail in Chapter 5. For the steady-state situation, the method of second harmonic detection described below is commonly used.

The second harmonic detection technique involves the application of a small ac frequency modulation to the laser output. The transmitted power through the absorption cell is synchronously detected at twice the modulation frequency. If the frequency excursion is small compared to the linewidth of the measured transition, then this method in effect takes the second derivative of the lineshape. As the second derivative of a sloping background is zero, this method removes the background and allows concentrations on the order of parts-per-million or better to be detected. The theory of this technique has been examined in detail by

Reid et al.[22] so will not be described in more detail here.

2.5 Summary

This chapter has presented the infrared spectroscopy theory that is required for an understanding of the measurements made in this thesis. Direct detection lineshapes and analysis methods used to extract molecular parameters such as linestrength and linewidth have been outlined. In addition, the method of second harmonic detection to greatly enhance the sensitivity of the measurements in a steady-state situation was briefly examined.

CHAPTER 3

DIAGNOSTICS IN CO_2, NH_3 AND HTO SYSTEMS

3.1 Introduction

The tunable diode laser diagnostic techniques that were discussed in the previous chapter have been applied to studies of 3 different gases. In initial experiments, the digital data recording system was verified for accuracy in the determination of linestrength and linewidth for a weak transition in CO_2 for which these parameters are accurately known. Having tested the measurement system, detailed measurements were made on several vibration-rotation transitions in the ν_2 fundamental band of NH_3. These transitions are of importance in both cw and pulsed NH_3 laser systems. In addition, several transitions in the ν_2 band of HTO were examined. These data will be of importance in studies on the sensitivity limits for detection of HTO with tunable diode lasers.

3.2 System Calibration with CO_2

In order to calibrate the linestrength and line-broadening information obtained from the digital data recording system, a weak isotopic line in CO_2 was chosen. The CO_2 transition P(17) (1246.89079 cm^{-1}) of the 628 isotope ($^{12}C^{16}O^{18}O$) in the 10002 - 00001 band[23] was decided upon as the tunable diode laser was single mode in this region, and molecular parameters associated with this line are known to a few percent accuracy. For these measurements

the TDL was directed through a multi-pass White cell, which was easily filled with pure CO_2 or emptied. The pressure in the cell was monitored with a 0 - 1000 Torr capacitance manometer (accuracy 0.5 Torr), and the cell path length was set at 40 passes (4017 cm). Measurements were made at pressures of 50 Torr and 158 Torr, which gave linecentre absorptions on the P(17) transition that were on the order of 13 %. A measurement cycle consisted of TDL scans across the absorption line both with and without gas in the cell, and with a Ge etalon in the beam to give a wavenumber calibration. The background was obtained from the scan with no gas in the cell. Due to the extreme curvature of the background, a linear fit to the wings of the absorption line would not have been appropriate. It was not necessary to scale the background down as is the case when the cell is physically removed from the beam. Analysis of the data consisted of Voigt fits to the absorption curves and detailed information on the methods used is given in the next section with the NH_3 measurements.

The linestrength for the P(17) transition in CO_2 as determined from the measurements is $S = 1.42(5) \times 10^{-5}$ cm^{-2} atm^{-1}. This agrees very closely with the value 1.40×10^{-5} cm^{-2} atm^{-1} that is given by Toth (with a stated accuracy of 0.4 %).[23] For the pressure broadening coefficient, Brimacombe and Reid recently averaged many linewidth measurements in the 9 and 10 μm bands of CO_2 and with a least squares fit to the data arrived at a coefficient:[24]

$$\gamma = 0.1149 - 9.2 \times 10^{-4}|m| \quad \text{cm}^{-1}\ \text{atm}^{-1}$$

where $m = -J$ for the P-branch and $m = J + 1$ for the R-branch. For the

transition P(17) this equation gives γ_{CO_2} = 0.0993 cm^{-1} atm^{-1} (1.31 x 10^{-4} cm^{-1} $Torr^{-1}$). This gives excellent agreement with the measured value of 1.30(3) x 10^{-4} cm^{-1} $Torr^{-1}$. It can be concluded that the procedures used to extract linestrength and linewidth are correct, allowing further measurements on NH_3 and HTO to be performed with confidence.

3.3 Linewidths and Linestrengths in NH_3

3.3.1 Introduction

The infrared absorption spectrum of the ν_2 band of NH_3 has been studied extensively. Excellent data are available for the frequencies of the individual vibration-rotation transitions.[25-27] Several measurements have been made of the dipole moment or bandstrength of the ν_2 band.[28-30] Poynter and Margolis[26] used a dipole moment of 0.24 Debye in their calculation of linestrength, and this value has been confirmed by very recent measurements made by Nakanaga et al.[30] (average dipole moment in the ν_2 band = 0.242(7) Debye, where the values in parentheses are the absolute errors in the last significant figure). However, there is little information available on linewidths of the ν_2 band transitions. Self-broadened widths are reported by Benedict et al.[31,32] and Taylor,[29] while limited measurements have been published on collisional broadening by H_2[28,33,34] and N_2[35] in the infrared. Foreign-gas broadening measurements in the far-infrared and microwave regions are more abundant.[36-38] The recent development of pulsed and cw 12 μm NH_3 lasers operating in dilute mixtures of N_2 and Ar[39-41] has led to a renewed interest in buffer gas broadening of the ν_2 band of NH_3.

Detailed modelling of this laser system requires accurate pressure broadening coefficients for the individual vibration-rotation transitions.[42-44]

In this section we report measurements of collisional broadening coefficients for a total of 18 transitions in the P branch of the NH_3 ν_2 band. These transitions are of particular interest in line-tunable NH_3 lasers. The majority of the measurements are made with a tunable lead-salt diode laser interfaced to a micro-computer. Voigt profiles are fit to the recorded data, and we estimate that linewidths and linestrengths can be measured with an accuracy of better than 4 % on most transitions. Results are reported for N_2-broadening, Ar-broadening, and self-broadening. Measurements made on pure NH_3 in a short gas cell allow an accurate determination of individual linestrengths, and hence the dipole moment of the ν_2 band. The results are in good agreement with previous measurements of band strength. Also reported are limited measurements of linestrength and linewidth in the $(2\nu_2 \leftarrow \nu_2)$ band of NH_3.[14]

3.3.2 Experimental Apparatus

Figure 3.1 is a schematic diagram of the apparatus. A monochromator is initially used to determine the lasing wavelength of the tunable diode laser (TDL), and to search for good single-mode regions of operation. The monochromator is removed during measurements to ensure maximum signal-to-noise ratio in the recorded spectra. A chopper and conventional amplitude detection is used to record the TDL scans, while an analog-to-digital converter (Ithaco Model 385E0-2)

Fig. 3.1: Schematic diagram of the apparatus. Lens L_1 collimates the output of the TDL and lens L_2 focuses the TDL beam onto the detector. Pure NH_3 and mixtures with N_2 and Ar are flowed from a flask through cells varying in length from 0.57 cm to 15 cm. A germanium etalon can be placed in the beam to calibrate the wavenumber scale. The lock-in amplifier signal is digitized and stored in a micro-computer for subsequent analysis.

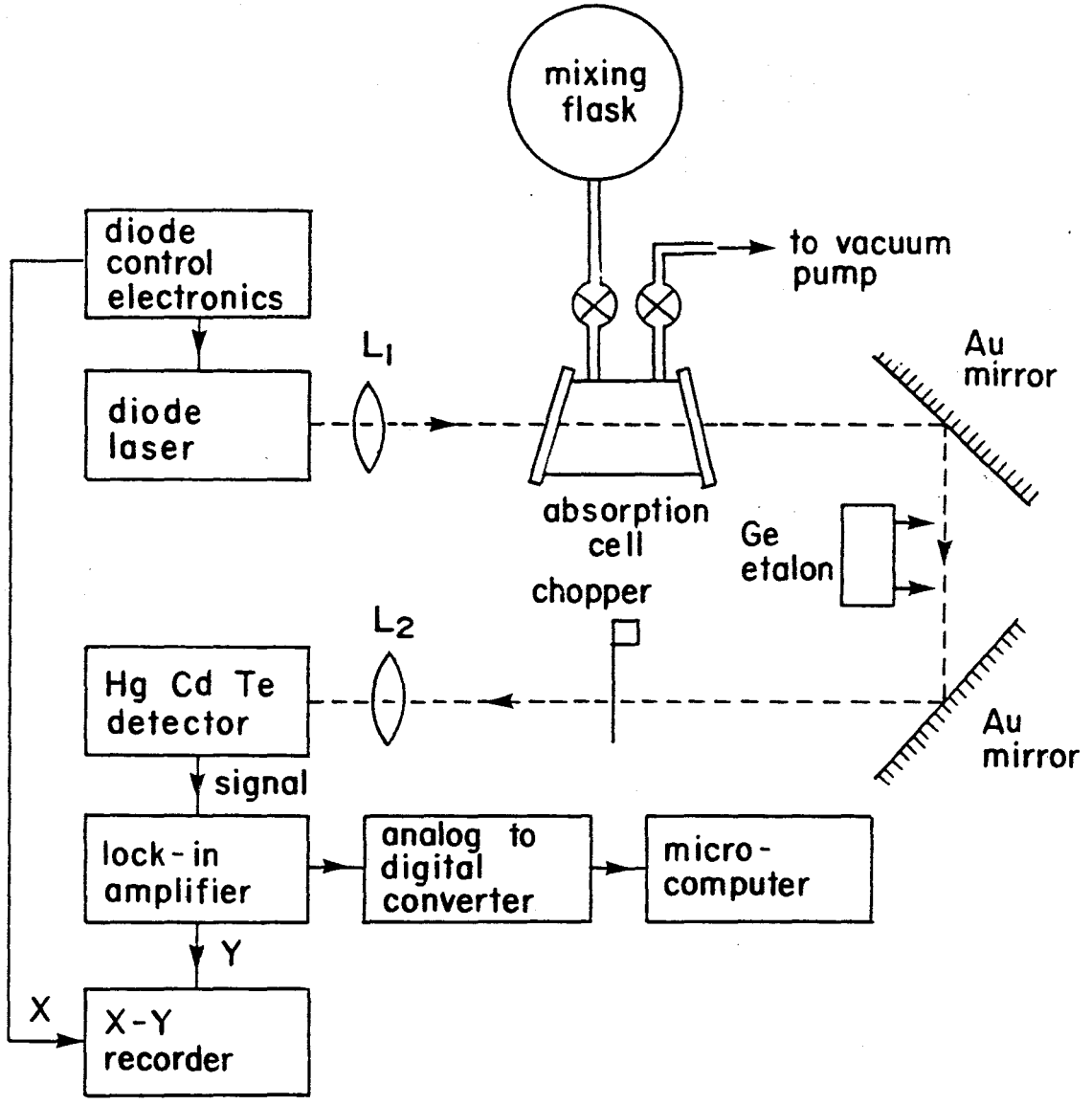
mixing flask
to vacuum pump
diode control electronics
diode laser
L_1
Au mirror
absorption cell
Ge etalon
chopper
L_2
Hg Cd Te detector
Au mirror
signal
lock-in amplifier
analog to digital converter
micro-computer
Y
X
X-Y recorder

interfaces the lock-in amplifier to an IBM PC micro-computer. Use of a digital technique[45,46] to measure linewidth and linestrength is an improvement over most previous methods involving manual digitization[47] or manual analysis of data from X-Y recorders. Gas cells ranging from 0.57 cm to 15 cm in length were used for the measurements. The cell length was chosen such that the linecentre absorptions were always in the intermediate range of 20 to 60 % per pass. In view of the systematic errors which can arise in fitting measured and calculated line profiles,[48-51] care was taken to ensure that wide TDL scans were obtained at slow speeds to eliminate line distortion and account for wing absorption. A second cell of length 10 cm containing 2 Torr pure NH_3 (totally absorbing at linecentre on most transitions) was periodically placed in the laser beam to check the zero transmission baseline, and a careful optical alignment maintained random laser noise well below the 1 % level. A calibrated Ge etalon with a fringe spacing of 0.01627 cm^{-1} was used to determine the tuning rate of the TDL.

Figure 3.2 shows a typical TDL scan over an NH_3 absorption line, together with an etalon scan (the TDL showed very little drift, and successive scans recorded over a period of 10 minutes or so were identical). A linear fit is made to the position of successive etalon peaks to determine the TDL tuning rate, and these data are used to produce a plot of absorption coefficient versus wavenumber, as shown in Fig. 3.3. Superimposed on the data in Fig. 3.3 is the theoretical Voigt profile[52] calculated by numerical integration using the method of Drayson.[20] The high quality of the data can be seen in the plot of residuals (measured - calculated) as a percentage of linecentre

Fig. 3.2: Typical TDL scans of an NH_3 absorption line in the 0.57 cm cell, and a calibration etalon scan. The analog signal from the output of the lock-in amplifier is sampled at a 12 Hz rate, digitized, and stored. Approximately 500 data points are recorded in each scan with a digitization error of < 1 %. The "smoothness" of the displayed data in this and other Figures is limited by the printer resolution.

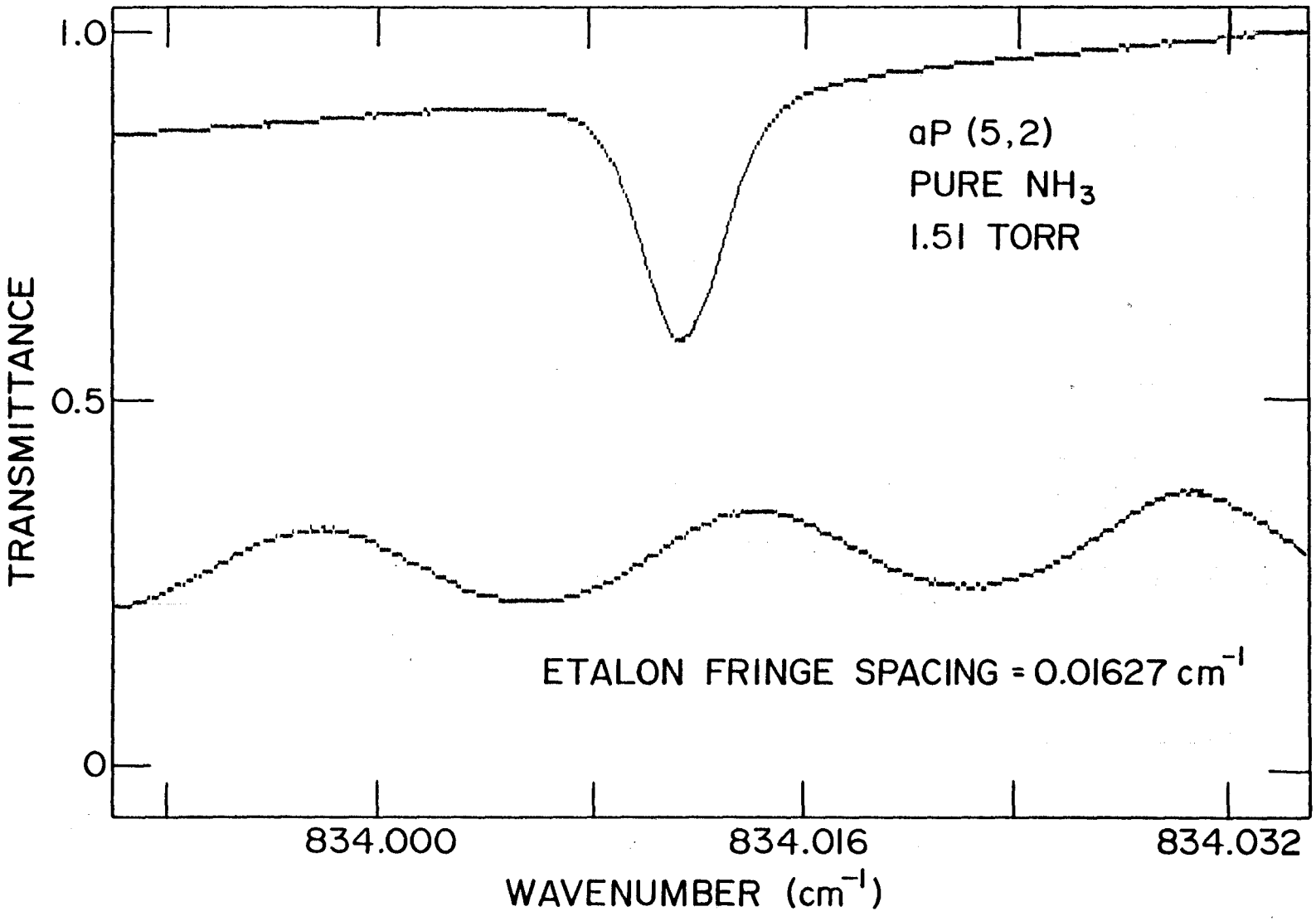
1.0
0.5
0
TRANSMITTANCE
aP (5,2)
PURE NH3
1.51 TORR
ETALON FRINGE SPACING = 0.01627 cm-1
834.000
834.016
834.032
WAVENUMBER (cm-1)

Fig. 3.3: Measured and calculated lineshapes for the data of Fig. 3.2. The upper scan shows the residuals (measured - calculated) as a percentage of the linecentre absorption α_o. These residuals are minimized to optimize the fit. The calculated Voigt profile[20] gives a best fit with a linecentre absorption of 0.8044 cm^{-1} at 834.012 cm^{-1}, and a HWHM pressure broadening coefficient, γ, of 14.60 MHz/Torr. The Doppler width is fixed at its theoretical value ($\Delta\nu_D = 1.255 \times 10^{-3}$ cm^{-1}).

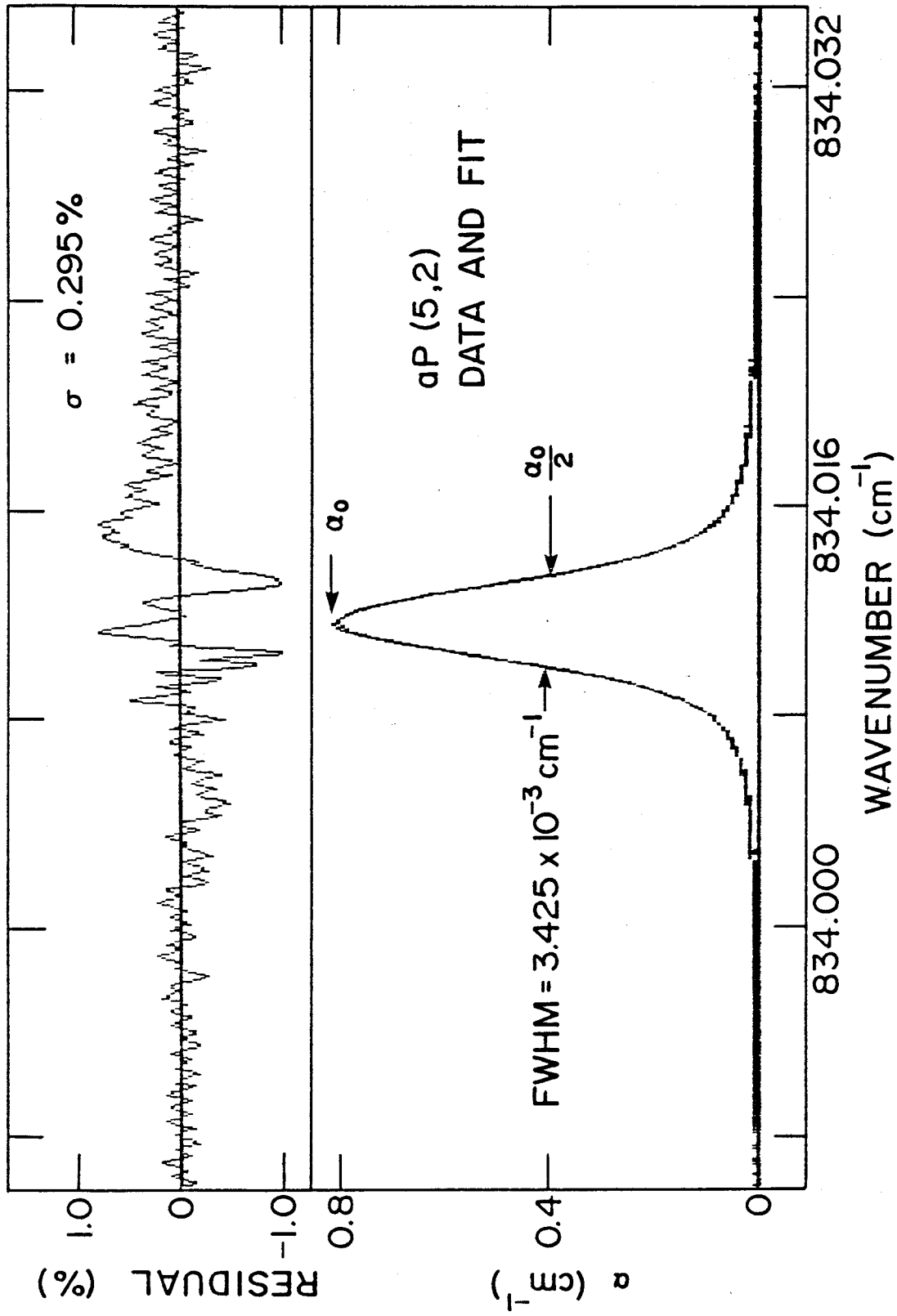
σ = 0.295 %
aP (5,2)
DATA AND FIT
α_0
$\frac{\alpha_0}{2}$
FWHM = 3.425 x 10^{-3} cm^{-1}
RESIDUAL (%)
1.0
0
-1.0
α (cm^{-1})
0.8
0.4
0
834.000
834.016
834.032
WAVENUMBER (cm^{-1})

absorption. Note that in the wings of the line, random noise is ~ 0.25 % peak-to-peak, or < 0.1 % of the total laser power. The maximum deviation in the fit is less than 1 % of the linecentre absorption. These data are typical of many scans taken over a wide range of pressures and mixtures and are comparable with the best previously attained with TDLs[47,53] or high resolution Fourier transform spectrometers.[54] The mean square deviation of the residuals, σ , is always less than 0.5 % (When required, the Voigt fitting procedure incorporated a linear background slope to account for the variation of TDL power with wavenumber). There is a small but systematic pattern observed in the residuals at linecentre as can be seen, for example, in Fig. 3.3. It has been suggested that this pattern is characteristic of collisional narrowing effects[53,55,56] and could possibly be reduced by the use of Galatry lineshapes instead of Voigt profiles. This type of analysis was not attempted in the present work as a simple Voigt profile gave more than adequate agreement with experimental lineshapes.

3.3.3 Results

a) Buffer gas broadening

In this series of measurements, 1 % NH_3 in N_2 and 1 % NH_3 in Ar mixtures were prepared in a pyrex flask at 600 Torr, and then slowly flowed through a 10 cm long Monel cell. The low concentrations of NH_3 were chosen to minimize the corrections required for the NH_3 self-broadening in the determination of the foreign gas broadening coefficients. The total pressure in the absorption cell was measured with a 0 - 100 Torr capacitance manometer with an accuracy of

0.05 Torr. The TDL was tuned to a series of isolated ν_2 transitions, and scans were taken as a function of pressure. Shown in Fig. 3.4 are the effects of pressure broadening by N_2 on the NH_3 transition aP(4,2) (852.725 cm^{-1}). In each case the concentration of NH_3 in N_2 is constant (1 %) and the total pressure is varied. Data fits similar to those shown in Fig. 3.3 were used to determine the total linewidth, and the Lorentz portion of the linewidth, as a function of pressure. These two components are plotted in Fig. 3.5 for aP(4,2), and several other transitions. The theoretical curves in the upper plots were generated following Minguzzi and Di Lieto.[21] Removal of the Doppler component results in the linear plots of the lower section. Further results for N_2 and Ar broadening are given in Table 3.1. The linewidth of the TDL used in these measurements had neglible effect on the results.[57] Also included in Table 3.1 are N_2-broadening coefficients measured previously at McMaster.[58,59] These results were determined from X-Y plotter recordings, and are not as accurate as those determined from the digital data.

b) Linestrengths and self-broadening coefficients

As typical linecentre absorption coefficients in a few Torr of pure NH_3 are 1 cm^{-1}, a short 0.57 cm cell was used for the majority of these measurements. Pure NH_3 flowed slowly through the cell at pressures ranging from 0.5 to 6.5 Torr. This technique minimizes problems due to adsorption and desorption from the cell walls, and consistent results were obtained for several different transitions over a range of pressures. From plots similar to those shown in Fig. 3.5,

Fig. 3.4: Effects of pressure broadening by N_2 on a transition in NH_3. The low pressure scan (19.84 Torr) is shown relative to 0 and 100 % transmission of the TDL, the other scans are offset for clarity. The etalon scan (fringe spacing = 0.01627 cm^{-1}) is used to calibrate the tuning rate of the TDL and thus allows determination of the linewidths.

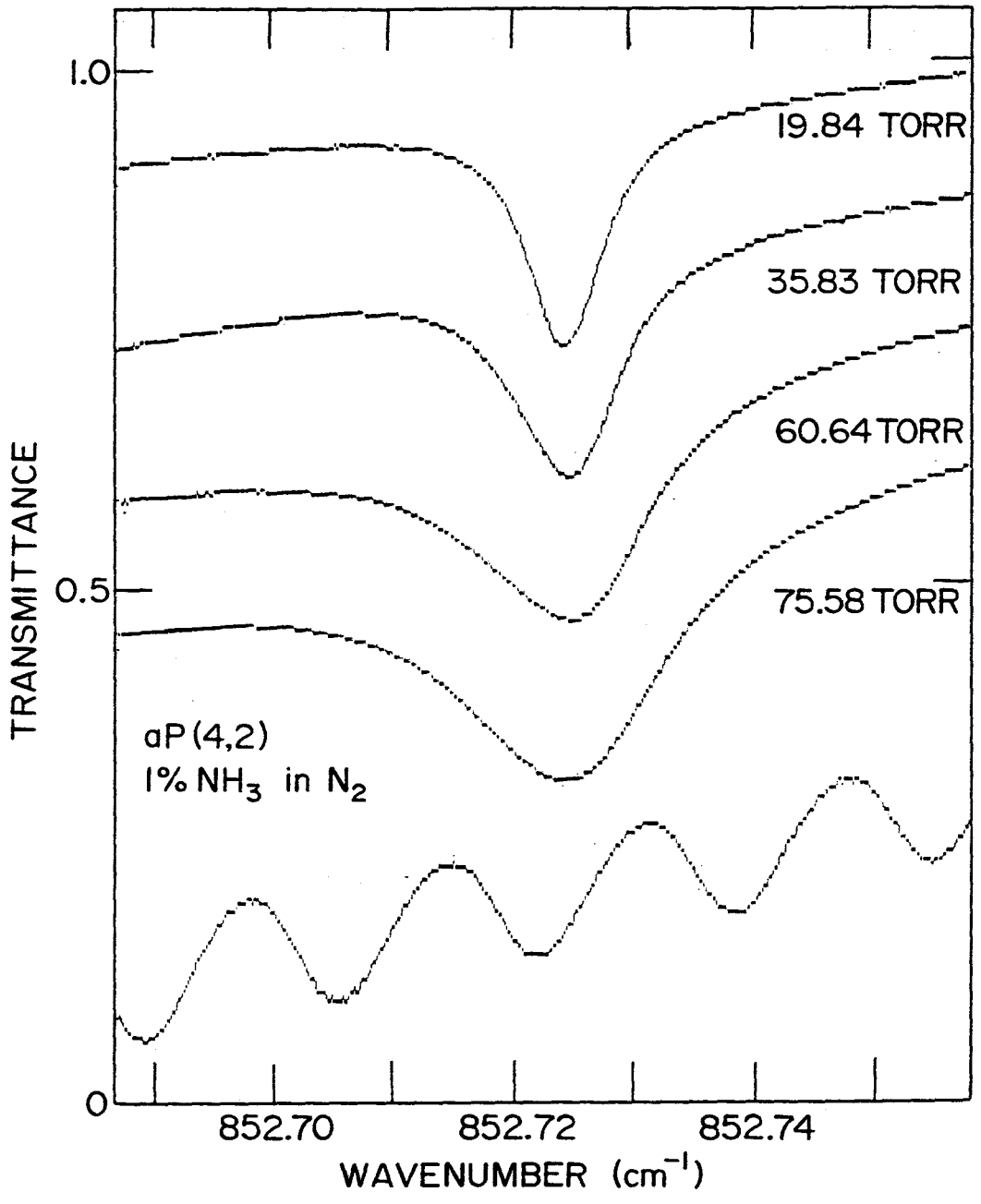
1.0
0.5
0
TRANSMITTANCE
19.84 TORR
35.83 TORR
60.64 TORR
75.58 TORR
aP(4,2)
1% NH3 in N2
852.70
852.72
852.74
WAVENUMBER (cm-1)

Fig. 3.5: Plots of total linewidth (Doppler plus Lorentz), and the Lorentz component only, as a function of pressure for a selected number of transitions. Shown in the upper trace are the linewidths and the theoretical fits as generated by Pade approximations.[21] The straight-line least square fits in the lower traces give the listed pressure broadening coefficients, with their respective standard deviations.

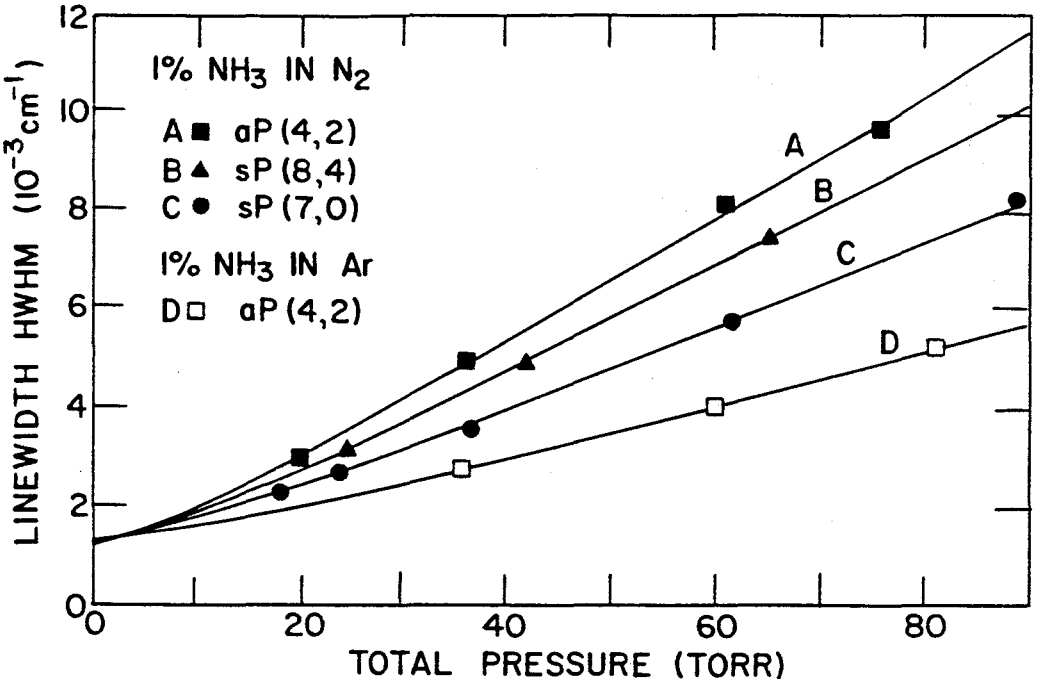
1% NH3 IN N2
A ■ aP(4,2)
B ▲ sP(8,4)
C ● sP(7,0)
1% NH3 IN Ar
D □ aP(4,2)
A
B
C
D
LINEWIDTH HWHM (10-3cm-1)
TOTAL PRESSURE (TORR)
0
2
4
6
8
10
12
0
20
40
60
80

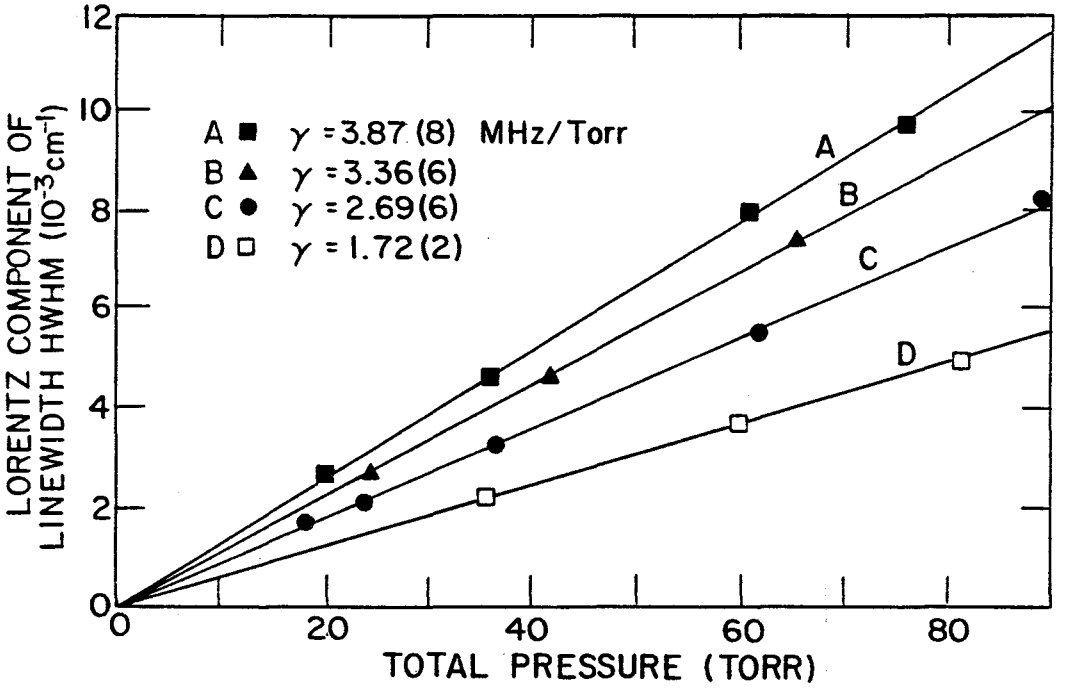
A ■ γ = 3.87(8) MHz/Torr
B ▲ γ = 3.36(6)
C ● γ = 2.69(6)
D □ γ = 1.72(2)
A
B
C
D
LORENTZ COMPONENT OF LINEWIDTH HWHM (10-3cm-1)
TOTAL PRESSURE (TORR)
0
2
4
6
8
10
12
0
20
40
60
80

Table 3.1: Line intensities, self-broadened widths, nitrogen-broadened widths, and argon-broadened widths in the ν_2 band of NH_3 at 296 K. Theoretical linestrengths were computed using a band strength of 546 cm^{-2} atm^{-1}.

a Ref. 26

b The numbers in brackets represent the estimated accuracy derived from the scatter in linestrength values obtained over an order of magnitude of NH_3 pressure.

c Ref. 29

d The numbers in brackets represent one standard deviation to the fits as displayed in Fig. 3.5.

e Refs. 58, 59. The numbers in brackets represent the estimated accuracy of the measurements.

Transition	$S_{calculated}$[a] ($cm^{-2}atm^{-1}$)	$S_{measured}$[b] ($cm^{-2}atm^{-1}$)	$\gamma_{NH_3-NH_3}$[c] calculated HWHM (MHz/Torr)	$\gamma_{NH_3-NH_3}$[d] measured HWHM (MHz/Torr)	$\gamma_{NH_3-N_2}$[e] HWHM (MHz/Torr)	$\gamma_{NH_3-N_2}$[d] measured HWHM (MHz/Torr)	γ_{NH_3-Ar}[d] measured HWHM (MHz/Torr)
aR(1,1)	2.68		18.17		4.34(28)		1.91(20)[e]
aP(4,0)	5.14		9.537			3.79(10)	1.63(3)
aP(4,2)	2.06	2.13(5)	17.80	15.59(25)		3.87(8)	1.72(2)
aP(4,3)	2.64		21.93		4.33(27)		
sR(5,0)	6.13		8.915		3.62(20)		
aP(5,1)	1.89		12.46		3.72(8)		
aP(5,2)	1.74	1.78(2)	15.84	14.60(18)			
sP(5,2)	1.83	1.72(8)	15.84	14.72(29)		3.52(12)	1.51(5)
aP(5,3)	2.90		19.22			3.82(18)	1.61(3)
aP(6,0)	2.55		8.915		3.63(9)		
aR(6,0)	3.98		8.877		2.88(10)		
aP(6,1)	1.26	1.30(10)	11.70	11.39(52)	3.50(10)	3.55(2)	1.42(4)
sP(6,1)	1.32		11.70		3.40(31)	3.10(6)	
sP(6,2)	1.27		14.49		3.64(27)	3.47(10)	
sP(6,3)	2.35	2.34(8)	17.27	16.37(30)	3.42(25)	3.71(5)	
sP(7,0)	1.55		8.877			2.69(6)	
sP(7,1)	0.771		11.20		3.15(9)		
sP(7,2)	0.762		13.53		3.35(14)		
sP(7,5)	0.590		20.51			3.41(11)	1.46(3)
sP(7,6)	0.778	0.766(42)	22.84	20.45(77)		3.85(4)	1.75(4)
sP(8,4)	0.398		16.73			3.36(6)	1.27(3)
2sP(4,2)	0.0214[c]	0.0303(23)	17.80	7.85(50)			
2sR(4,3)	0.0611[c]		19.22		3.67(15)		
2sP(5,3)	0.0300[c]	0.0462(8)	19.22	9.02(6)			

self-broadening coefficients were determined. Results are given in Table 3.1. Standard deviations on the self-broadening coefficients ranged from 1 to 4.6 %. Linestrengths for the various transitions were determined from the area of the calculated best-fit Voigt profiles. Typically, the measured linestrength would vary by less than 5 % when the NH_3 pressure was varied by an order of magnitude. Finally, a limited number of measurements were made on ($2\nu_2 \leftarrow \nu_2$) transitions. These weak transitions were measured in pure NH_3 flowing in a 15 cm cell, and results are given at the bottom of Table 3.1.

3.3.4 Discussion and Conclusions

Data have been obtained for NH_3 linestrengths, self-broadening coefficients, and foreign-gas broadening coefficients for a selected number of transitions. Table 3.1 summarizes the present series of measurements, and compares the results with previous work. For the fundamental ν_2 band of NH_3, the calculated linestrengths at 296 K are taken from Poynter and Margolis[26] and are corrected for the vibrational partition function. Poynter and Margolis used a dipole moment of 0.240 Debye. Our measured linestrengths were determined on six transitions at room temperature (296(1) K), and have a mean deviation from the calculated values of less than 3 %. However, it is interesting that the measured s$\leftarrow$a transitions have slightly stronger linestrengths than the calculated values, while the a$\leftarrow$s transitions are slightly weaker than calculated. If we treat this difference as significant, we derive a dipole moment of 0.244 D for $\mu_{s\leftarrow a}$ and 0.237 D for $\mu_{a\leftarrow s}$.[60] This result is in excellent agreement with recent measurements of 0.248(7) D and

0.236(4) D, respectively, by Nakanaga et al.[30] Our average value for the dipole moment is 0.240(10) D.

Present measurements of self-broadening coefficients (10 - 20 MHz/Torr) in the fundamental ν_2 band follow the general trends given by Taylor[29], but typically the measured values are 8 % lower. For the foreign-gas broadening measurements, several of the NH_3 in N_2 transitions have been previously measured[58,59] and agree with the new values. On average, the N_2-broadening coefficients are larger than the Ar-broadening coefficients by the factor ~2.4. Although there is little information recorded in the infrared on N_2- and Ar-broadening of NH_3, there is an abundance of data in the far infrared and microwave regions.[36-38] It is interesting to note that for these regions the pressure broadening coefficients are in the ranges 3.1 - 4.5 MHz/Torr HWHM for N_2 and 1.6 - 1.8 MHz/Torr for Ar, and are thus comparable to the values in the infrared.

From the linestrengths measured in the $(2\nu_2 \leftarrow \nu_2)$ band one derives a transition dipole moment of μ = 0.285(10) D for the a↞s transitions. This disagrees with the value used by Taylor[29] (see linestrength data in Table 3.1), but is in good agreement with the Bischel et al. value of 0.27(5) D.[61] Takami et al.[62] derive a value of 0.36(3) D from the measurements of Siemsen and Reid,[63] while Bulanin et al.[64,65] report a value of 0.395(3).[66] The measured $(2\nu_2 \leftarrow \nu_2)$ self-broadening coefficients differ significantly from the values given by Taylor,[29] but are in good agreement with the range of values (6.5 - 13 MHz/Torr) measured by Baldacchini et al.[67,68] and the range of values (7.0 - 9.6 MHz/Torr) measured by Bulanin et al.[64] Clearly, as seen above, there is not universal agreement in the literature on these values.

While the data given in Table 3.1 do not provide a complete list of broadening coefficients for all transitions of interest, they do allow more accurate modelling to be carried out on the dynamics of pulsed and cw NH_3 lasers. The narrow linewidths in NH_3/Ar mixtures partially accounts for the improved behaviour observed in cw NH_3 lasers with Ar buffer gas.[41] The anomalously small N_2 pressure broadening coefficient of 2.69 MHz/Torr for the sP(7,0) transition contributes to the anomalously high gain observed on this transition in both cw and pulsed laser systems.[41,58] The $(2\nu_2 \leftarrow \nu_2)$ band measurements will be useful for modelling 16 - 21 μm NH_3 lasers.[69]

In a recent series of measurements on (V→T,R) relaxation in NH_3/N_2 mixtures, a TDL was used to determine the percentage of NH_3 in a gas mixture confined in a capillary tube.[70] Absorption measurements made on several different P-branch transitions gave significantly different concentrations when a constant value of the N_2 pressure broadening coefficient was assumed for all transitions. However, when the pressure broadening coefficients determined in the present study were used, the concentrations calculated from measurements on different transitions agreed to better than 5 %.

3.4 Linewidths and linestrengths in HTO

Leakage of tritium into the air is a recognized health hazard in both fission and fusion reactor environments. Once in the air, tritium commonly takes on the forms HTO and HT through isotope exchange. HTO is a much more dangerous form of tritium than HT, thus there is interest in developing a monitor for tritium in the specific form of HTO.

Sensitivity required for such a device is in the parts-per-billion to parts-per-trillion range.

In order to evaluate the performance of a TDL instrument for the detection of HTO, certain spectroscopic information is required. In this section measurements made on the strong ν_2 band of HTO are described. A sample of tritiated water vapor was introduced into a multipass optical cell, and TDL scans were taken of six of the stronger HTO absorption lines in the 1250 to 1400 cm^{-1} region. These lines were identified from Fourier transform spectra taken at Los Alamos laboratories.[71]

Measurements were made with a chopper, a lock-in amplifier and conventional amplitude detection. The output of the lock-in amplifier was digitized and stored on an IBM PC. The tuning rate of the TDL was found by using a 7.65 cm Ge etalon. The measured lineshapes were compared with calculated Voigt profiles to determine linestrengths and linewidths. As in the previous work on NH_3, the data were generally of high quality with residuals rarely exceeding 1 % of the linecentre absorption. Typical data are shown in Fig. 3.6, while the corresponding fit and residuals are shown in Fig. 3.7. Pressure broadening coefficients for both air and water broadening were determined to better than 5 %. Typical data are shown in Fig. 3.8, while the total linewidth and Lorentz component of the linewidth versus pressure for several lines is given in Fig. 3.9. A summary of the results is given in Table 3.2.

Also shown in Table 3.2 are the linestrengths of the measured lines. Relative linestrengths are accurate to 2 %. The absolute linestrength error is larger (10 %) due to uncertainty in the

Fig. 3.6: Typical TDL scan of an HTO absorption line at 1384.694 cm^{-1}, together with a calibration etalon scan. Optical pathlength is 4 m through 7 Torr of an HTO/H_2O mixture with a nominal specific activity of 5 Ci/ml. The analog signal from the output of the lock-in amplifier is sampled at a 12 Hz rate, digitized, and stored. Approximately 500 data points are recorded in each scan with a digitization error of < 0.1 %. The "smoothness" of the displayed data in this and other Figures is limited by the printer resolution.

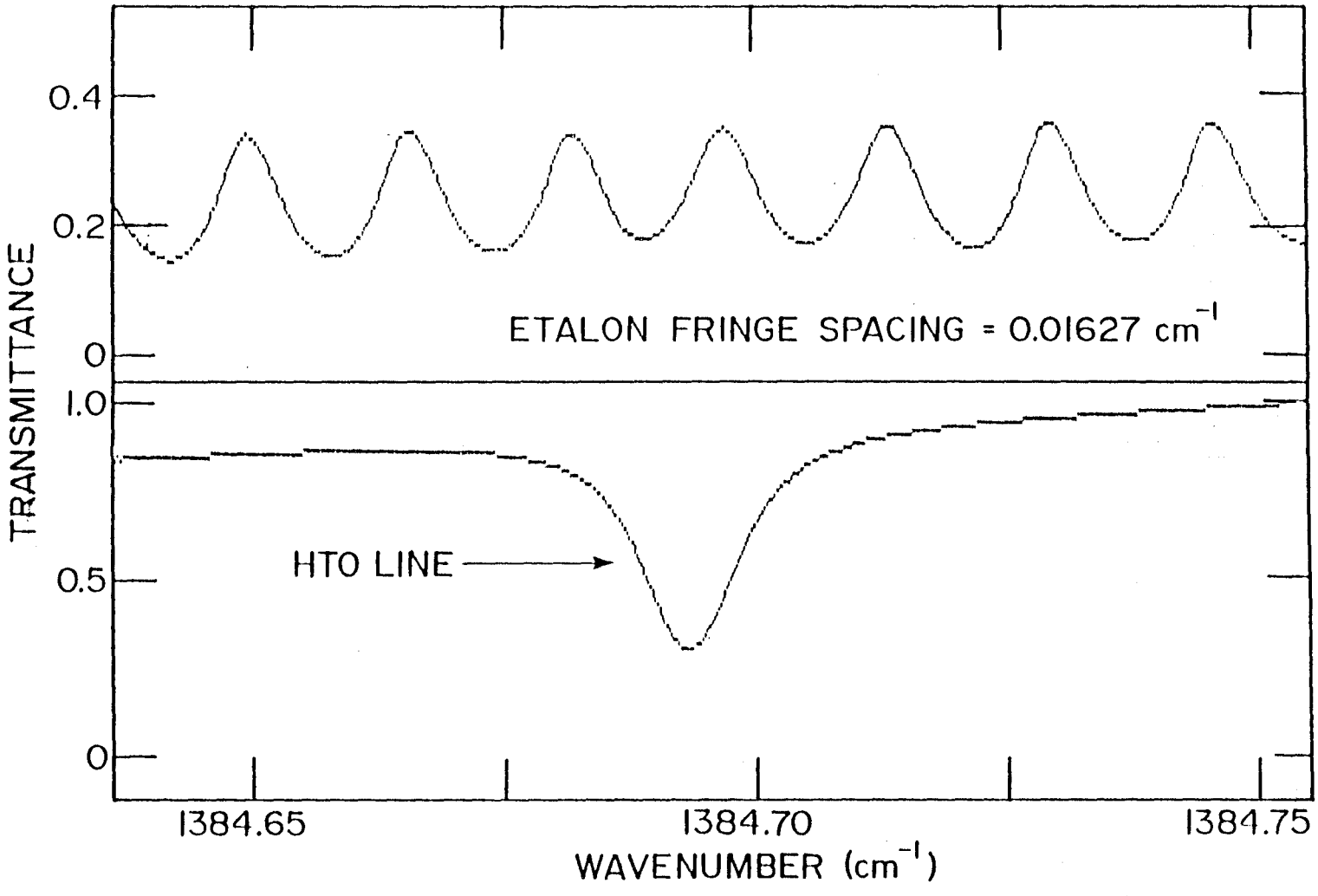
0.4
0.2
0
1.0
0.5
0
TRANSMITTANCE
ETALON FRINGE SPACING = 0.01627 cm⁻¹
HTO LINE
1384.65
1384.70
1384.75
WAVENUMBER (cm⁻¹)

Fig. 3.7: Measured and calculated lineshapes for the data of Fig. 3.6. The upper scan shows the residuals (measured - calculated) as a percentage of the linecentre absorption α_0. The calculated Voigt profile gives a best fit with a linecentre absorption of 2.8×10^{-1} m^{-1} with a HWHM pressure broadening coefficient of 16.8 MHz/Torr.

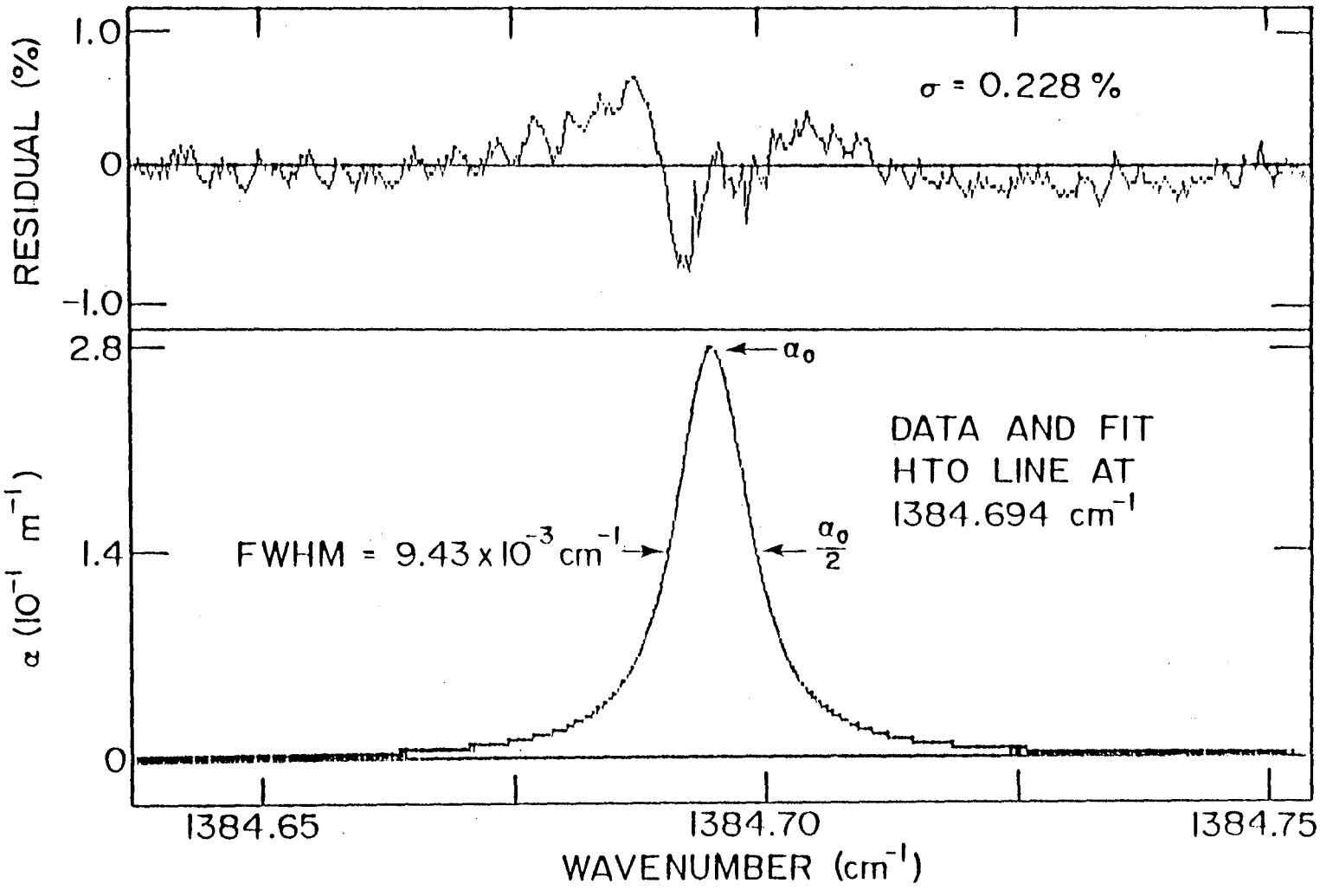
RESIDUAL (%)
1.0
0
-1.0
σ = 0.228 %
2.8
1.4
0
α (10⁻¹ m⁻¹)
α₀
α₀/2
FWHM = 9.43 x 10⁻³ cm⁻¹
DATA AND FIT
HTO LINE AT
1384.694 cm⁻¹
1384.65
1384.70
1384.75
WAVENUMBER (cm⁻¹)

Fig. 3.8: Effects of pressure broadening by H_2O on a transition in HTO. The low pressure scan (2.1 Torr) is shown relative to 0 and 100 % transmission of the TDL, the other scans are offset for clarity.

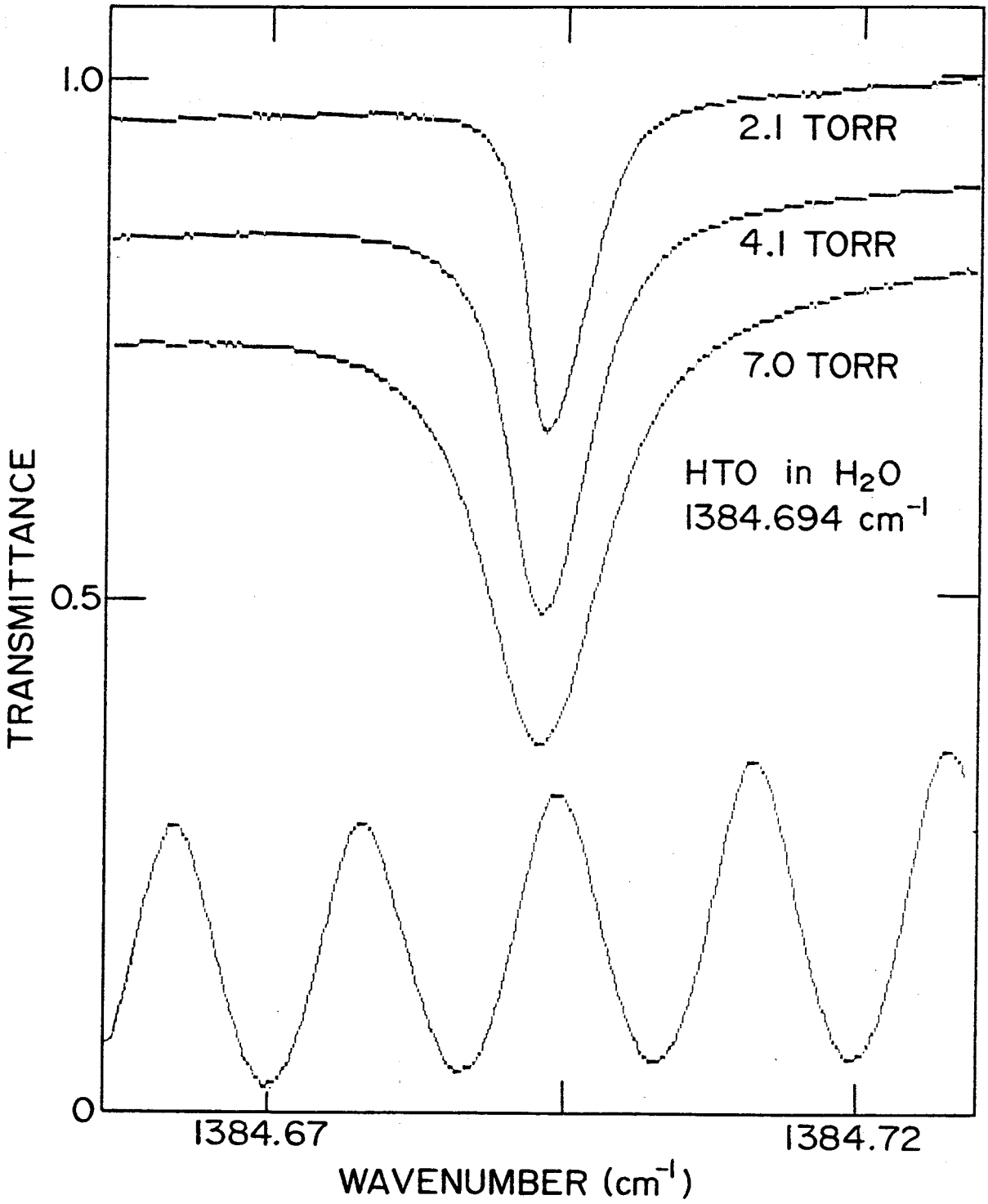
1.0
0.5
0
TRANSMITTANCE
2.1 TORR
4.1 TORR
7.0 TORR
HTO in H_2O
1384.694 cm^{-1}
1384.67
1384.72
WAVENUMBER (cm^{-1})

Fig. 3.9: Plots of the total linewidth (Doppler plus Lorentz), and the Lorentz component only, as a function of pressure for three HTO transitions. The HTO transitions are identified by their respective wavenumber.[71] The straight-line least square fits in the lower traces give the pressure broadening coefficients, with their respective standard deviations.

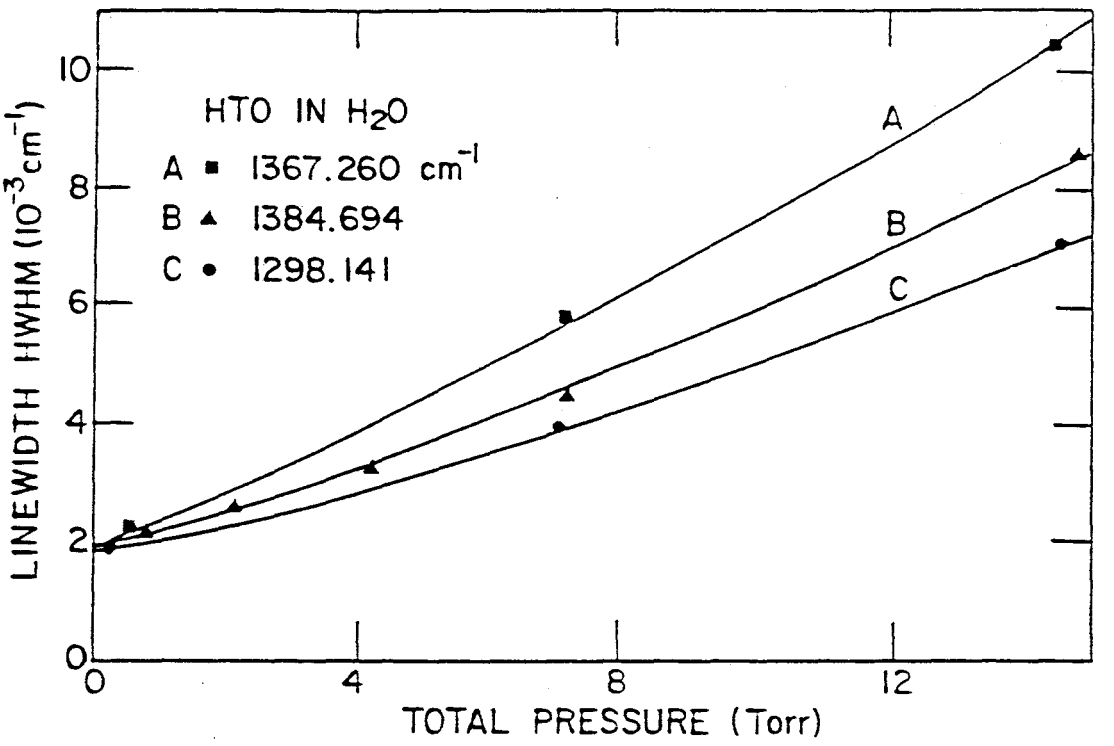
HTO IN H_2O
A ■ 1367.260 cm^{-1}
B ▲ 1384.694
C ● 1298.141
A
B
C
LINEWIDTH HWHM ($10^{-3}cm^{-1}$)
TOTAL PRESSURE (Torr)
0
2
4
6
8
10
0
4
8
12

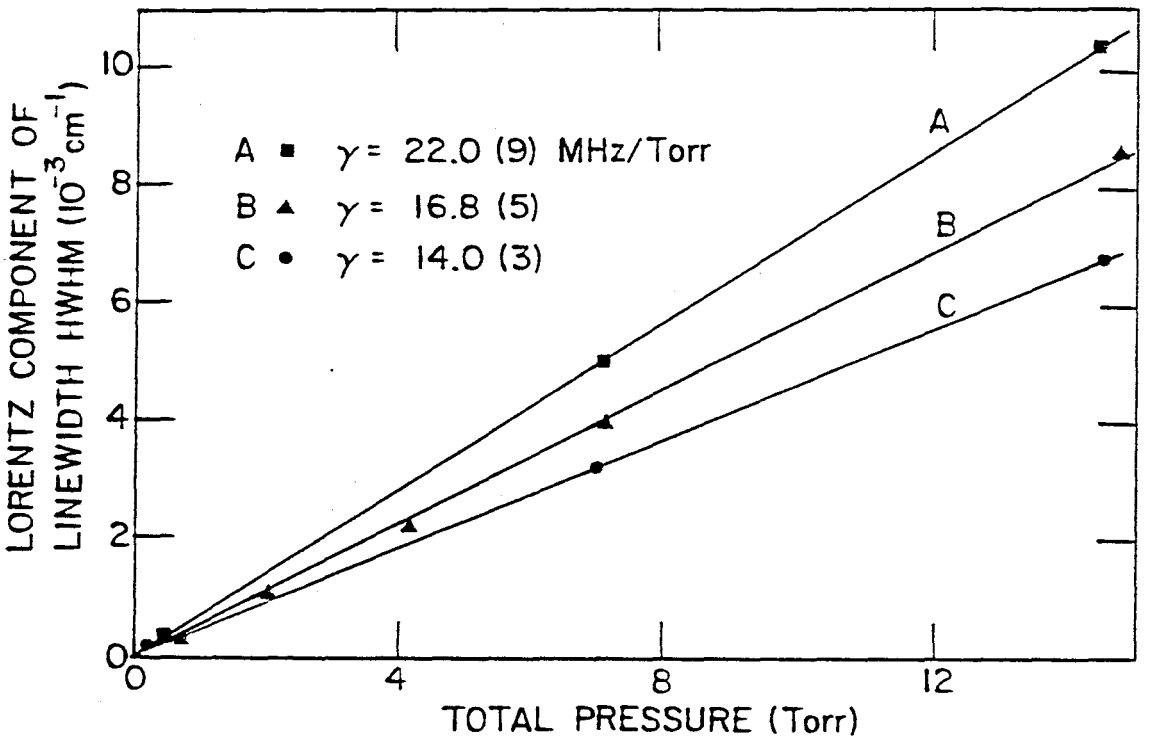
A ■ γ = 22.0 (9) MHz/Torr
B ▲ γ = 16.8 (5)
C ● γ = 14.0 (3)
A
B
C
LORENTZ COMPONENT OF LINEWIDTH HWHM ($10^{-3}cm^{-1}$)
TOTAL PRESSURE (Torr)
0
2
4
6
8
10
0
4
8
12

Table 3.2: Line positions, line intensities, water-broadened widths, and air-broadened widths in the ν_2 band of HTO at 297 K.

a Uncertainty on line positions is 0.005 cm^{-1}

b Absolute linestrengths are estimated to be accurate to 10 %, relative linestrengths are good to 2 %.

Line Position (cm^{-1})[a]	Linestrength (cm^{-2}/atm)[b]	Water Broadening (MHz/Torr)	Air Broadening (MHz/Torr)
1262.480	1.10	16.8(8)	-
1266.339	0.47	15.0(2)	3.23(6)
1266.461	1.47	16.8(1)	3.80(6)
1298.141	1.62	14.0(3)	3.91(7)
1367.079	1.62	18.6(9)	4.56(13)
1367.260	0.64	22.0(9)	3.82(12)
1384.694	1.51	16.8(5)	4.02(9)

concentration of HTO in H_2O. For the absolute linestrength determination, a series of measurements were made on the line at 1367.019 cm^{-1} using a water sample which was calibrated both before and after the infrared measurement; calibration was carried out using scintillation counters and NBS standards.

The results given in Table 3.2 can be used to determine the minimum level of HTO that can be detected with a TDL monitor. Details can be found in work by Cherrier et al.[15,72]

3.5 Summary

This chapter illustrates the application of a tunable diode laser to the measurement of linestrength and linewidth in a variety of gaseous systems. The diagnostic technique is quite general, and allows spectral parameters to be measured to accuracies of a few percent from a limited number of measurements. Data on linestrength and linewidth is required in order to determine concentrations of the species of interest from infrared absorption measurements. The majority of the work reported in this chapter is described in publications by Beckwith, Danagher, and Reid (Accepted in J. Mol. Spectrosc.)[14] and Cherrier, Beckwith, and Reid (Submitted to J. Mol. Spectrosc.).[15] In particular, acknowledgements are due to D. J. Danagher for his collaboration in obtaining the data shown in Figs. 3.2, 3.4, 3.5 and Table 3.1, and to P. P. Cherrier for his collaboration in obtaining the data shown in Figs. 3.6, 3.8, 3.9, Table 3.2, and the CO_2 calibration. The next chapter will discuss the application of the TDL diagnostics to photochemistry experiments.

CHAPTER 4

DIAGNOSTICS IN $CDCl_3$ DISSOCIATION

4.1 Introduction

Tunable diode lasers remain relatively unexploited as a tool in analytical chemistry. In this chapter it is demonstrated that TDLs are a sensitive analytical tool for investigating the products of photochemical reactions in the gas phase. Examples are given from experiments on the infrared photochemistry of chloroform. The sensitivity of the TDL technique is such that one can measure the few parts per million of DCl formed by photolysis of natural abundance $CDCl_3$ in $CHCl_3$.[13]

To illustrate the advantages of the TDL technique both chemical and isotopic analyses made after TEA - CO_2 laser infrared multiphoton dissociation (IRMPD) of chloroform[73] will be described. The basic concepts of this method are explained in terms of parameters for DCl and CO detection. The CO that was observed is formed in the photolysis cell as a result of $:CCl_2$ reacting with the walls of the cell. The detection method used is applicable to other irradiation sources such as metal vapour resonance lamps, flash lamps, Nd:YAG or excimer lasers. Thus, the TDL techniques are applicable to chemical and isotopic product analysis of most types of gas phase reactions.

The next section (Section 4.2) describes the experimental apparatus and calibration procedures, and illustrates the high sensitivity that can be attained with harmonic techniques. In

Section 4.3 typical results are described, including the detection of DCl after irradiation of naturally occuring $CDCl_3$ in $CHCl_3$. The importance of wall reactions is also illustrated. Discussion and conclusions are given in the final section (Section 4.4).

4.2 Experimental Apparatus and Calibration Procedure

Figure 4.1 is a schematic diagram of the apparatus. The sample is irradiated in a conventional 10 cm long pyrex or Monel gas cell with NaCl or KCl windows tilted slightly to avoid feedback to either the CO_2 laser or the TDL. The TEA CO_2 laser pulses have energies in the range 0.3 to 2 J and are focussed into the gas cell with a 25 cm focal length BaF_2 lens. The pulses are produced by a Lumonics K-922S laser, and approximately half the energy is contained in a 100 ns gain-switched spike, with the remainder in the tail of the pulse, which lasts 1 μs. In general, the gas cell was irradiated by several successive pulses, and then the TDL was used to monitor the product formation.

To demonstrate the application of the TDL as a diagnostic tool, the formation of DCl was monitored after irradiation of $CHCl_3/CDCl_3$ mixtures with 11 μm radiation. At the CO_2 transition 10P(48) (10.911 μm) $CHCl_3$ is almost transparent while $CDCl_3$ gives strong absorption. Thus, $CDCl_3$ should be the principle molecule dissociated. Herman *et al.* examined the multiphoton dissociation of $CDCl_3$ in a molecular beam and showed that the dominant dissociation channel (> 99%) was elimination of DCl.[73] It is noteworthy that although this study was performed with sophisticated mass spectrometer equipment, no direct detection of DCl was carried out. In contrast, DCl is an ideal molecule

Fig. 4.1: Schematic diagram of the apparatus. Lens L_1 collimates the output of the TDL, lens L_2 focuses both the TDL and the CO_2 beams into the photolysis cell, and lens L_3 focuses the TDL onto the detector. Mirror M_1 (Ge) transmits ~75 % of the TEA CO_2 pulse, and reflects ~85 % of the TDL radiation. The LiF filter prevents any 11 μm radiation from reaching the detector.

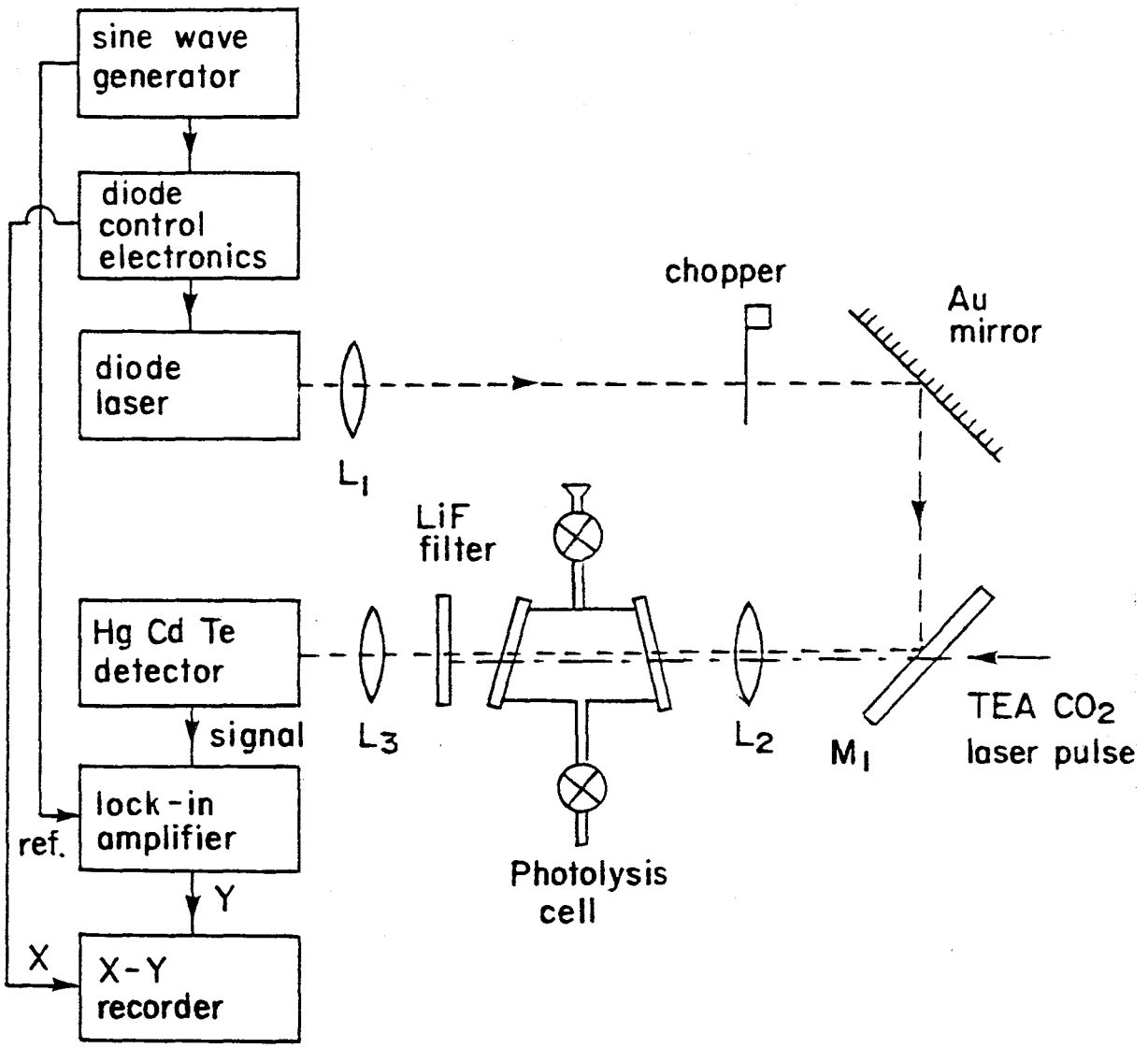
sine wave generator
diode control electronics
diode laser
chopper
Au mirror
L_1
LiF filter
Hg Cd Te detector
signal
L_3
L_2
M_1
TEA CO_2 laser pulse
lock-in amplifier
ref.
Y
X
X-Y recorder
Photolysis cell

for TDL detection; it has a strong infrared spectrum consisting of isolated lines in the 4.8μm region. The positions of these lines have been accurately measured.[74,75] Refer to Fig. 4.2 for an illustrated spectrum of DCl for the ^{35}Cl and ^{37}Cl transitions, and to Table 4.1 for the wavenumbers of these transitions.[75]

The first part of the experiment consisted of finding suitable conditions of temperature and current for operating the TDL. The TDL beam was directed through a 0.5 m grating spectrometer which was calibrated with a HeNe laser. With a little care, the TDL operating wavenumber could be determined to 0.1 cm^{-1}. This accuracy was more than sufficient to identify $D^{35}Cl$ or $D^{37}Cl$ absorption lines when a gas cell containing low pressure DCl was placed in the beam. Several potential operating regions were determined. For each one, the TDL tuned smoothly through a DCl line with no mode hops and a minimum of laser power in satellite modes. The spectrometer was then removed, and additional scans were taken through a gas cell containing sufficient DCL to be opaque at line centre. Typical scans are shown in Fig. 4.3. A chopper and conventional amplitude detection were employed, and the TDL temperature was carefully adjusted to maximise the laser power in the required laser mode. In general > 90 % of the total laser power could be obtained in the mode tuning through the DCl line. The $D^{35}Cl$ line R(7) was finally used for DCl monitoring. Throughout the experimental measurements, periodic checks were made of the DCl optical zero as shown in Fig. 4.3, and all calculations of absorption coefficients were performed using only the laser power actually in the DCl mode.

Figure 4.4 shows results of TDL scans taken after irradiation of

Fig. 4.2: Infrared spectrum of the deuterium chloride fundamental (2240 cm^{-1} - 1890 cm^{-1}) as measured on an IR grating spectrometer. Shown are the $D^{35}Cl$ and $D^{37}Cl$ transitions for the P and R branches and the operating wavenumber range of the lead-salt TDL used in the DCl detection. The illustrated spectrum is based on scans of 1 Torr DCl for a 3 m path length.[75]

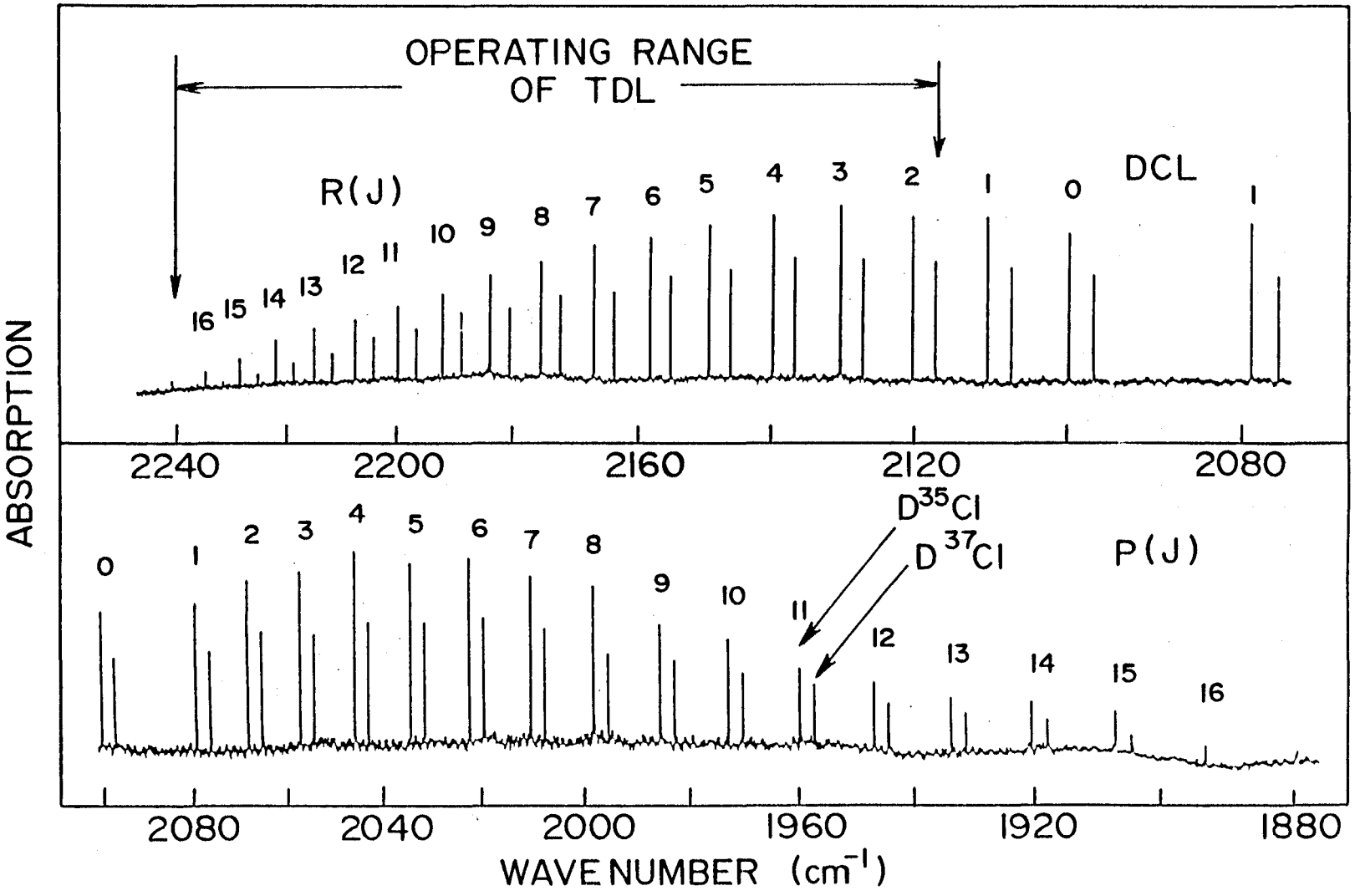
OPERATING RANGE
OF TDL
R(J)
DCL
16
15
14
13
12
11
10
9
8
7
6
5
4
3
2
1
0
1
2240
2200
2160
2120
2080
ABSORPTION
D35Cl
D 37Cl
P(J)
0
1
2
3
4
5
6
7
8
9
10
11
12
13
14
15
16
2080
2040
2000
1960
1920
1880
WAVE NUMBER (cm-1)

Table 4.1: Line positions in the fundamental band of DCl.

Line Pair Designation	$D^{35}Cl$ Wavenumber (cm^{-1})	$D^{37}Cl$ Wavenumber (cm^{-1})	Line Pair Designation	$D^{35}Cl$ Wavenumber (cm^{-1})	$D^{35}Cl$ Wavenumber (cm^{-1})
R(0)	2101.620	2098.590			
R(1)	2111.951	2108.891	P(1)	2080.277	2077.310
R(2)	2122.051	2118.961	P(2)	2069.272	2066.337
R(3)	2131.915	2128.798	P(3)	2058.048	2055.147
R(4)	2141.542	2138.398	P(4)	2046.610	2043.743
R(5)	2150.927	2147.758	P(5)	2034.960	2032.129
R(6)	2160.068	2156.875	P(6)	2023.103	2020.308
R(7)	2168.962	2165.746	P(7)	2011.041	2008.283
R(8)	2177.605	2174.368	P(8)	1998.779	1996.058
R(9)	2185.995	2182.737	P(9)	1986.319	1983.637
R(10)	2194.128	2190.852	P(10)	1973.666	1971.023
R(11)	2202.001	2198.708	P(11)	1960.822	1958.219
R(12)	2209.613	2206.303	P(12)	1947.792	1945.230
R(13)	2216.959	2213.634	P(13)	1934.579	1932.059
R(14)	2224.037	2220.698	P(14)	1921.187	1918.709
R(15)	2230.845	2227.493	P(15)	1907.618	1905.185
R(16)	2237.379	2234.016	P(16)	1893.878	1891.491

Fig. 4.3: TDL scans taken during optimization of operating temperature. The laser beam passes through a gas cell containing 3.5 Torr of DCl in $CDCl_3$ (50 Torr total pressure) and is scanned in frequency over the R(7) line in $D^{35}Cl$ at 2168.962 cm^{-1}. From the central scan it can be seen that > 91 % of the laser energy is in the mode of interest. The two additional scans illustrate the effect of minor changes in operating temperature.

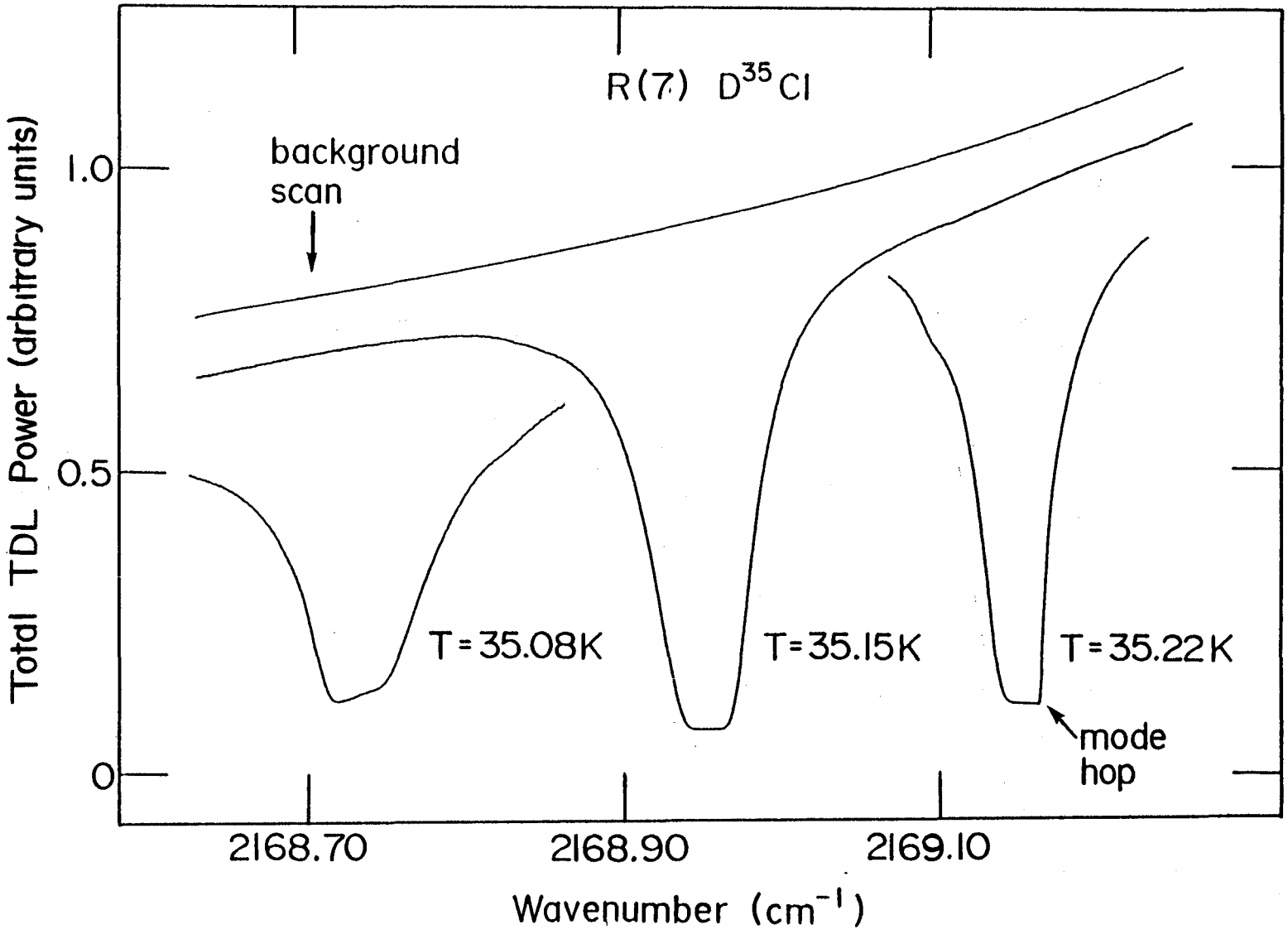
R(7) D35Cl
background scan
1.0
0.5
0
Total TDL Power (arbitrary units)
T = 35.08K
T = 35.15K
T = 35.22K
mode hop
2168.70
2168.90
2169.10
Wavenumber (cm-1)

Fig. 4.4: Typical TDL scans showing the formation of DCl and CO after irradiation of 2 Torr pure $CDCl_3$ with 80 pulses of 0.4 J energy per pulse. The CO_2 laser transition was 10P(48) (916.76 cm^{-1}). The etalon fringes are used to calibrate the wavenumber scale, and additional cells containing pure DCl and CO were used to confirm the line identifications. Also shown at the bottom of the figure are the calculated positions of the R(7) line in DCl (2168.962 cm^{-1}) and the R(6) line in CO (2169.1984 cm^{-1}).[75,76]

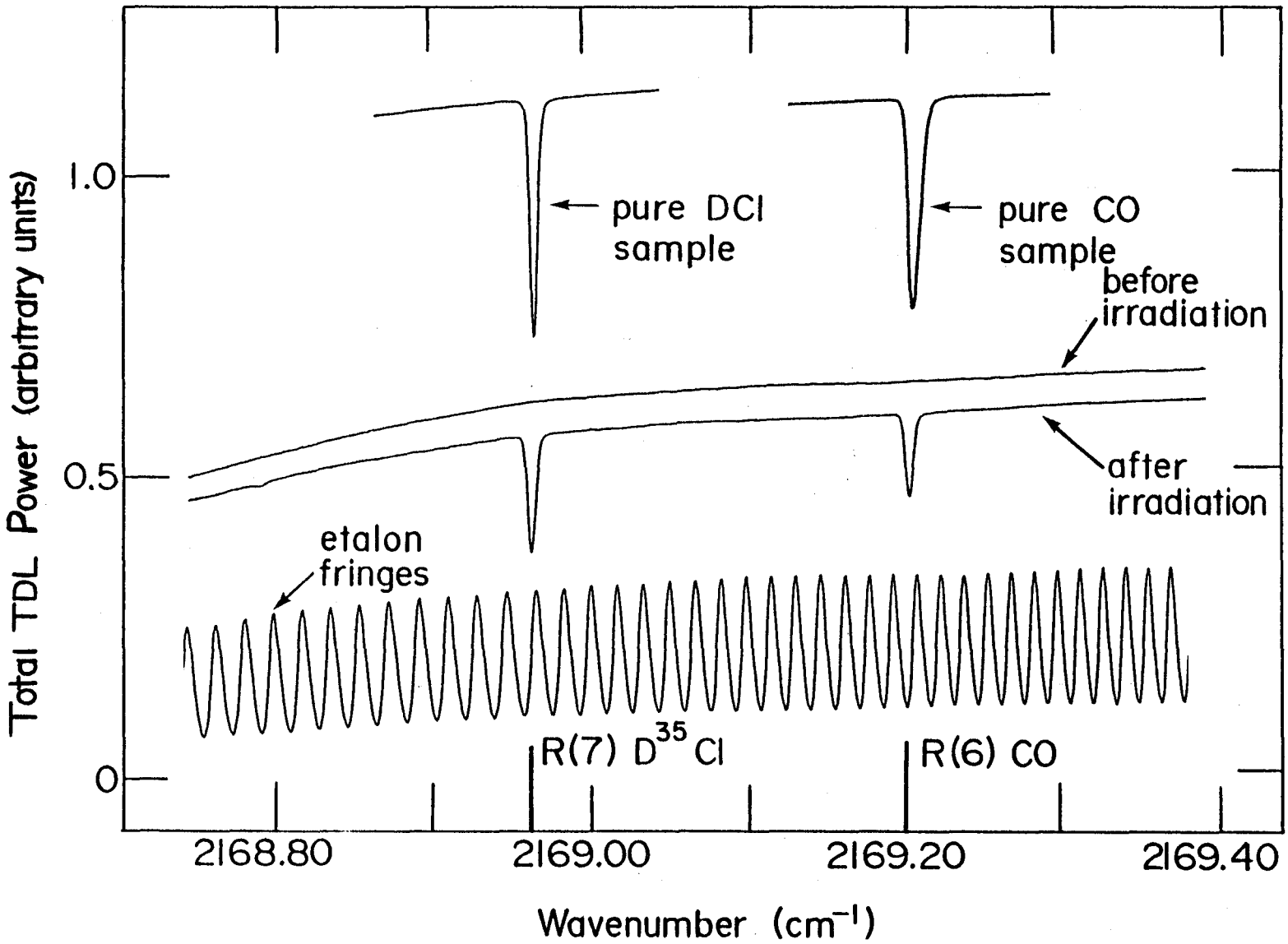
Total TDL Power (arbitrary units)
1.0
0.5
0
pure DCl sample
pure CO sample
before irradiation
after irradiation
etalon fringes
R(7) D35Cl
R(6) CO
2168.80
2169.00
2169.20
2169.40
Wavenumber (cm-1)

a cell containing pure $CDCl_3$. The measured DCl absorption corresponds to a dissociation of < 2 % of the parent $CDCl_3$ molecules. In addition to absorption at the DCl frequency (2168.962 cm^{-1}), a strong line also appeared near 2169.20 cm^{-1}. This was identified as the R(6) line of CO at 2169.1984 cm^{-1}.[76] By analogy with the wall reaction of CF_2,[77] it is believed that the CO is formed by wall reactions of $:CCl_2$ in the cell. CO is easily observed in the scans shown in Fig. 4.4, even though its concentration in the cell is only 0.3 %. When more intense CO_2 laser pulses were used for irradiation, the formation of DCl and CO was even more dramatic. A single 1.2 J pulse produces substantial absorption (> 50 %) on the R(7) DCl line, even though the "dog-bone" focussing geometry ensures that << 1 % of the gas in the cell is irradiated with intensities above the dissociation threshold. (In the experiments, sufficient time elapses between irradiation and the TDL measurement for the photolysis products to diffuse uniformly throughout the cell volume.)

Although the traces shown in Fig. 4.4 demonstrate the ease with which DCl formation can be detected after irradiation of pure $CDCl_3$, we are more interested in detecting the much lower concentrations of DCl formed when irradiating $CHCl_3/CDCl_3$ mixtures. $CDCl_3$ occurs naturally in $CHCl_3$ at 1 part in 7000, and hence even with complete dissociation, DCl would only appear as 140 part per million (ppm) after irradiation of chloroform at natural isotopic abundance. Fortunately, harmonic detection techniques allow the TDL to monitor DCl at concentrations in the ppm range. These techniques are fully described in Refs. 22 and 78 and are illustrated in Fig. 4.5. For the scans shown in Fig. 4.5, the

Fig. 4.5: Second harmonic detection with a TDL. Scan (a) is taken with a chopper and conventional amplitude detection. The DCl absorption is 35 % in a 10 cm path. Scan (b) is taken with the chopper removed and a 2.5 kHz modulation applied to the TDL current. Lock-in amplifier detection is carried out at 5 kHz. Scans (a) and (b) are taken with identical gain settings. For trace (c), amplification is increased by a factor of 1150, and there is only a trace of CO and DCl in 5 Torr $CDCl_3$ in the cell (noise is not minimized).

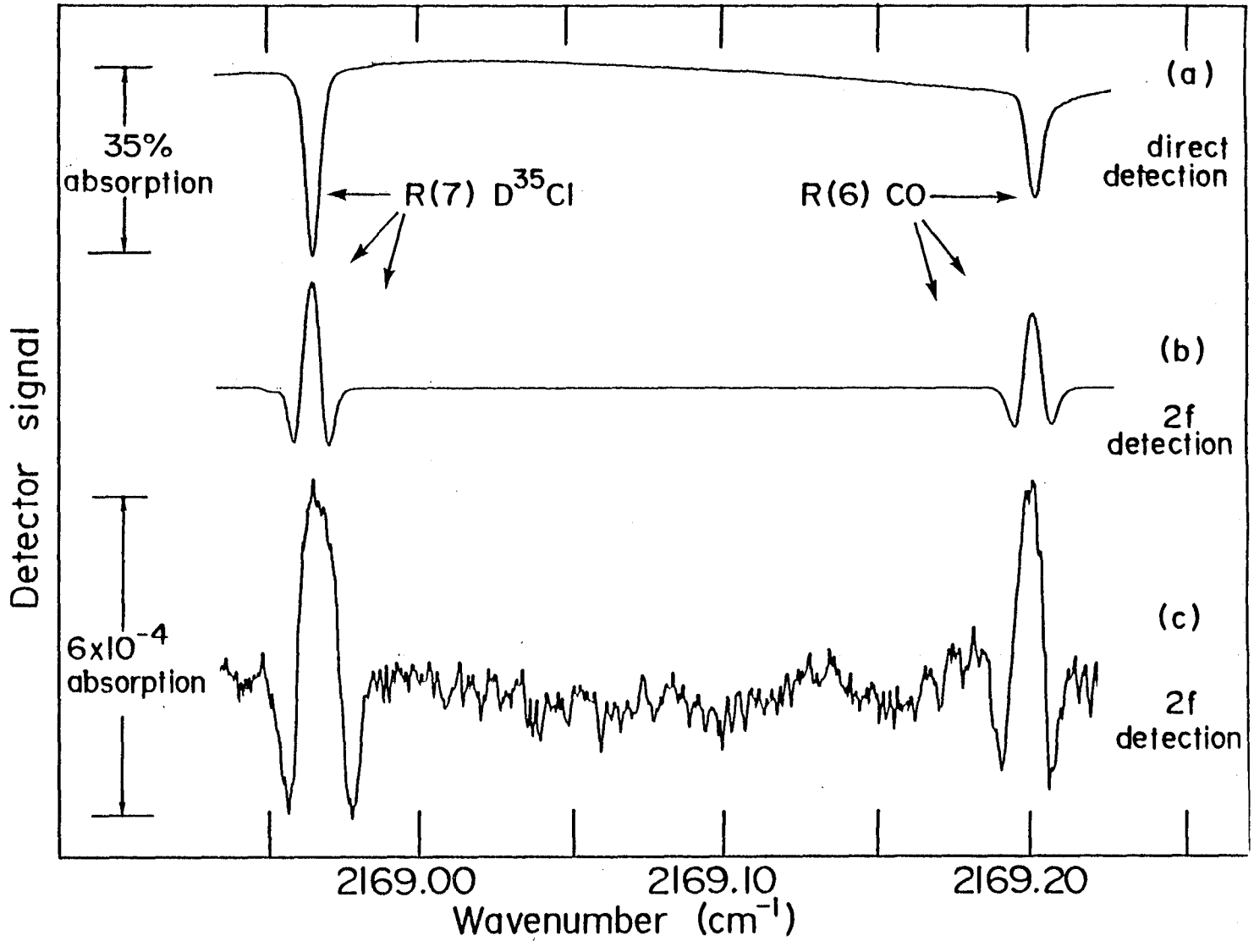
35%
absorption
R(7) D35Cl
R(6) CO
(a)
direct
detection
(b)
2f
detection
6x10-4
absorption
(c)
2f
detection
Detector signal
2169.00
2169.10
2169.20
Wavenumber (cm-1)

modulation amplitude is optimized to maximize the second harmonic signal. Under such conditions, the ratio of second harmonic signal (peak-to-peak) to direct signal is near unity,[22] and there is no loss in signal in switching to harmonic detection. There is, however, a very substantial reduction in noise,[78] and fractional absorptions of 2×10^{-5} can easily be detected using harmonic techniques. If one considers a single pass through the infrared cell, this corresponds to a minimum detectable absorption coefficient of 2×10^{-6} cm^{-1}, more than sufficient sensitivity for the present experiments.

A further advantage of the TDL technique is that the measurement of an infrared absorption coefficient gives an absolute calibration, provided linestrength and linewidth data are available. There is no need to prepare known samples to calibrate the instrument response. This point is illustrated by the experimental calibration plot shown in Fig. 4.6.[79] A series of $CO/CHCl_3$ mixtures were prepared on a grease-free vacuum system using a calibrated capacitance manometer to measure pressure. For mixtures containing less than 10 mTorr CO, successive dilutions were employed. It is estimated that mixtures could be prepared with a CO concentration known to better than 5 % . The TDL was used to scan over a line of CO as shown in the insert of Fig. 4.6. The area under the absorption line is directly proportional to the number of CO molecules in the path of the TDL beam. The proportionality constant is the linestrength, S_J, of the particular absorption line under investigation. Linestrengths have been measured for many of the simple molecules of interest to analytical chemists.[80] For CO, the most recent measurements of band and linestrengths[81] are listed in the AFGL

Fig. 4.6: Calibration plots for CO and $CO/CHCl_3$ mixtures. The measured absorption coefficients are shown to be linear with CO content for a dynamic range of ~4 orders of magnitude. The straight line through the pure CO data (line A), from the Doppler regime equation (2-3), yields a linestrength in agreement with the AFGL value, while line B is consistent with the intermediate pressure regime equation (2-5) (using the measured pressure broadening coefficient of 8.0×10^{-5} cm^{-1} $Torr^{-1}$). Both sets of data were measured on the R(8) transition of CO. The third set of data (line C) was measured on the R(6) transition and illustrates results with both direct and 2f detection. Very dilute mixtures of CO in $CHCl_3$ are measured with 2f detection, and are shown on expanded scales (x10 or x100) to demonstrate linearity. The insert defines the parameters used in the Beer-Lambert equation (2-1).

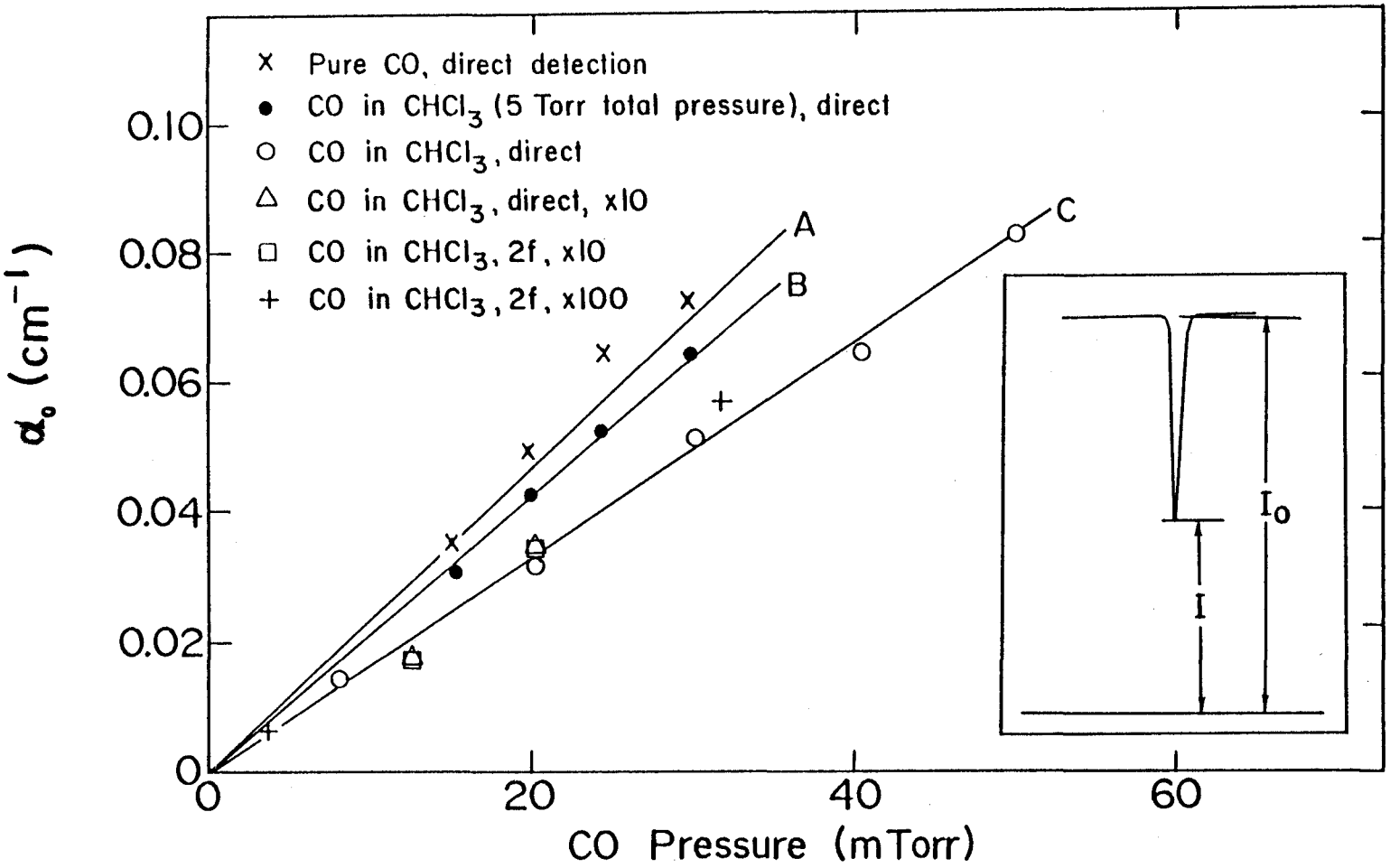
× Pure CO, direct detection
• CO in $CHCl_3$ (5 Torr total pressure), direct
○ CO in $CHCl_3$, direct
△ CO in $CHCl_3$, direct, x10
□ CO in $CHCl_3$, 2f, x10
+ CO in $CHCl_3$, 2f, x100
A
B
C
I_0
I
α_0 (cm^{-1})
0.10
0.08
0.06
0.04
0.02
0
0
20
40
60
CO Pressure (mTorr)

line parameters compilation.[82] Experimentally, it is much more convenient to measure the linecentre absorption, α_0, than the area of the absorption line. The procedure for relating α_0 to S_J and the number of absorbing molecules in the cell is described in the theory section (Chapter 2), and involves consideration of both Doppler and pressure broadening of the absorption line in the Voigt profile.

In Fig. 4.6 plots of α_0 for an isolated absorption line are shown as a function of pressure. The calibration lines A and B illustrate the transition from the low pressure Doppler regime to the intermediate pressure region where $\Delta\nu_L \sim \Delta\nu_D$. The measurements for line A are taken in pure CO and, using the equation of the Doppler regime, yield a linestrength of 9.7 ± 0.8 cm^{-2} atm^{-1} in agreement with the AFGL value of 10.43 cm^{-2} atm^{-1} for R(8). The pressure broadening coefficient for CO in $CHCl_3$ was measured to be $(8.0 \pm 0.5) \times 10^{-5}$ cm^{-1} Torr^{-1}, and using this value in the equation for the intermediate pressure regime gives good agreement with the data obtained for CO in 5 Torr $CHCl_3$ (line B). The third set of data in Fig. 4.6 illustrates that the linearity of calibration is maintained with both direct and second harmonic detection. Direct detection was employed whenever the linecentre absorption was > 5 %. Both direct and second harmonic detection were used for linecentre absorptions in the range 1 to 5 %, and the relative response of the two techniques was determined. (In Fig. 4.5, for example, the ratio of 2f signal (peak-to-peak) to direct detection is 0.85 and 1.00 for the DCl and CO lines, respectively. The slight difference in ratio arises from differences in linewidths and modulation amplitudes for the two lines). Once this relative response

is measured, second harmonic detection alone can be used to determine absorption coefficients when $\alpha_0 L$ lies in the range 10^{-1} to 10^{-5}. The data displayed in Fig. 4.6 demonstrate that once linestrength and linewidth are known, low pressure gas mixtures can be calibrated absolutely by simply measuring α_0. In view of the care taken in CO sample preparation for the measurements of bandstrengths,[81] it is thought that the measurements displayed in Fig. 4.6 serve more as a check on the mixture preparation than as a repeat calibration of CO linestrengths. However, it is worth pointing out that the combination of direct and 2f detection employed for Fig. 4.6 gives an absolute, linear calibration over 4 orders of magnitude of CO concentration ($\alpha_0 L$ ranges from 10^{-4} to 1). This dynamic range can easily be extended, if required, by varying L, for example by using multipass cells for low concentrations,[78] or a transverse geometry with a short pathlength for high concentrations.

The calibration procedures for DCl are very similar to those used for CO. The pressure broadening parameter on the R(7) DCl line was then measured for both $CHCl_3$ and $CDCl_3$. Results are shown in Fig. 4.7. The linewidths were measured by preparing cells containing $CDCl_3$ (or $CHCl_3$) with a trace of DCl to give a value for $\alpha_0 L$ in the range 0.2 to 0.5. Careful scans over the DCl line were taken with the TDL, and the tuning rate of the laser was calibrated using a 7.65 cm Ge etalon with a fringe spacing of 0.01627 cm^{-1} (see Fig. 4.4). The linewidth at half maximum (the width when $\alpha = \alpha_0/2$) was then measured from the X-Y recorder traces. As a check on the measurement technique, the Doppler width for DCl was determined in a low pressure sample. The measured

Fig. 4.7: Measured linewidths for the R(7) line of $D^{35}Cl$ buffered by $CHCl_3$ or $CDCl_3$. The solid line drawn through the data points is the calculated linewidth for $\gamma_m = 9.7 \times 10^{-5}$ cm^{-1} $Torr^{-1}$ (best fit value). The calculated linewidth is from Pade approximants of the Voigt profile as outlined by Minguzzi et al.[21]

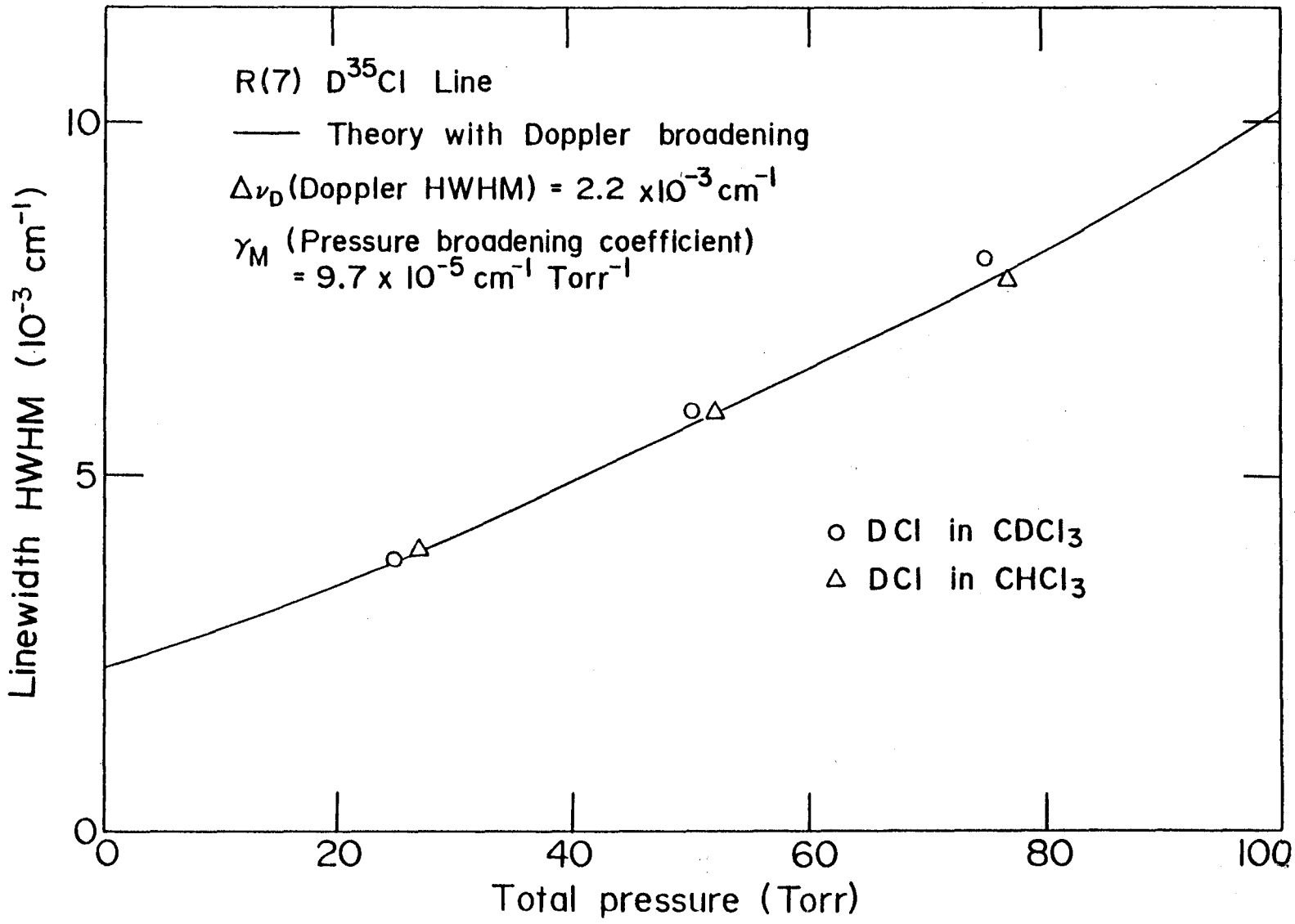
R(7) D35Cl Line
—— Theory with Doppler broadening
Δν_D (Doppler HWHM) = 2.2 x10^-3 cm^-1
γ_M (Pressure broadening coefficient)
= 9.7 x 10^-5 cm^-1 Torr^-1
o DCl in CDCl3
Δ DCl in CHCl3
Linewidth HWHM (10^-3 cm^-1)
Total pressure (Torr)
0
5
10
0
20
40
60
80
100

Doppler width was (2.2 ± 0.2) x 10^{-3} cm^{-1} compared with a calculated value of 2.18 x 10^{-3} cm^{-1}. This good agreement confirms that the TDL linewidth has a negligible effect on the measured linewidths.[83] From the data shown in Fig. 4.7, we estimate that the pressure broadening parameter for DCl collisions with chloroform is 9.7 x 10^{-5} cm^{-1} $Torr^{-1}$ ± 10 %. There appears to be no measurable difference between collisions with $CHCl_3$ and $CDCl_3$. Note that these measurements were made prior to the development of the computerized data collection and analysis methods that were used in the CO_2/NH_3/HTO measurements described in Chapter 3. However, the linewidth measurements shown in Fig. 4.7 are more than accurate enough to calibrate mixtures of DCl in chloroform. The accuracy of the calibration is limited by the accuracy of the available linestrength data. No attempt has been made to experimentally measure the bandstrength of the fundamental band of DCl. This type of measurement requires extreme care in preparing samples of a reactive gas such as DCl; the difficulties involved are described in detail in the excellent work of Pine et al.[18] For the bandstrength of DCl, it has been chosen to use the bandstrength of HCl as determined by Pine et al. and multiply it by the bandstrength ratio DCl/HCl (66.6/130) as measured by Benedict et al.[84] This experimental ratio agrees well with the theoretical value of 0.525.[85] Consequently, we use a value of 2.60 cm^{-2} atm^{-1} for the linestrength of the R(7) DCl line, and estimate that this value is accurate to better than 10 %.

4.3 Dissociation of $CDCl_3$ at Natural Abundance

An initial series of measurements was carried out to check on the linearity and reproducibility of the measurement system. A gas cell was filled with 2 Torr of pure $CDCl_3$ and irradiated with 0.4 J pulses of 10P(48) radiation (916.76 cm^{-1}) focussed by a 25 cm focal length BaF_2 lens. The cell was irradiated with 20 pulses, and then the DCl concentration was quickly measured. This process was repeated three times for a total of 60 pulses in several different experimental runs. Results confirm that the concentration of DCl increased linearly with the number of pulses. This is shown in the upper section of Fig. 4.8. This result is to be expected as the maximum DCl concentration is very low, and the entire measurement process is done quickly (~3 minutes) to prevent any significant loss of DCl to the cell walls. When the DCl concentration is larger, the linearity of DCl concentration with number of pulses can not be observed as there is significant DCl loss to the walls of the cell and the curve saturates as can be seen in the lower part of Fig. 4.8.

Further experiments were carried out to monitor the formation of DCl from the photolysis of natural abundance $CDCl_3$ in $CHCl_3$. These experiments required high sensitivity measurements of DCl at the ppm level. Initially, pyrex photolysis cells were used, but absorption and isotope exchange at the cell walls resulted in a steady decrease in DCl concentration in time after the initial irradiation in an unconditioned cell as can be seen in the upper section of Fig. 4.9. CO concentrations were constant. However in a cell that had been previously used (conditioned) and then evacuated there was a steady increase in DCl and CO concentrations with time as can be seen in the lower section of

Fig. 4.8: Formation of DCl as a function of the number of CO_2 irradiation pulses. Each pulse irradiates approximately 1 % of the total cell volume. Linearity in the upper section occurs with a small number of laser pulses, saturation in the lower section is due to DCl exchange reactions with the cell walls (with a larger number of laser pulses).

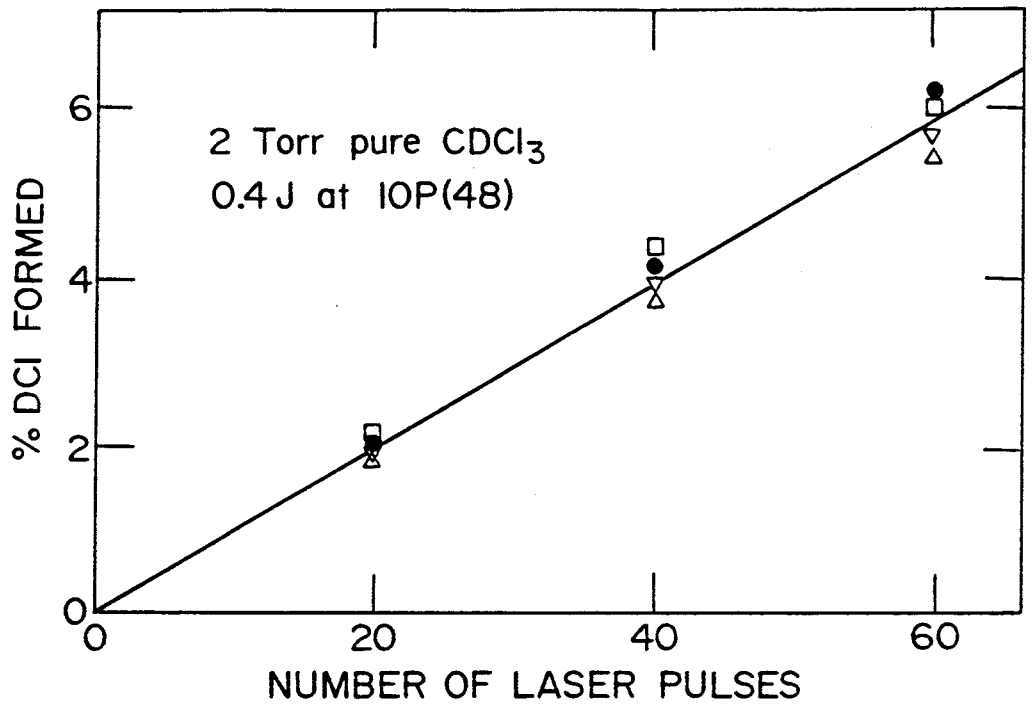
2 Torr pure $CDCl_3$
0.4 J at 10P(48)
% DCI FORMED
0
2
4
6
0
20
40
60
NUMBER OF LASER PULSES

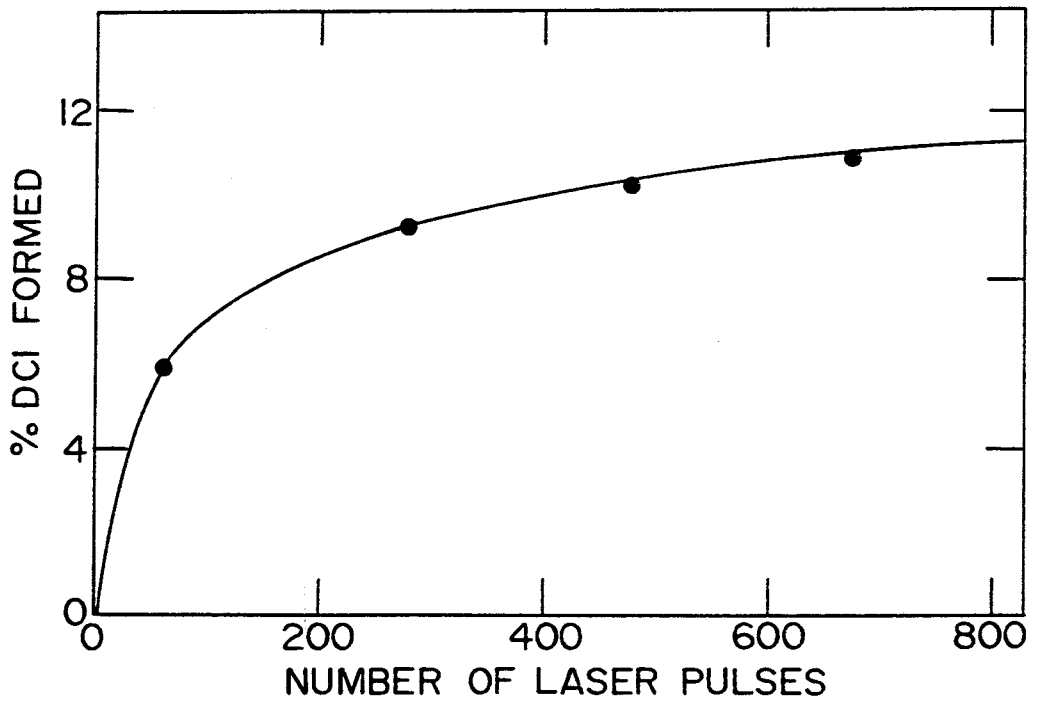
% DCI FORMED
0
4
8
12
0
200
400
600
800
NUMBER OF LASER PULSES

Fig. 4.9: Effect of wall reactions on gas concentrations in a pyrex cell. DCl and CO concentrations are measured as a function of time after (A): irradiation of 5 Torr $CDCl_3$ in a "clean" glass cell and (B): filling of a previously "conditioned" glass cell with 5 Torr of pure $CHCl_3$. A Monel cell is used to reduce the effect of these adverse wall reactions.

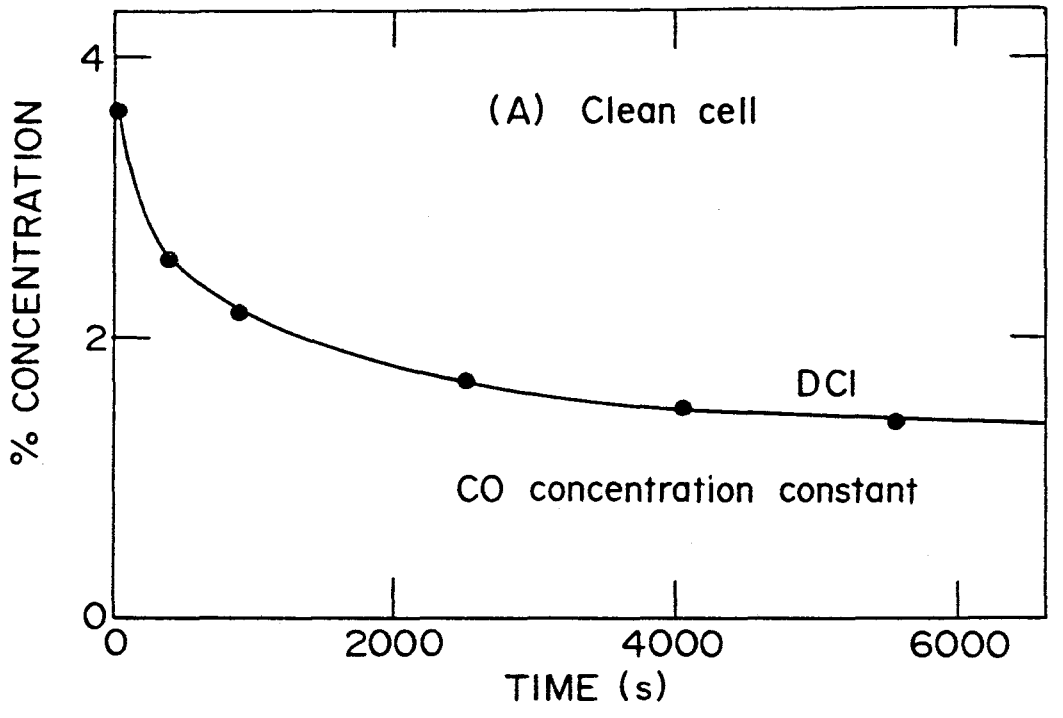
(A) Clean cell
DCl
CO concentration constant
% CONCENTRATION
TIME (s)
0
2
4
0
2000
4000
6000

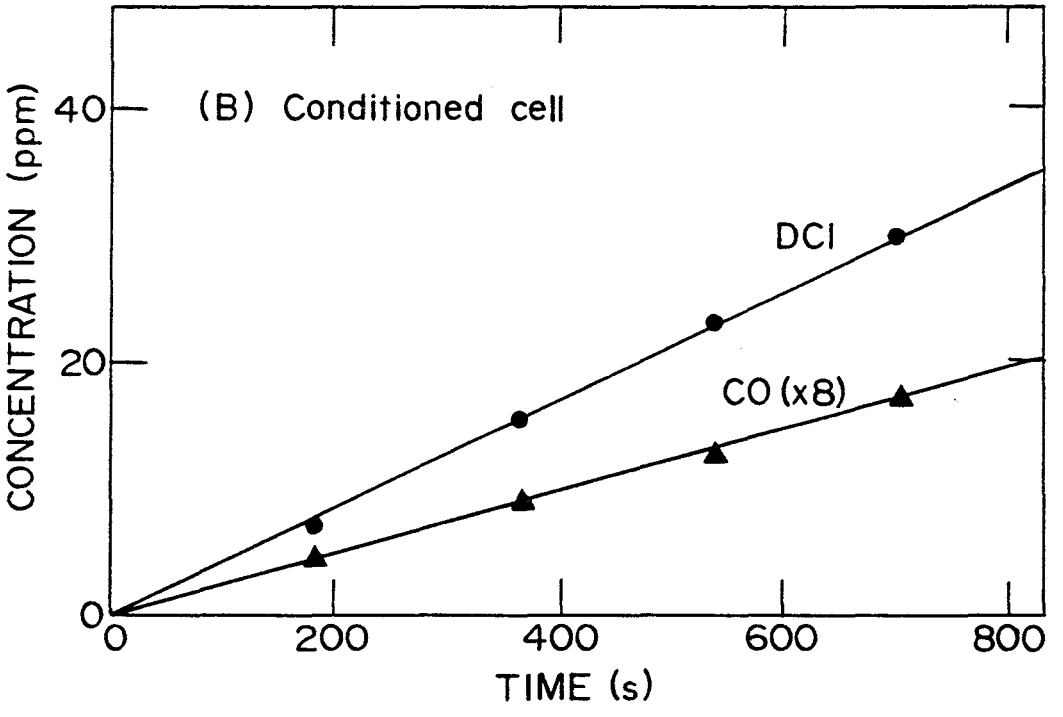
(B) Conditioned cell
DCl
CO (x8)
CONCENTRATION (ppm)
TIME (s)
0
20
40
0
200
400
600
800

Fig. 4.9. To eliminate these adverse effects a monel cell was used in which DCl and CO concentrations were stable at ppm levels.

Figure 4.10 shows successive second harmonic scans which monitor DCl and CO concentrations before and after irradiation with 10P(38) and 10P(48) CO_2 laser transitions. The irradiated volume was only 1 % of the total cell volume. Note the appearance of DCl after irradiation with 10P(48); the measured DCl concentration corresponds to 2.5 % of the $CDCl_3$ originally present in natural abundance in the cell. It is extremely significant that DCl only appears after irradiation with 10P(48). In a separate series of measurements on pure $CDCl_3$, it was determined that under identical conditions 10P(48) irradiation is ten times more effective at producing DCl than 10P(38) irradiation.[79] Thus the appearance of DCl in the upper scan of Fig. 4.10 can be attributed to the IRMPD of the $CDCl_3$ in the cell, and not to thermal or shock induced effects. The increase in CO concentration is probably caused by a reaction between photolytically produced $:CCl_2$ and the cell walls. (In this case, much of the CO derives from the photolysis of $CHCl_3$ which is the dominant species in the cell.)

4.4 Summary

Described here is the first reported measurement of DCl formation from the photolysis of natural abundance $CDCl_3$ in $CHCl_3$. This measurement could not have been made without the high sensitivity of the tunable diode laser technique. TDLs allow one to make accurate absolute measurements of trace gas concentrations immediately after photolysis, the technique is very rapid and does not require the removal of a sample

Fig. 4.10: Successive 2f scans taken of a sample of natural abundance chloroform after irradiation with 100 pulses of 10P(38) and 10P(48) radiation (0.4 J/pulse). The increase in DCl concentration after irradiation with 10P(48) is attributed to IRMPD of naturally occurring $CDCl_3$ in the sample. Gas pressure in the cell is 5 Torr. The noise level is equivalent to ~0.8 ppm DCl, or a fractional absorption of 2×10^{-5} in the 10 cm cell.

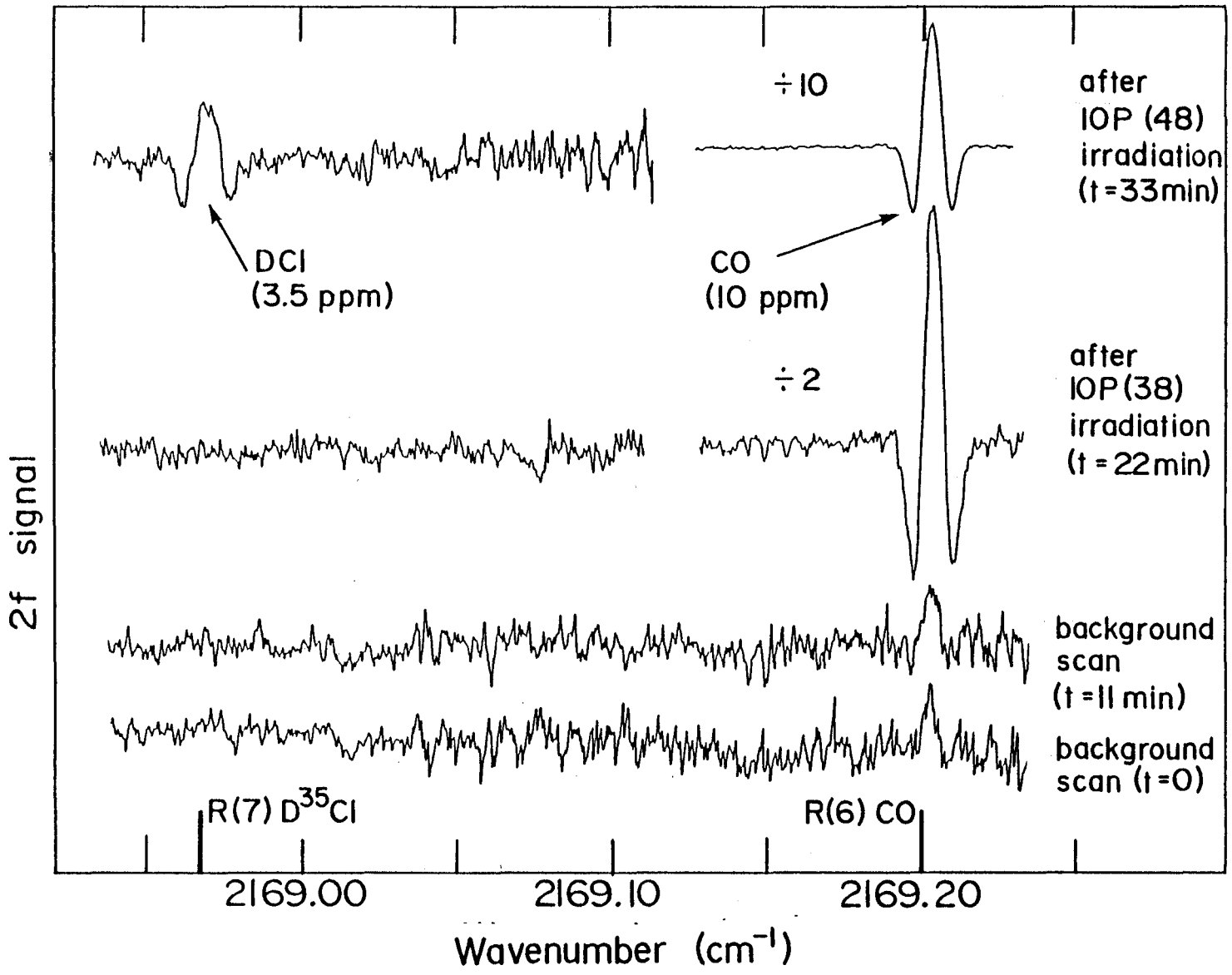
÷10
after
10P (48)
irradiation
(t=33min)
DCl
(3.5 ppm)
CO
(10 ppm)
÷2
after
10P(38)
irradiation
(t = 22min)
background
scan
(t=11 min)
background
scan (t=0)
R(7) D35Cl
R(6) CO
2f signal
2169.00
2169.10
2169.20
Wavenumber (cm-1)

of gas from the photolysis cell.

It is instructive to compare the present TDL results with other techniques for measuring DCl. (DCl is a favorable case for TDL detection, nevertheless, it is a molecule of primary importance in proposed tritium from deuterium separation schemes.[12]) Fourier transform infrared spectroscopy (FTIR) has many similarities to the TDL technique. However, even the best commercially available FTIR instruments require 16 minutes to complete a measurement with 0.004 cm^{-1} resolution. For a low pressure DCl gas sample, the minimum detectable absorption is ~0.1 %[86] - two orders of magnitude worse than with a TDL. Another technique that does not compare favorably with the TDL for DCl detection is gas chromatography.[87] In addition to monitoring DCl with the TDL, infrared multiphoton dissociation of COF_2 (which is difficult due to the low density of vibrational states[88]) produces CO that has been detected with high sensitivity.[89]

Clearly, the use of a tunable diode laser provides an analytical chemist with a powerful technique for investigating gas phase reactions. It is thought that TDLs will become much more widely used in this type of application, and that TDL measurements will prove invaluable in determining the mechanisms of photochemical reactions. The majority of the work reported in this chapter is described in a publication by Beckwith, Orlando, Reid, and Smith (Accepted for publication in J. Photochem.).[13] In particular, acknowledgements are due to J. J. Orlando for his collaboration in obtaining the data shown in Figs. 4.4 and 4.10, and for obtaining the data shown in Fig. 4.6.

CHAPTER 5

TRANSIENT DETECTION OF CF_2 RADICALS

5.1 Introduction

Over the past decade, the use of lead-salt tunable diode lasers for high resolution infrared spectroscopy has become routine. TDLs are used extensively for high sensitivity spectroscopy, particularly in applications such as atmospheric monitoring,[2,3] detection of rare isotopes,[90] and the measurement of very weak infrared transitions.[91] The combination of high sensitivity and high resolution has led to TDLs finding increasing application in the detection of unstable species such as radicals[92] and molecular ions.[93] In the applications described above, the TDL monitors a constant concentration of the species of interest and integration time constants of ~1 s are commonly used. Source modulation and harmonic detection are often employed to increase sensitivity, but laser noise and the presence of optical fringes limit the minimum detectable absorptance to $> 10^{-5}$ in these cw experiments.[78] (For special cases, where the absorption itself can be modulated, detection levels of $\sim 10^{-6}$ have been reported[94,95]).

In recent years, TDLs have also been widely used to detect transient infrared absorptions. In particular, TDLs are used to probe the transient absorption created in a gas after the passage of an excimer laser pulse. The ultraviolet pulse produces radicals such as SO,[96] CCO[97] or CH_3,[98] and these radicals are monitored by tuning the TDL probe to a characteristic absorption line. Other types of transient

experiments with TDLs involve probing gases which have been perturbed by Q-switched CO_2 lasers,[99,100] Nd:YAG lasers,[101] and excimer lasers.[102] Generally, the detection system has a response time ranging from 1 μs to 1 ms, and the minimum detectable transient absorbance appears to have been limited to > 10^{-3} for TDL systems.[103]

In this section a novel technique for monitoring transient infrared absorption with TDLs is described. The technique is essentially a high frequency version of the sweep integration technique pioneered by Jennings[104] and modified by Cassidy and Reid.[105] The TDL is wavelength modulated on the absorption line of interest at modulation frequencies up to ~250 kHz. Response time can be as short as ≈2 μs, and sensitivity is presently limited solely by detector noise at the 10^{-5} level of absorbance. The technique provides excellent discrimination between true absorption and spurious effects such as probe-beam deflection. These spurious effects caused by thermal lensing and shock wave phenomena, are often a major problem in detection schemes that do not involve modulation.

The modulation technique is illustrated by describing the detection of CF_2 radicals formed by the infrared multiphoton dissociation (IRMPD) of C_3F_6 and C_2F_3Cl (in collaboration with C. E. Brown).[16] In a second series of experiments using a Q-switched CO_2 laser the modulation technique is compared with a more conventional detection technique in which the TDL is simply tuned to an absorption linecentre. Very similar results are obtained in terms of sensitivity and response time. It is shown that more laser power or a better detector allow the sensitivity limit to be lowered to 10^{-6}.

It is worth noting that it is very easy to achieve detector noise-limited performance in transient detection with TDLs. This is not the case in cw detection systems where detector noise is often negligible in comparison with beam noise or optical fringing.[78] Using the same laser, detector and optics, it is easier to detect a transient absorption of 10^{-4} than it is to detect the same absorption on a cw basis. More CF_2 absorption is generated with a single TEA CO_2 laser pulse than with an optimized multi-pass cw microwave discharge cell. Pulsed rather than cw experiments may be much more suitable for the spectroscopy of transient species such as radicals and molecular ions.

In the next section the experimental apparatus and the detection of CF_2 radicals is described. Section 5.3 deals in detail with the modulation technique and the sensitivity obtainable. In section 5.4 the conventional technique of tuning the laser diode to linecentre and monitoring the absorption as a function of time is examined. A summary is presented in the final section.

5.2 Detection of CF_2 Radicals

5.2.1 Apparatus

Figure 5.1 is a schematic diagram of the apparatus. The beam from a thyratron pulsed TEA CO_2 laser (Lumonics model 801A) is combined on a ZnSe beamsplitter with a collimated TDL probe beam, and both beams are focussed with a BaF_2 lens into a capillary waveguide cell. The cell consists of a 1 mm bore capillary tube 15.5 cm long enclosed in a pyrex tube 25 cm long. After passing through the cell, the two laser beams are separated with a grating and focussed onto separate detectors.

Fig. 5.1: Schematic diagram of the apparatus for detection of CF_2 transients. Lens L_1 collimates the output beam of the TDL, lens L_2 compensates for the divergence of the CO_2 beam, and lens L_3 focuses both beams into the capillary waveguide cell. Mirror M_1 transmits ~70 % of the TDL radiation and reflects ~80 % of the TEA CO_2 pulse. Cells C_1 and C_2 contain either ethylene or cyclopropane, and prevent any scattered radiation from reaching the TDL or the sensitive HgCdTe detector.

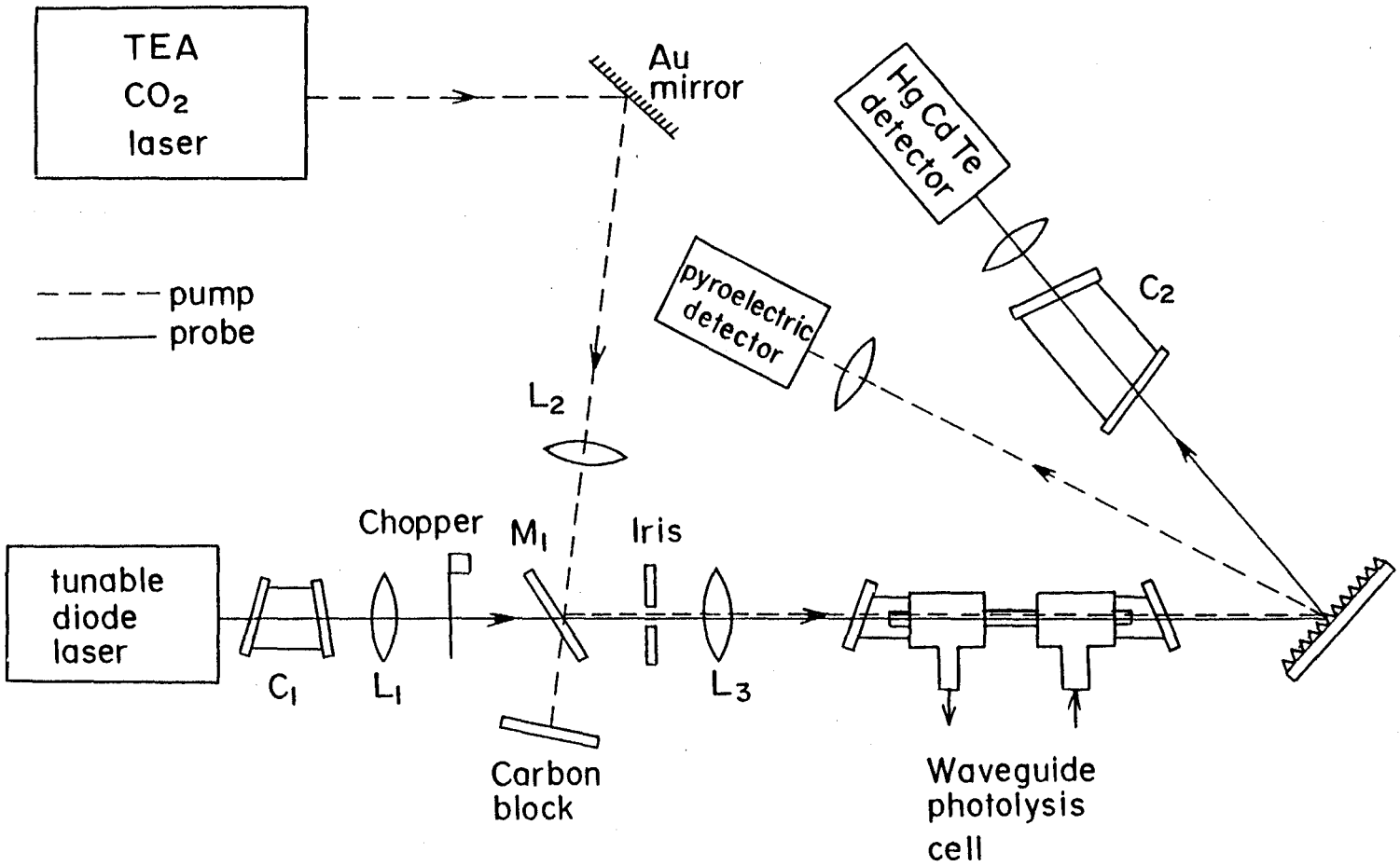
TEA
CO_2
laser
Au
mirror
Hg Cd Te
detector
pyroelectric
detector
C_2
pump
probe
L_2
Chopper
M_1
Iris
tunable
diode
laser
C_1
L_1
L_3
Carbon
block
Waveguide
photolysis
cell

Either hexafluoropropene (C_3F_6) or chlorotrifluoroethene (CF_2=CFCl) flow slowly through the waveguide photolysis cell at pressures ranging from 0.5 to 2 Torr. Infrared multiphoton dissociation of C_3F_6 is carried out using the 9P(36) transition of the CO_2 laser,[106] while the 9P(14) transition is used for the C_2F_3Cl.[107] Pulse energies of ~300 mJ at ~5 Hz repetition rate are obtained from the CO_2 laser, allowing fluences as high as 30 J/cm^2 inside the capillary tube of the photolysis cell.

The initial intention was to tune the TDL to the centre of a strong CF_2 absorption line, and look for absorption of the TDL beam immediately after passage of the CO_2 pulse. However it was first necessary to carry out preliminary spectroscopic measurements on CF_2 as described below.

5.2.2 cw Spectroscopy of CF_2

Experiments were performed with a conventional microwave discharge to characterize the CF_2 absorption spectra in a region of good single mode operation of the TDL probe. More specifically, the $^RQ_3$ branch of the ν_1 band of CF_2 ($\tilde{X}^1A_1$) at 1243 cm^{-1} was chosen. N_2O and CH_4 reference lines were used as frequency standards, while a reference cell containing CF_2O provided numerous lines which allowed the exact determination of CF_2 line positions in the later pulsed work. Refer to Fig. 5.2 for these microwave spectra and the results of Davies *et al.*[108] Note that in the discharge cell ~10 % absorption was observed on the strongest CF_2 lines. The optimum gas conditions differ significantly from those of Davies *et al.*[108] who used much more buffer gas than parent

Fig. 5.2: TDL spectrum of CF_2 in the 1243 cm^{-1} region. The upper section shows the absorption lines created in a microwave discharge by Davies *et al.*[108], and in the present work. The lower trace shows an expanded section of the spectrum. The optimum gas mixture in the 2450 MHz microwave discharge was C_2F_3Cl/Ar in a 4:1 ratio at 280 mTorr, and the strongest CF_2 absorption lines observed in the present work had linecentre absorptions of ~10 % (4 passes, 2.4 m total pathlength).

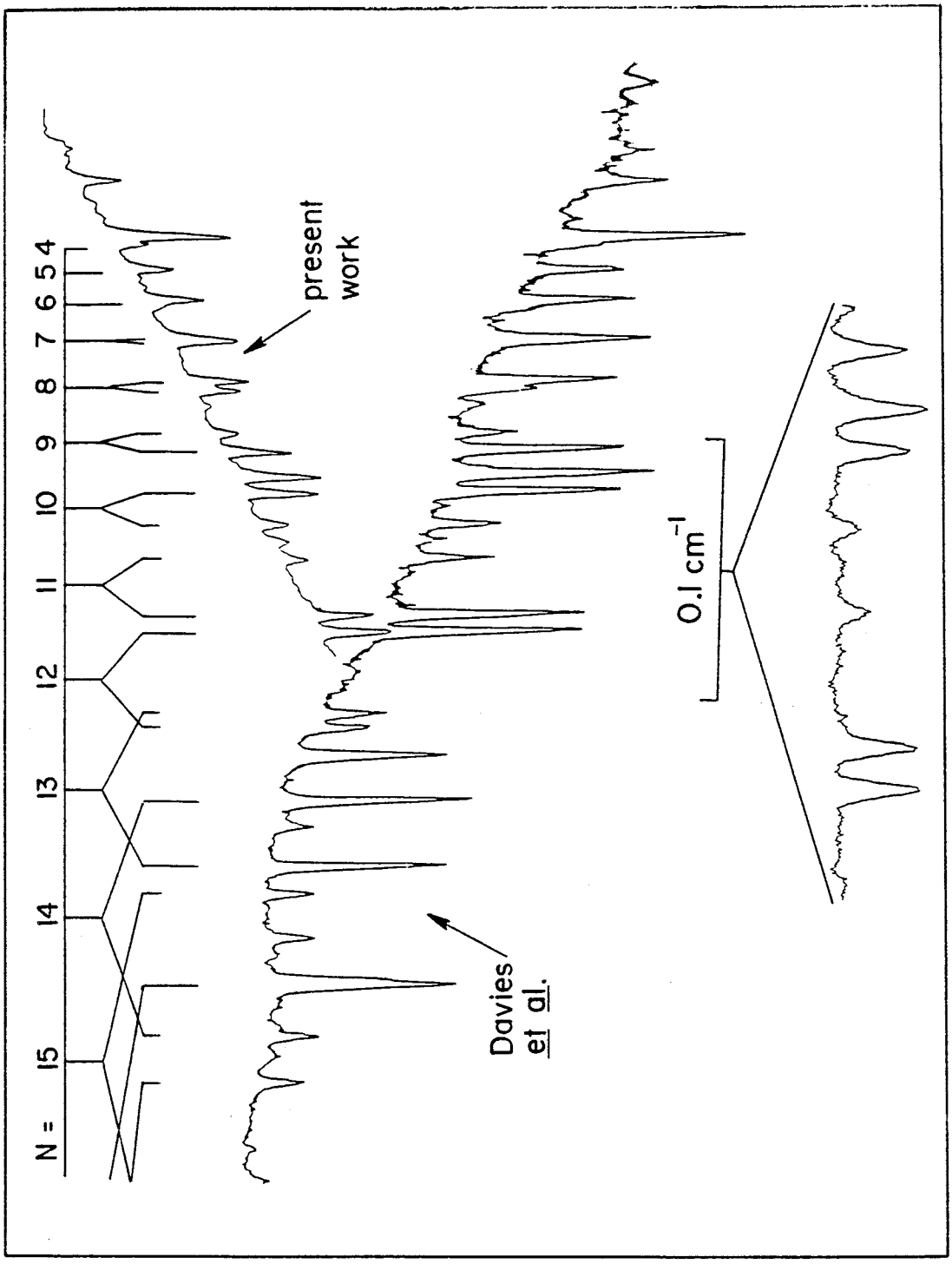
N = 15 14 13 12 11 10 9 8 7 6 5 4
present work
Davies et al.
0.1 cm⁻¹

at lower pressures. This difference is thought to be due to different flow rates and cell geometry.

5.2.3 Transient Spectoscopy of CF_2

In initial attempts to detect CF_2 a conventional photolysis cell (2.5 cm diameter) was used, and the TDL was tuned to the centre of a strong CF_2 absorption line. However, passage of the intense TEA CO_2 laser pulse through the gas in the cell caused thermal shocks, and deflection of the TDL probe beam away from the detector. It was impossible to distinguish between beam deflections and true absorption. Switching to a capillary waveguide cell allowed for better confinement of the probe beam, and also ensured that the pump beam had a high fluence over a long interaction length. However, the main improvement in technique was to take advantage of the tunability of the TDL, and to modulate the probe wavelength at high frequency. Figure 5.3 illustrates the transient detection technique. Current-modulation of the TDL leads to both amplitude and wavelength modulation of the laser beam. At present, the technique is limited to modulation frequencies < 250 kHz,[109] and the AM component is typically < 10 % of the total laser signal. It can be seen in Fig. 5.3 that the absorptions are superimposed on the amplitude modulation signal. Wavelength scanning leads to sampling the CF_2 doublet twice per cycle, in opposite directions. For example, at a 100 kHz modulation frequency the doublet is sampled every 5 μs. The magnitude of the doublet absorption is proportional to the concentration of CF_2 in the photolysis cell.

It is a simple matter to record both the signal and the AM

Fig. 5.3: Schematic illustration of transient detection of CF_2 using a wavelength modulated TDL. The TDL scans past the CF_2 doublet twice every cycle, and the detector output consists of an AM sine wave plus the absorption doublet.

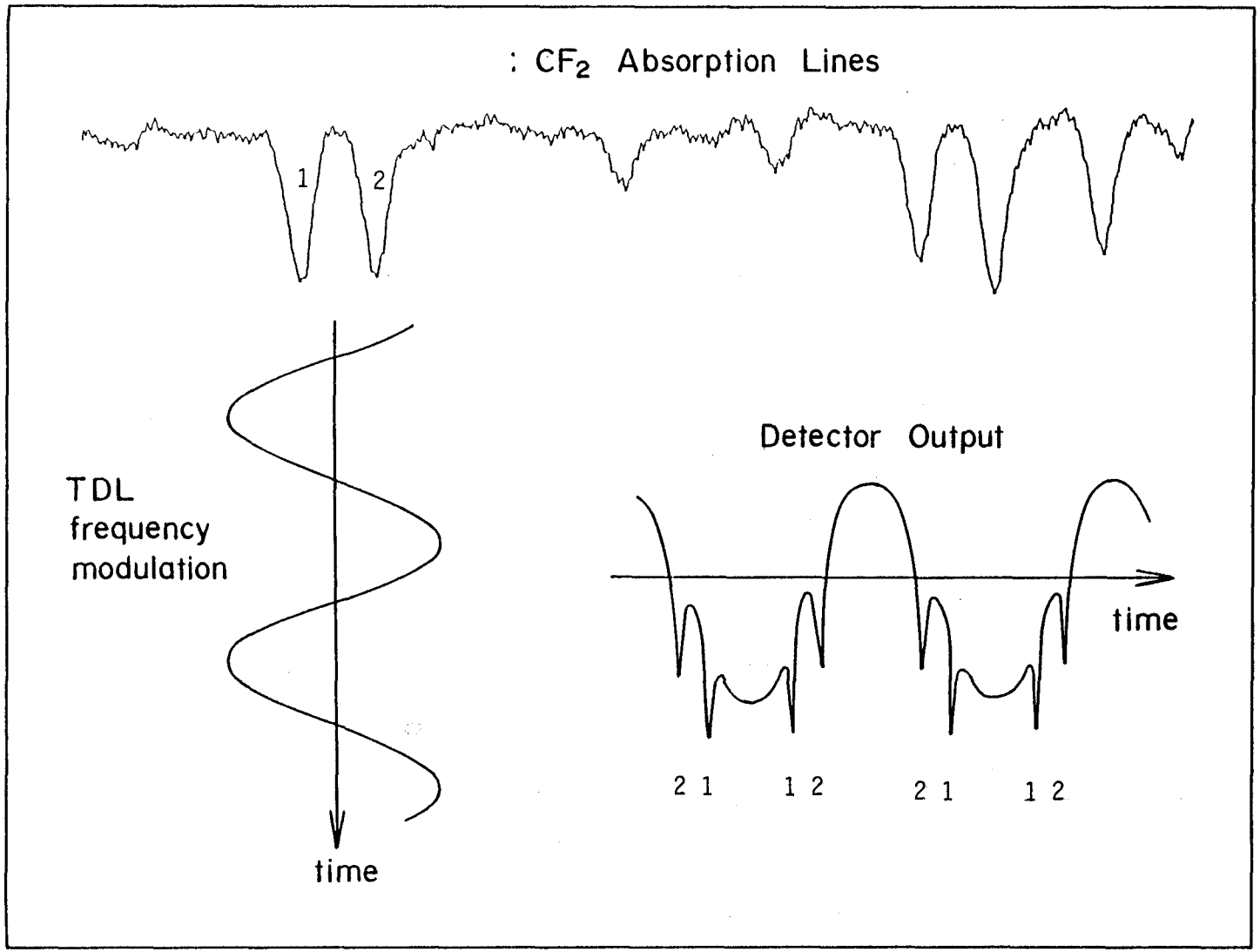
: CF_2 Absorption Lines
1
2
TDL
frequency
modulation
time
Detector Output
time
2 1
1 2
2 1
1 2

background with a digital oscilloscope, and to subtract the background. Figure 5.4 illustrates this at a 2.5 kHz modulation frequency for a CF_2 doublet with a spacing of 0.007 cm^{-1}. Notice that the doublet is clearly resolved and provides an unambiguous identification of the presence of CF_2. Any beam deflection simply causes a minor reduction in the amplitude of the signals due to part of the beam missing the detector. In Fig. 5.4 the CF_2 concentration is constant over the timescale of 2 ms. However, varying the timescale of the sampling allows one to observe the formation of CF_2 after the CO_2 laser pulse and its subsequent decay. Figure 5.5 illustrates how one can monitor the increase of CF_2 concentration on a fast timescale using high frequency modulation, and then observe the much slower fall in concentration using low frequency modulation. (The decay time of ~15 ms is the time it takes for gas to flow through the capillary tube in the photolysis cell.)

Figures 5.4 and 5.5 clearly demonstrate the usefulness of the present detection technique. Weak, transient infrared absorptions can be unambiguously identified on a fast timescale. However, in attempts to measure the ultimate sensitivity of the technique the limitation is detector noise. Therefore, a more powerful TDL was used in a simpler apparatus with better throughput of the TDL beam. An N_2O cell gave an easily controlled infrared absorption line. Results of sensitivity measurements using this apparatus are described in the next section.

5.3 Sensitivity of the Modulation Technique

These measurements were made with a TDL which operated in a

Fig. 5.4: Experimental results on detection of CF_2. The CF_2 doublet (absorptions at 1242.9453 cm^{-1} and 1242.9523 cm^{-1}) observed in the middle trace is produced by irradiating 0.5 Torr of C_2F_3Cl in the capillary waveguide cell with a 9P(14) CO_2 pulse of fluence 10 J/cm^2. Trace B is recorded with no gas in the cell, and both traces are averages performed by a digital storage oscilloscope of 32 successive scans.

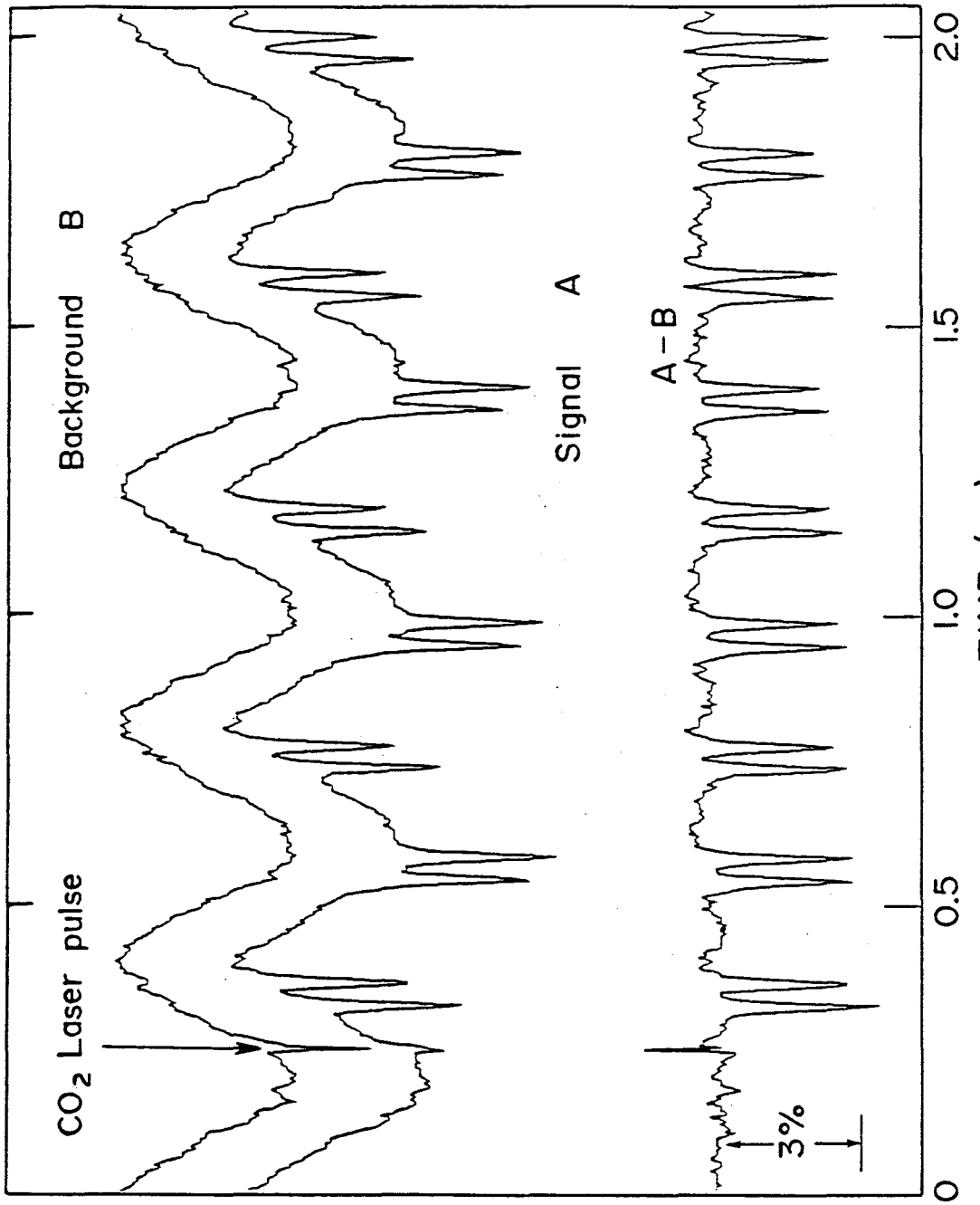
CO_2 Laser pulse
Background B
Signal A
A-B
3%
0
0.5
1.0
1.5
2.0
TIME (ms)

Fig. 5.5: Concentration of CF_2 monitored as a function of time. The upper trace, an average of 256 scans, illustrates the growth of CF_2 following CO_2 irradiation of 1.5 Torr C_2F_3Cl. The lower section shows the CF_2 decay, each trace is an average of 50 scans. Trace B was obtained with gas in the cell and the CO_2 beam blocked to allow subtraction of the steady-state C_2F_3Cl absorptions and enhancement of the transient CF_2 absorptions. TDL modulation frequencies in the upper and lower sections were 14 kHz and 470 Hz respectively.

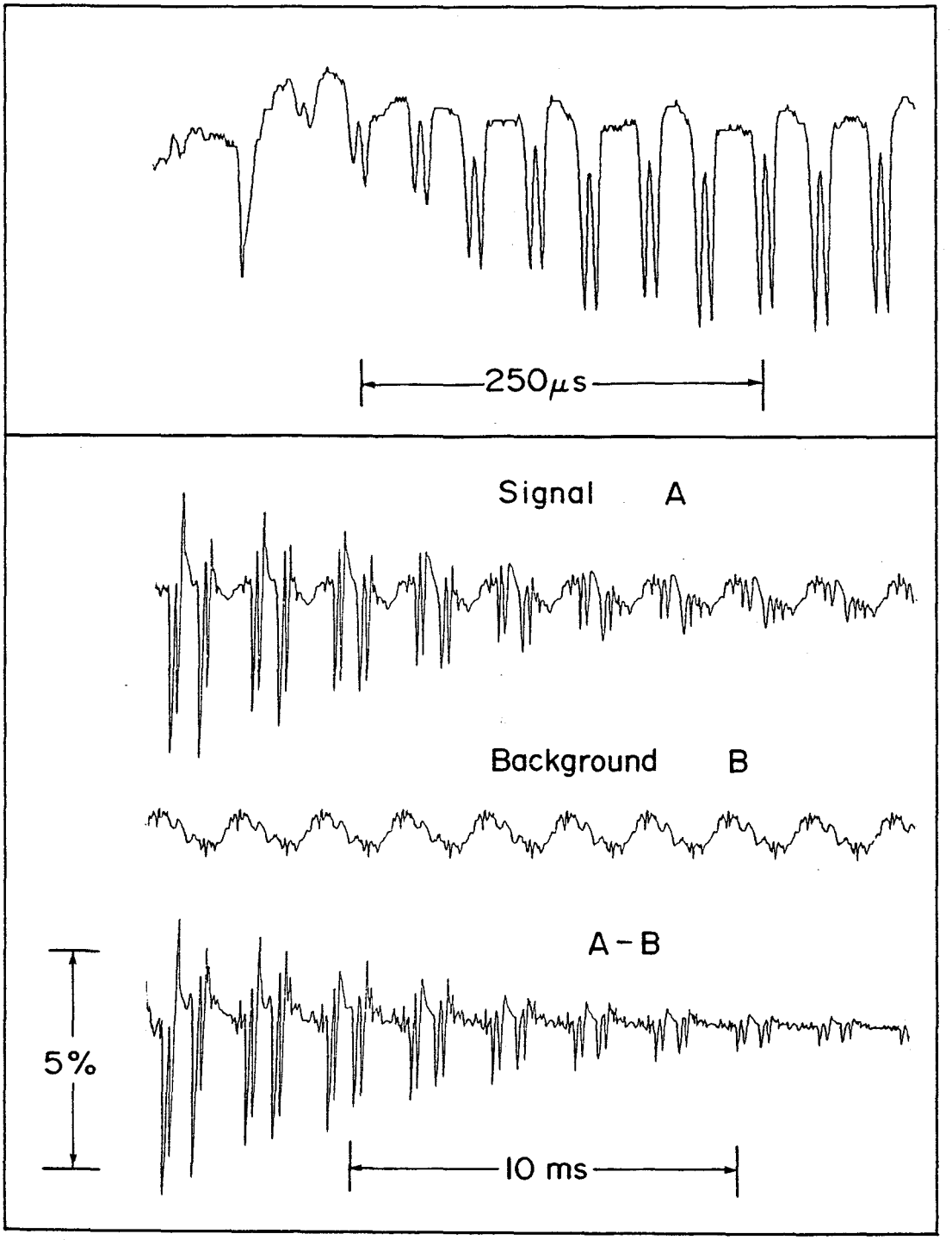
250μs
Signal A
Background B
A-B
5%
10 ms

single mode near 1260 cm^{-1}, and gave an output power of ~0.5 mW. The laser beam was focussed onto a HgCdTe detector, and a 10 cm long N_2O cell was placed in the beam. This cell had a cold finger attached, which allowed the N_2O pressure, and hence the infrared absorption, to be easily adjusted. One further modification was made to the apparatus - the detector output was combined at a differential amplifier with a sine wave derived from the modulation frequency signal. The sine wave was adjusted in amplitude and phase to cancel out the AM background component of the detector signal. By using this analog subtraction technique, the background AM signal was reduced from ~5 % to $< 10^{-3}$ equivalent absorption. This procedure allows the full dynamic range of the digital oscilloscope (8 bits) to be utilised in detecting small absorption lines.[105]

Results obtained using the analog subtraction technique are shown in Fig. 5.6. The TDL was modulated over one or two closely spaced N_2O lines. Note that the absorption lines appear on a relatively flat background as the analog subtraction has removed almost all the AM sine wave. The final traces in Fig. 5.6 were recorded with most of the N_2O frozen out of the cell, and demonstrate that the minimum detectable absorbance is $\sim 3 \times 10^{-5}$. Identical noise levels were obtained with the laser beam blocked, i.e., sensitivity was limited by detector noise. By optimizing the laser power falling on the detector (~0.5 mW), and using a better detector (higher D^*) the noise level was reduced to $\sim 10^{-5}$ absorbance. These measurements were very easy to perform - there were no problems with laser noise or optical fringes which tend to plague cw TDL experiments.

Fig. 5.6: TDL scans taken with the AM background reduced by analog subtraction. Modulation frequency is 2.5 kHz, and the modulation amplitude and DC current can be adjusted to sweep over one or both of the N_2O lines recorded in direct detection in the upper trace. For the lower trace, most of the N_2O is frozen out of the cell, and the remaining linecentre absorption is only 0.03 %. Each trace is the average of 256 scans.

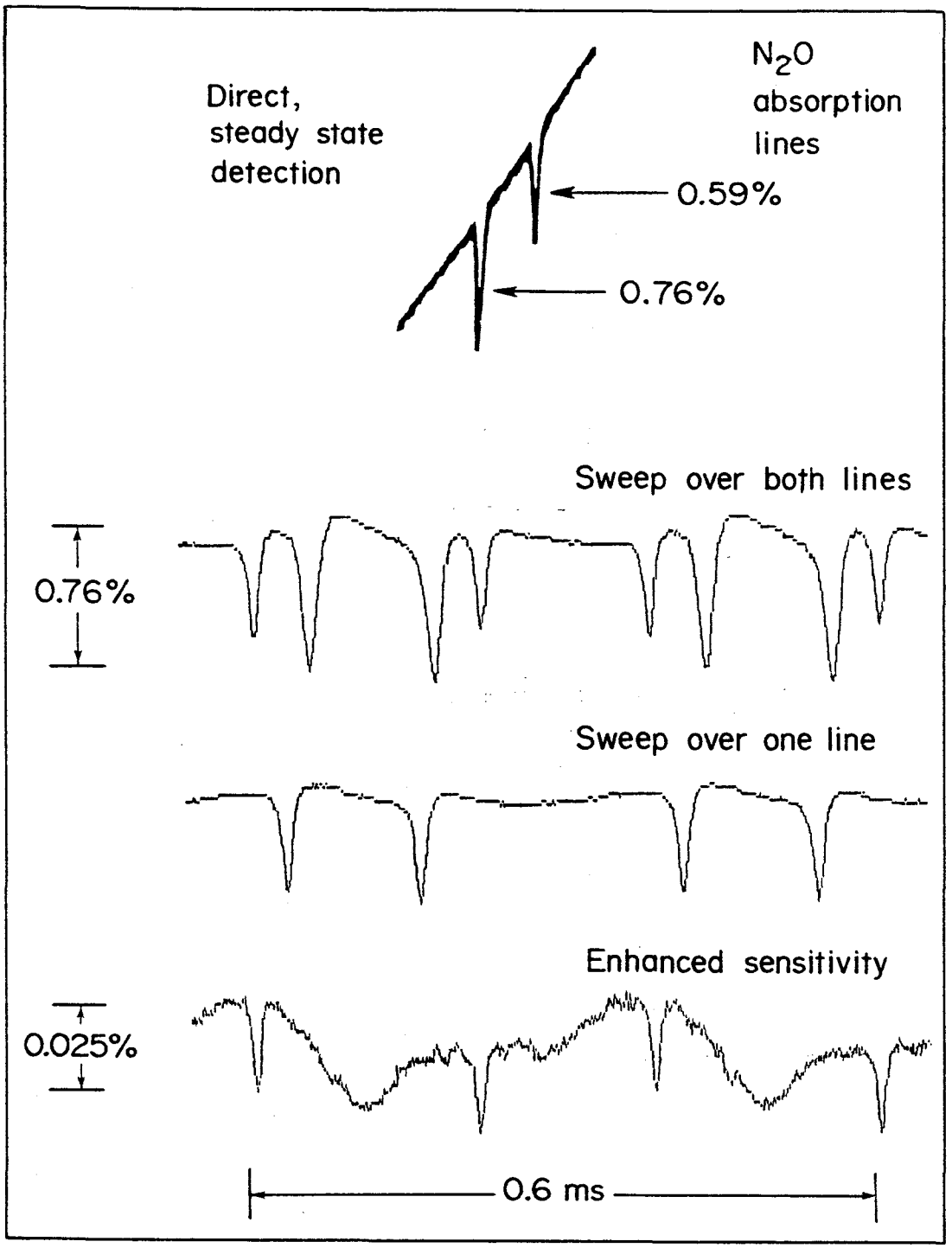
Direct,
steady state
detection
N_2O
absorption
lines
0.59%
0.76%
Sweep over both lines
0.76%
Sweep over one line
Enhanced sensitivity
0.025%
0.6 ms

The results given in Fig. 5.6 were obtained at the relatively slow modulation frequency of 2.5 kHz, corresponding to sweeping past an absorption line every 0.2 ms. Many experiments on transient absorption require a much higher sampling rate. At present, the maximum modulation frequency is limited by a combination of detector speed and the TDL power supply.[109] Modulation at frequencies at high as 250 kHz has been successful, and the work of Gehrtz et al.[110] indicate that TDLs can be wavelength modulated at frequencies > 100 MHz.

Figure 5.7 shows results obtained with a modulation frequency of 100 kHz. In this case, the noise level corresponds to an absorbance of $\sim 4 \times 10^{-5}$, and is once again entirely caused by detector noise. Thus, it appears that the high frequency modulation technique allows detector-limited detection of transient absorptions at all modulation frequencies from 1 to 100 kHz(at 250 kHz, the modulation is only over part of the line). In the next section, the performance is compared with that obtained by a more conventional TDL technique.

5.4 Direct Detection of Transient Absorption

As mentioned in Section 5.1, the more conventional method of detecting a transient absorption is to fix the TDL wavelength at linecentre of an absorption line, and directly monitor changes in transmission. Experiments of this type have been performed by using a Q-switched CO_2 laser to induce absorption changes in NH_3 gas. The apparatus is described in detail elsewhere,[70] however the spectroscopy involved is illustrated in Fig. 5.8. A Q-switched CO_2 laser operating on the 9R(30) transition transfers population from the ground state to the $\nu_2 = 1$ level of NH_3. The rotational populations in the two

Fig. 5.7: Results obtained with a modulation frequency of 100 kHz. The N_2O is frozen out of the cell after the first trace. Note the substantial reduction in the AM background after analog subtraction is employed. A further reduction in background is obtained by digitally subtracting successive traces, i.e., by subtracting the background from signal-plus-background. Residual noise is detector noise. Each trace is the average of 256 scans.

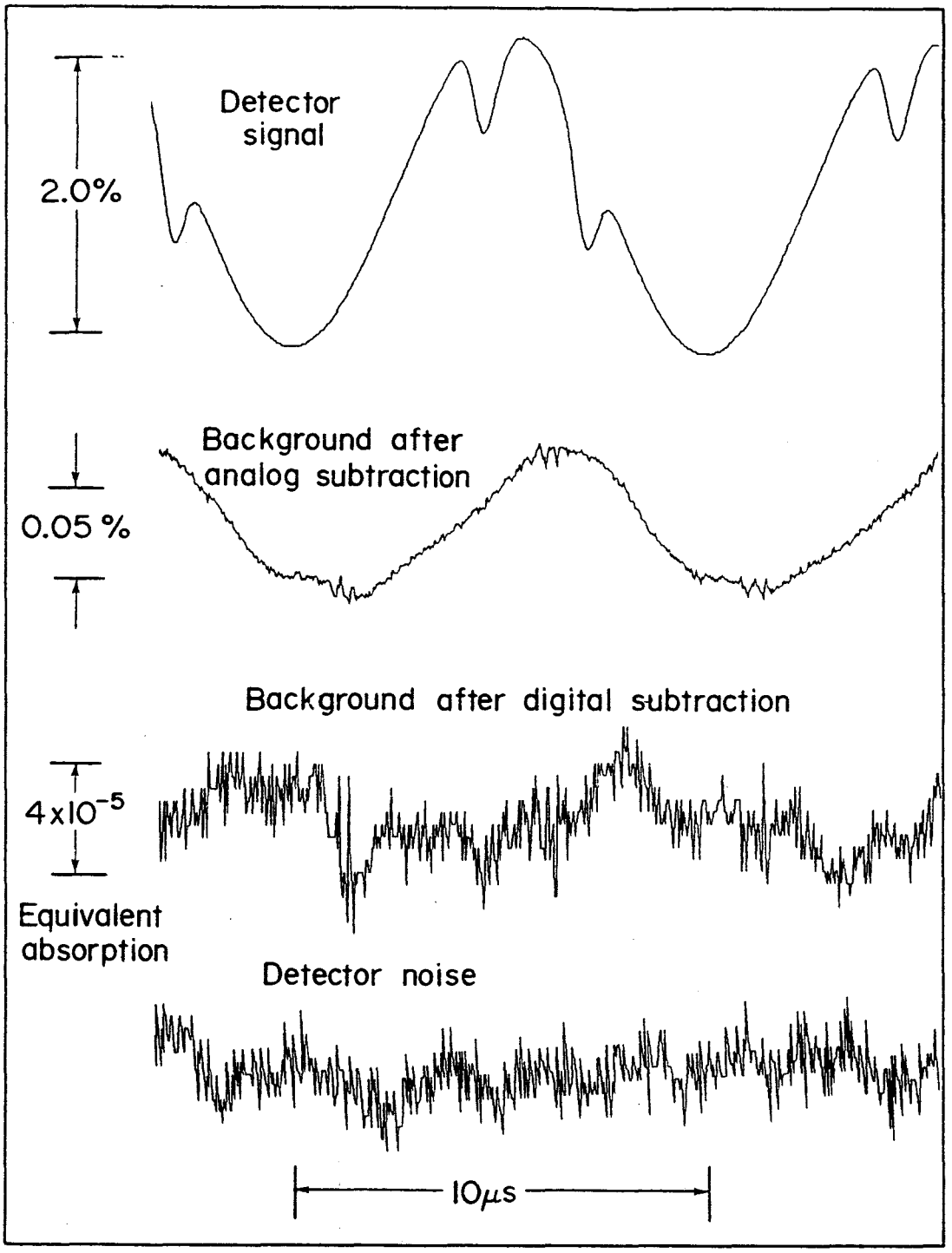
Detector signal
2.0%
Background after analog subtraction
0.05 %
Background after digital subtraction
4x10⁻⁵
Equivalent absorption
Detector noise
10μs

Fig. 5.8: Direct detection of transient absorption with the TDL fixed at linecentre. The relevant energy levels are illustrated in the upper part of the Figure, along with a direct detection scan over the NH_3 aP(4,0) transition. The NH_3/N_2 mixture is pumped with a Q-switched CO_2 laser, shown in the lower traces are the CO_2 pump pulse and the transient probe signals.

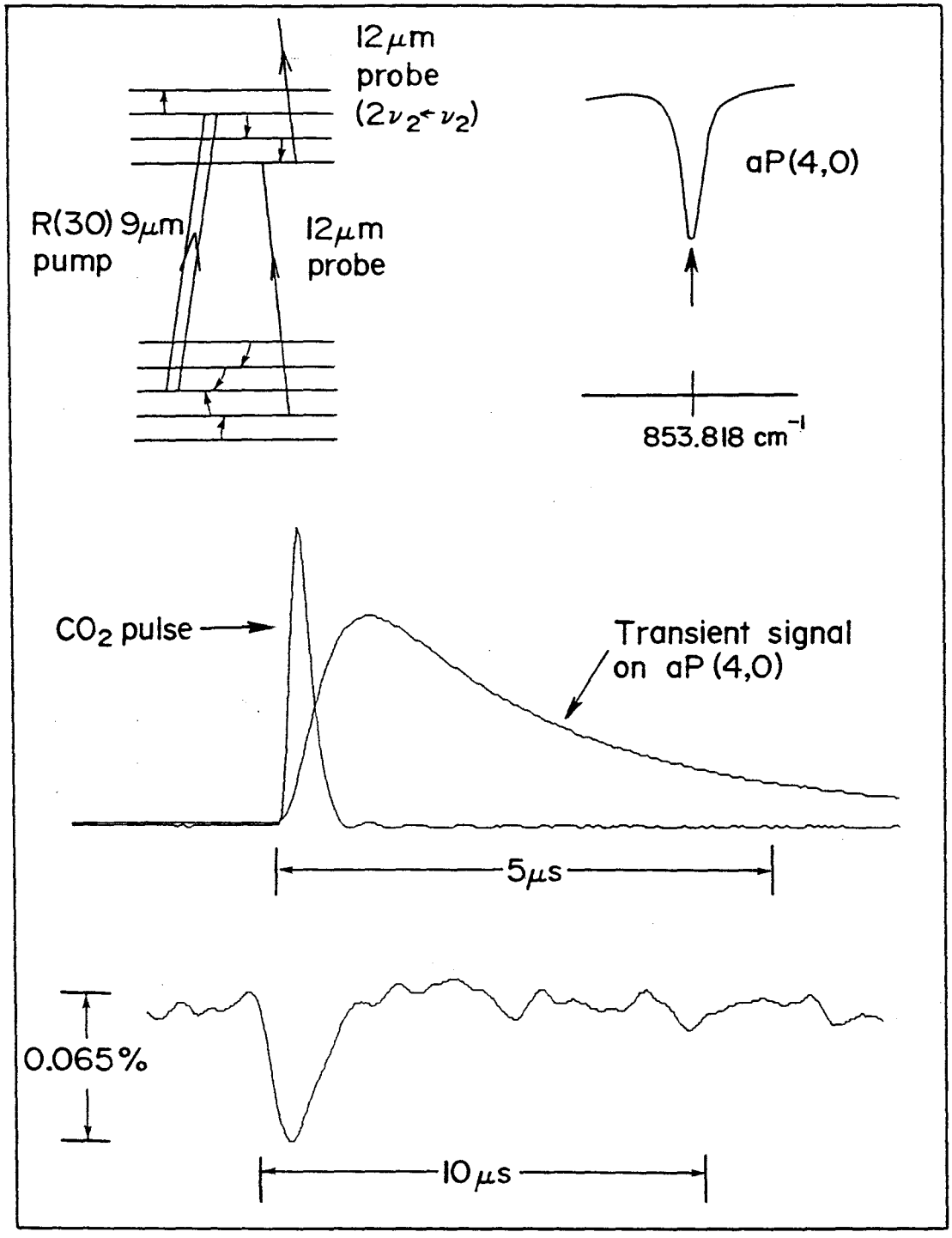
12μm
probe
(2ν2←ν2)
R(30) 9μm
pump
12μm
probe
aP(4,0)
853.818 cm⁻¹
CO2 pulse
Transient signal
on aP (4,0)
5μs
0.065%
10μs

vibrational levels are thermalized by collisions with a buffer gas (typical gas mixtures are 1 % NH_3 in N_2), and hence transient changes in absorption can be monitored by probing with a 12 μm TDL in the ($\nu_2 \leftarrow 0$) band (decrease in absorption) or ($2\nu_2 \leftarrow \nu_2$) band (increase in absorption). Transient probe signals illustrating these two cases are given in the lower traces of Fig. 5.8, for both large and small signal-to-noise ratios using different NH_3/N_2 mixtures. In the small signal case a change in absorption of 0.065 % can be detected with a noise level of approximately 0.01 %. As with the modulation technique, this noise level in the direct detection method is limited by detector noise. Experimentally it has been verified that by averaging a larger number of scans or by using a more powerful probe laser or a more sensitive detector this noise level can be reduced down to $\sim 10^{-5}$.

To further reduce the level of detector noise a final experiment was performed in which a more powerful probe laser was utilized. It is difficult to obtain TDLs that have significantly more power than the 0.5 mW (single mode) that was available. Switching to a cw CO_2 laser as a probe gave more power and allowed tuning to the 9P(24) CO_2 line in close coincidence with the 2sR(4,3) transition in NH_3.[111] Although the cw CO_2 laser gave much more power than the TDL, only 3 mW could be used before the HgCdTe detector response became non-linear. In the experiment, population is transferred to the ν_2 level using the 9R(30) Q-switched pump pulse and monitored with the cw CO_2 laser. Signals observed are of the type shown in Fig. 5.9. The increased absorption has a lifetime corresponding to that of the $\nu_2 = 1$ level.[70] Reduction of the signal to examine the noise levels was achieved by lowering the NH_3

Fig. 5.9: Sensitivity limits obtained with a cw CO_2 laser as a probe. The upper trace shows the probe signal at NH_3/N_2 mixture pressures of 100 Torr (large signal-to-noise ratio), and trace A is recorded at 1.2 Torr. The background trace is recorded with the gas cell evacuated. Subtraction of the background from the signal allows determination of the true induced absorption signal. The noise level corresponds to detector noise, and has been minimized by averaging over 4096 scans using the digital oscilloscope and the micro-computer.

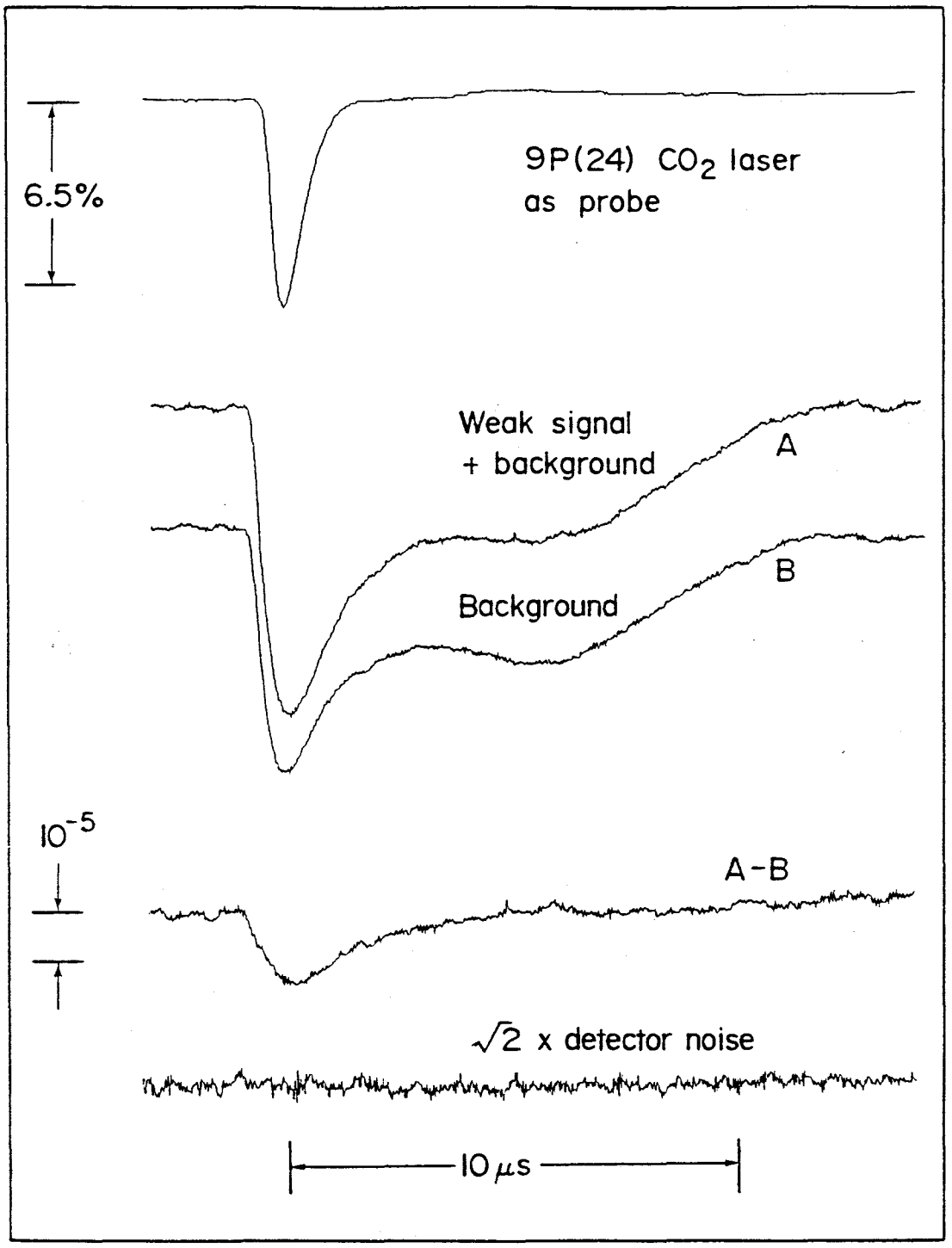
6.5%
9P(24) CO_2 laser
as probe
Weak signal
+ background
A
B
Background
10^{-5}
A-B
$\sqrt{2}$ x detector noise
10 μs

gas pressure in the cell. With no NH_3 in the cell (background scan) a drop in transmission of the probe is observed when the pump laser passes through the cell. This is attributed to pump-induced deflection of the probe away from the detector. Clearly, the modulation technique is advantageous in this respect as it discriminates between deflection and a true induced absorption. In the present case, subtracting the background from the signal eliminates the deflection signal leaving behind the true induced absorption in NH_3. Subtraction results in a 14 ppm absorption signal riding on a noise level of $\simeq$1 ppm (detector noise). This detector noise could be further reduced by averaging for longer time periods. At present, the averaging is limited to 256 scans on the Tektronix 468 digital oscilloscope. This number can be extended by storing 16 successive files, for example, and then performing additional averaging on the computer as was done in Fig. 5.9.

5.5 Summary

In this chapter a novel technique for monitoring transient infrared absorptions with TDLs has been described. The TDL is wavelength modulated on the absorption lines of interest at modulation frequencies of up to ~250 kHz. This allows absorption line sampling every $\sim$2 μs, with sensitivities as high as 10^{-5} equivalent absorption. These sensitivities match those in the direct detection case in which one tunes to linecentre of an absorption and monitors induced change. In both cases the limiting factor in the sensitivity is the detector noise. Factors that influence the detector noise are discussed in detail by Shimoda.[112] Better detectors (higher D^*) can be used to

increase the sensitivity. Alternatively, more laser power for the probe would increase the sensitivity, provided that the dynamic range of the detector was not exceeded. Replacement of the tunable TDL probe with a cw CO_2 laser allowed absorptions on the 10^{-6} level to be detected. However, for the fixed frequency laser probe one relies on fortuitous coincidences between the probe frequency and the transition frequency to be monitored.

Thus far, the modulation technique has been applied in the measurement of transient CF_2 absorptions created by IRMPD with a TEA CO_2 laser pulse, transient NH_3 absorptions created by a Q-switched CO_2 laser, and steady-state N_2O absorptions. In a further application, the technique has been utilized to monitor the formation and decay of DCl produced in CO_2 laser IRMPD of $CDCl_3$.[113] The majority of the work reported in this chapter is described in a publication by Beckwith, Brown, Danagher, Smith, and Reid (Submitted to Appl. Opt.).[16] In particular, acknowledgements are due to C. E. Brown for his collaboration in obtaining the data shown in Figs. 5.2, 5.3, 5.4, 5.5 and to D. J. Danagher for his collaboration in obtaining the data shown in Figs. 5.8 and 5.9. Acknowledgements are also due to J. J. Orlando for his collaboration in obtaining the data shown in Fig. 5.2.

CHAPTER 6

CONCLUSIONS

This thesis has attempted to illustrate the importance of the tunable diode laser as a probe to monitor processes occuring in gaseous molecular photochemical systems. The high sensitivity and fast response time of the diagnostic system promises to lead to many applications both now and in the near future.

In the course of this work a computerized digital technique has been developed whereby accurate data can be obtained on the molecular parameters of linestrength and linewidth from infrared absorption scans. Application of the digital technique to NH_3 measurements are expected to be important in modelling NH_3 laser systems (both cw and pulsed). Further measurements on HTO are useful for evaluating the sensitivity limits of an HTO detection system, which is of importance as HTO is a health hazard and levels need to be monitored. This work is described in Chapter 3.

The next chapter illustrates the application of the TDL diagnostic system to measurements in a photochemical environment. A TEA CO_2 laser is used to dissociate $CDCl_3$; the DCl formed was then monitored directly with the TDL probe. This dissociation procedure is thought to be a good candidate for H/D laser isotope separation. The high sensitivity of the detection scheme is illustrated by monitoring the dissociation of natural abundance $CDCl_3$ in $CHCl_3$, this is reported for the first time.

Chapter 5 describes the detection of the transient radical CF_2 by current-modulation of the TDL at high frequencies. This technique allows the sampling on microsecond time scales of transient infrared absorptions on the level of 10^{-5} equivalent absorbance. The technique is very versatile, non-intrusive, and could be applied to the detection of any infrared-active transient molecule of interest.

In summary, the TDL diagnostic technique leaves open many avenues of possible research. Important insight can be obtained on many infrared multiphoton dissociation processes, and on the feasibility of laser isotope separation systems. Presently, transient absorptions can be monitored on microsecond time scales at 10^{-5} absorbance levels. This enables chemical reactions and dissociation processes to be studied quantitatively on a non-intrusive basis. Further areas of investigation should be focused on improvement of the diagnostic system by increasing the modulation frequency of the lead-salt diode laser to allow detection on nanosecond time scales. In addition, long term averaging, and more sensitive detectors should enable sensitivity levels to be increased.

References

1. J. C. Hill and G. P. Montgomery, Jr, "Diode lasers for gas analysis: some characteristics," Appl. Opt. 15, 748-755 (1976).

2. H. I. Schiff, D. R. Hastie, G. I. Mackay, T. Iguchi and B. A. Ridley, "Tunable diode laser systems for monitoring trace gases in tropospheric air," Environ. Sci. Technol. 17, 352A-364A (1983).

3. C. R. Webster and R. T. Menzies, "In situ measurement of stratospheric nitric oxide using a balloon-borne tunable diode laser spectrometer," Appl. Opt. 23, 1140-1142 (1984).

4. Articles listed in "Infrared Laser Spectroscopy Applications and Techniques", Reprint List, published Spring, 1985 by Spectra Physics, Laser Analytics Division, 25 Wiggins Ave., Bedford, MA. 01730

5. E. D. Hinkley, "High-resolution infrared spectroscopy with a tunable diode laser," Appl. Phys. Lett. 16, 351-354 (1970).

6. TDLs are commercially available covering the wavenumber range 300 to 3000 cm^{-1}, with a given TDL typically being tunable over 100 cm^{-1}. The linewidth is generally less than 0.001 cm^{-1}.

7. H. R. Schlossberg and P. L. Kelly, "Infrared spectroscopy using tunable lasers," from Spectroscopic Techniques, Vol. II, Academic Press, p. 161-239 (1981).

8. R. S. Eng, G. Petagne, and K. W. Nill, "Ultrahigh (10^{-4} cm^{-1}) resolution study of the 8.2-μm and 11.3-μm bands of H_2SO_4: accurate determination of absorbance and dissociation constants," Appl. Opt. 17, 1723-1726 (1976).

9. P. B. Davies, C. J. Kho, W. K. Leong, and W. Lewis-Bevan, "The $N_2F_4 \rightleftharpoons 2NF_2$ equilibrium studied with a tunable diode laser," J. Chem. Soc., Chem. Commun. 70, 690-691 (1982).

10. G. E. Streit, J. S. Wells, F. C. Fehsenfeld, and C. J. Howard, "A tunable diode laser study of the reactions of nitric and nitrous acids: $HNO_3 + O_3$," J. Chem. Phys. 70, 3439-3443 (1979).

11. B. A. Thrush, G. S. Tyndall, "Reactions of HO_2 studied by flash photolysis with diode-laser spectroscopy," J. Chem. Soc. Faraday Trans. 2, 78, 1469-1475 (1982).

12. R. D. McAlpine and D. K. Evans, "Laser isotope separation by the selective multiphoton decomposition process," chapter in Photodissociation and Photoionization, Ed. K. P. Lawley, John Wiley and Sons Ltd. p. 31-98 (1985).

13. P. H. Beckwith, J. J. Orlando, J. Reid, and D. R. Smith, "Analysis of the products of photochemistry using tunable diode lasers, with application to the multiphoton dissociation of chloroform," Accepted for publication in J. Photochem. (1986).

14. P. H. Beckwith, D. J. Danagher, and J. Reid, "Linewidths and linestrengths in the ν_2 band of NH_3 as measured with a tunable diode laser," Accepted for publication in J. Mol. Spectrosc. (1986).

15. P. P. Cherrier, P. H. Beckwith, and J. Reid, "Linewidths and linestrengths in the ν_2 band of HTO as measured with a tunable diode laser," Submitted to J. Mol. Spectrosc. (1986).

16. P. H. Beckwith, C. E. Brown, D. J. Danagher, D. R. Smith, and J. Reid, "High sensitivity detection of transient infrared absorptions using tunable diode lasers," Submitted to Appl. Opt. (1986).

17. P. L. Varghese and R. K. Hanson, "Tunable infrared diode laser measurements of line strengths and collision widths of $^{12}C^{16}O$ at room temperature," J. Quant. Spectrosc. Radiat. Transfer 24, 479-489 (1980).

18. A. S. Pine, A. Fried, and J. W. Elkins, "Spectral intensities in

the fundamental bands of HF and HCl," J. Mol. Spectrosc. 109, 30-45 (1985).

19. E. Kreyszig, Advanced Engineering Mathematics, John Wiley and Sons Inc., p. 774-777 (1962).

20. S. R. Drayson, "Rapid computation of the Voigt profile," J. Quant. Spectrosc. Radiat. Transfer 16, 611-614 (1976).

21. P. Minguzzi and A. Di Lieto, "Simple Pade approximations for the width of Voigt profile," J. Mol. Spectrosc. 109, 388-394 (1985).

22. J. Reid and D. Labrie, "Second-harmonic detection with tunable diode lasers - Comparison of experiment and theory," Appl. Phys. B, 26, 203-210 (1981).

23. R. A. Toth, "Line positions and strengths of CO_2 in the 1200 - 1430-cm^{-1} region," Appl. Opt. 24, 261-274 (1985).

24. R. K. Brimacombe and J. Reid, "Accurate measurements of pressure-broadened linewidths in a transversely excited CO_2 discharge," I.E.E.E. J. Quant. Electr. QE-19, 1668-1673 (1983).

25. S. Urban, D. Papousek, J. Kauppinen, K. Yamada, and G. Winnewisser, "The ν_2 band of $^{14}NH_3$: A calibration standard with better than 1 x 10^{-4} cm^{-1} precision," J. Mol. Spectrosc. 101, 1-15 (1983).

26. R. L. Poynter and J. S. Margolis, "The ν_2 spectrum of NH_3," Mol. Phys. 51, 393-412 (1984).

27. L. R. Brown and R. A. Toth, "Comparison of the frequencies of NH_3, CO_2, H_2O, N_2O, CO, and CH_4 as infrared calibration standards," J. Opt. Soc. Am. B 2, 842-856 (1985).

28. P. Varanasi, "Shapes and widths of ammonia lines collision-broadened by hydrogen," J. Quant. Spectrosc. Radiat. Transfer 12, 1283-1289 (1972).

29. F. W. Taylor, "Spectral data for the ν_2 bands of ammonia with applications to radiative transfer in the atmosphere of Jupiter," J. Quant. Spectrosc. Radiat. Transfer 13, 1181-1217 (1973).

30. T. Nakanaga, S. Kondo, and S. Saeki, "A determination of the transition dipole moment of $\mu_{a\leftarrow s}$ and $\mu_{s\leftarrow a}$ of the ν_2 band of NH_3," J. Mol. Spectrosc. 112, 39-44 (1985).

31. W. S. Benedict, E. K. Plyler, and E. D. Tidwell, "Vibration-rotation bands of ammonia: 1. The combination bands $\nu_2 + (\nu_1, \nu_3)$," J. Res. Natn. Bur. Stand. 61, 123-147 (1958).

32. W. S. Benedict, E. K. Plyler, and E. D. Tidwell, "Vibration-rotation bands of ammonia. III. The region 3.2 - 4.3

microns," J. Chem. Phys. 29, 829-845 (1958).

33. J. S. Margolis, "Hydrogen broadened half-widths of ammonia," J. Quant. Spectrosc. Radiat. Transfer 15, 627-640 (1975).

34. J. S. Margolis and S. Sarangi, "Measurement of hydrogen- and self-broadened half-widths of ammonia at 200 and 300 K," J. Quant. Spectrosc. Radiat. Transfer 16, 405-408 (1976).

35. W. L. France and D. Williams, "Total absorptance of ammonia in the infrared," J. Opt. Soc. Am. 56, 70-74 (1966).

36. J. Bonamy, "The role of K = 3 transitions in collision-broadened NH_3," J. Quant. Spectrosc. Radiat. Transfer 16, 213-215 (1976).

37. R. L. Legan, J. A. Roberts, E. A. Rinehart, and C. C. Lin, "Linewidths of the microwave inversion spectrum of ammonia," J. Chem. Phys. 43, 4337-4345 (1965).

38. J. S. Murphy and J. E. Boggs, "Collision broadening of rotational absorption lines. IV. Pressure broadening of the ammonia inversion spectrum," J. Chem. Phys. 50, 3320-3329 (1969).

39. C. Rolland, J. Reid, and B. K. Garside, "Line-tunable oscillation of a cw NH_3 laser from 10.7 to 13.3 μm," Appl. Phys. Lett. 44, 380-382 (1984).

40. K. J. Siemsen, J. Reid, and D. J. Danagher, "Improved cw lasers in 11 to 13-μm wavelength region by optically pumping NH_3," Accepted for publication in Appl. Opt. (1986).

41. D. F. Kroeker and J. Reid, "High power, line-tunable cw NH_3 lasers operating at wavelengths of 11 to 14-μm," Accepted for publication in Appl. Opt. (1986).

42. R. L. Sinclair, J. Reid, H. D. Morrison, B. K. Garside, and C. Rolland, "Dynamics of the line-tunable 12-μm continuous-wave NH_3 laser as measured with a tunable-diode laser," J. Opt. Soc. Am. B 2, 800-806 (1985).

43. H. D. Morrison, B. K. Garside, and J. Reid, "Gain dynamics in pulsed 12-μm NH_3 lasers," J. Opt. Soc. Am. B 2, 535-540 (1985).

44. H. D. Morrison, B. K. Garside, and J. Reid, "Modeling of high-pressure 12-μm NH_3 lasers," Appl. Phys. B 37, 165-170 (1985).

45. S. Lundqvist, J. Margolis, and J. Reid, "Measurements of pressure-broadened coefficients of NO and O_3 using a computerized tunable diode laser spectrometer," Appl. Opt. 21, 3109-3113 (1982).

46. L. R. Brown, J. S. Margolis, R. H. Norton, and B. D. Stedry, "Computer measurement of line strengths with application to the

methane spectrum," Appl. Spectrosc. 37, 287-292 (1983).

47. D. -W. Chen, E. R. Niple, and S. K. Poultney, "Determining tunable diode laser spectrometer performance through measurement of N_2O line intensities and widths at 7.8 μm," Appl. Opt. 21, 2906-2911 (1982).

48. B. Fridovich, "Correcting measured line half-widths," J. Mol. Spectrosc. 105, 53-60 (1984).

49. J. H. Shaw, N. Tu, and D. L. Agresta, "Sources of systematic errors in line intensities," Appl. Opt. 24, 2437-2441 (1985).

50. E. Niple and J. H. Shaw, "Information in spectra of collision-broadened absorption lines," Appl. Spectrosc. 33, 569-574 (1979).

51. Y. S. Chang and J. H. Shaw, "A nonlinear least squares method of determining line intensities and half-widths," Appl. Spectrosc. 31, 213-220 (1977).

52. B. H. Armstrong, "Spectrum line profiles: The Voigt function," J. Quant. Spectrosc. Radiat. Transfer 7, 61-88 (1967).

53. P. L. Varghese and R. K. Hanson, "Tunable diode laser measurements of spectral parameters of HCN at room temperature," J. Quant. Spectrosc. Radiat. Transfer 31, 545-559 (1984).

54. V. M. Devi, C. P. Rinsland, M. -A. H. Smith, and D. C. Benner, "Measurements of $^{12}CH_4$ ν_4 band halfwidths using a tunable diode laser system and a Fourier transform spectrometer," Appl. Opt. 24, 2788-2791 (1985).

55. P. L. Varghese and R. K. Hanson, "Collisional narrowing effects on spectral line shapes measured at high resolution," Appl. Opt. 23, 2376-2385 (1984).

56. F.Herbert, "Spectrum line profiles: A generalized Voigt function including collisional narrowing," J. Quant. Spectrosc. Radiat. Transfer 14, 943-951 (1974).

57. TDL scans taken of pure NH_3 at very low pressure (~60 mTorr) gave measured linewidths which exceeded the theoretical Doppler width by only 7 %. This degree of instrumental broadening has an insignificant effect on measurements made at higher pressures.

58. H. D. Morrison, Ph. D. Thesis "Dynamics of optically pumped pulsed mid-infrared NH_3 lasers," McMaster University, Hamilton, Ontario, Canada (1984).

59. H. D. Morrison, (unpublished work), McMaster University, Hamilton, Ontario, Canada (1984).

60. To obtain the dipole moment $\mu_{s\leftarrow a}$, for example, one considers the three measured s←a transitions and notes that, on average, they have linestrengths 3 % greater than the calculated values. As linestrength is proportional to μ^2, one derives a dipole moment 1.5 % larger than the one used in Ref. 26, i. e. , 0.244 D as opposed to 0.240 D.

61. W. K. Bischel, P. J. Kelly, and C. K. Rhodes, "High-resolution Doppler-free two-photon spectroscopic studies of molecules. II. The ν_2 bands of $^{14}NH_3$," Phys. Rev. A 13, 1829-1841 (1976).

62. M. Takami, H. Jones, and T. Oka, "Transition dipole moments of NH_3 in excited vibrational states determined by laser Stark spectroscopy," J. Chem. Phys. 70, 3557-3558 (1979).

63. K. J. Siemsen and J. Reid, "Technique for obtaining cw CO_2 sequence laser lines using an incavity NH_3 cell," Appl. Opt. 17, 3523-3525 (1978).

64. M. O. Bulanin, Y. M. Ladvishchenko, and Y. M. Sveshnikov, "Effect of vibrational excitation on the parameters of vibration-rotation line contours in the ν_2 mode of ammonia," Opt. Spectrosc. (USSR) 54, 116-117 (1983).

65. M. O. Bulanin, Y. M. Ladvishchenko, and E. B. Khodos, "Measurement of the pressure broadening and shift of the asR(0,0) line of the

$^{15}NH_3$ ammonia ν_2 band," Opt. Spectrosc. (USSR) 53, 119-120 (1982).

66. Although Ref. 64 reports a value of 0.395 D, the experimental data of Bulanin et al. is consistent with a dipole moment of $\mu = 0.302$ D.

67. G. Baldacchini, S. Marchetti, V. Montelatici, V. Sorge, G. Buffa, and O. Tarrini, "Self-broadening and self-shifting of ammonia lines in the $2\nu_2$ band," J. Chem. Phys. 78, 665-667 (1983).

68. G. Baldacchini, S. Marchetti, V. Montelatici, G. Buffa, and O. Tarrini, "Self-broadening and self-shifting of ammonia lines in the $2\nu_2$ band around 16 μm," J. Chem. Phys. 83, 4975-4977 (1985).

69. H. D. Morrison, J. Reid, and B. K. Garside, "16-21-μm line- tunable NH_3 laser produced by two-step optical pumping," Appl. Phys. Lett. 45, 321-323 (1984).

70. D. J. Danagher and J. Reid, "Vibrational relaxation of the $\nu_2 = 1$ level of ortho and para NH_3," Submitted to J. Chem. Phys. (1986).

71. Private communication with Dr. L. H. Jones, Los Alamos Scientific Laboratories.

72. P. P. Cherrier and J. Reid, "High sensitivity detection of HTO using tunable diode lasers," to be submitted to Nuc. Inst. Meth. (1986).

73. I. P. Herman, F. Magnotta, R. J. Buss and Y. T. Lee, "Infrared multiple-photon dissociation of $CDCl_3$ in a molecular beam," J. Chem. Phys. 79, 1789-1794 (1983).

74. D. H. Rank, D. P. Eastman, B. S. Rao, T. A. Wiggins, "Rotational and vibrational constants of the HCl^{35} and DCl^{35} molecules," J. Opt. Soc. Am. 52, 1-7 (1962).

75. A. R. H. Cole, Tables of Wavenumbers for the Calibration of Infrared Spectrometers, IUPAC, Pergamon Press, p 44-45 (1977).

76. G. Guelachvili, "Absolute wavenumbers and molecular constants of the fundamental bands of $^{12}C^{16}O$, $^{12}C^{17}O$, $^{12}C^{18}O$, $^{13}C^{16}O$, $^{13}C^{17}O$, $^{13}C^{18}O$ and of the 2-1 bands of $^{12}C^{16}O$ and $^{13}C^{16}O$, around 5 μm, by Fourier spectroscopy under vacuum," J. Mol. Spect. 75, 251-269 (1979).

77. J. M. Birchall, R. N. Haszeldine, and D. W. Roberts, "Cyclopropane chemistry. Part II. Cyclopropanes as sources of difluorocarbene," J. Chem. Soc., Perkin I, 1071-1076 (1973).

78. J. Reid, M. El-Sherbiny, B. K. Garside, and E. A. Ballik,

"Sensitivity limits of a tunable diode laser spectrometer, with application to the detection of NO_2 at the 100-ppt level," Appl. Opt. 19, 3349 (1980).

79. J. J. Orlando, published in Ref. 13.

80. K. N. Rao, Molecular Spectroscopy: Modern Research, Volume III, Academic Press, p. 111-248 (1985).

81. P. Varanai and S. Sarangi, "Measurements of intensities and nitrogen-broadened linewidths in the CO fundamental at low temperatures," J. Quant. Spectrosc. Radiat. Transfer 15, 473-482 (1975).

82. L. S. Rothman, "AFGL atmospheric absorption line parameters compilation: 1980 version," Appl. Opt. 20, 791-795 (1980).

83. J. Reid, D. T. Cassidy and R. T. Menzies, "Linewidth measurements of tunable diode lasers using heterodyne and etalon techniques," Appl. Opt. 21, 3961-3965 (1982).

84. W. S. Benedict, R. Herman, G. E. Moore and S. Silverman, "Infrared line and band strengths and dipole moment function in HCl and DCl," J. Chem. Phys. 26, 1671-1677 (1957).

85. S. Pinchas, I. Laulight, Infrared spectra of labelled compounds,

Academic Press, p. 297-299 (1971).

86. Private communication with J. W. C. Johns, NRC, Canada. Results are quoted for the Boman DA3.002 instrument.

87. F. Magnotta and I. P. Herman, "Infrared laser multiple-photon dissociation of $CTCl_3$: Wavelength dependence, collisional effects, and tritium/deuterium isotope selectivity," J. Chem. Phys. 81, 2363-2374 (1984).

88. A. Karbach, C. Sayer and P. Hess, "Vibrational relaxation in COF_2 and Xe, C_2H_6 mixtures following intense laser excitation," Chem. Phys. 96, 461-471 (1985).

89. C. E. Brown, J. J. Orlando and D. R. Smith, McMaster University, unpublished work.

90. D. Labrie and J. Reid, "Radiocarbon dating by infrared laser spectroscopy, A feasibility study," Appl. Phys. 24, 381-386 (1981).

91. J. Reid, R. L. Sinclair, A. M. Robinson, and A. R. W. Mckellar, "Observation of electric quadrupole transitions in the fundamental band of O_2 in the 1600-cm^{-1} region," Phys. Rev. A 24, 1944-1949 (1981).

92. E. Hirota, High-resolution spectroscopy of transient molecules, Springer-Verlag, Berlin, Germany, 1985.

93. C. S. Gudeman and R. J. Saykally, "Velocity modulation infrared laser spectroscopy of molecular ions," Ann. Rev. Phys. Chem. 35, 387-419 (1984).

94. D. J. Nesbitt, H. Petek, C. S. Gudeman, C. Bradley Moore, and R. J. Saykally, "A study of the ν_1 fundamental and bend-excited hot band of DNN^+ by velocity modulation absorption spectroscopy with an infrared difference frequency laser," J. Chem. Phys. 81, 5281-5287 (1984).

95. J. C. Owrutsky, C. S. Gudeman, C. C. Martner, L. M. Tack, N. H. Rosenbaum, and R. J. Saykally, "Determination of the equilibrium structure of protonated nitrogen by high resolution infrared laser spectroscopy," J. Chem. Phys. 84, 605-617 (1986).

96. H. Kanamori, J. E. Butler, K. Kawaguchi, C. Yamada, and E. Hirota, "Infrared diode laser kinetic spectroscopy of transient molecules produced by excimer laser photolysis: Application to the SO radical," J. Mol. Spectr. 113, 262-268 (1985).

97. C. Yamada, H. Kanamori, H. Horiguchi, S. Tsuchiya, and E. Hirota, "Infrared diode laser kinetic spectroscopy of the CCO radical in the $\tilde{x}^3\Sigma^-$ state generated by the excimer laser photolysis of carbon

suboxide," J. Chem. Phys. 84, 2573-2576 (1986).

98. G. A. Laguna and S. L. Baughcum, "Real-time detection of methyl radicals by diode laser absorption at 608 cm^{-1}," Chem. Phys. Lett. 88, 568-571 (1982).

99. C. Dang, J. Reid, and B. K. Garside, "Dynamics of the CO_2 upper laser level as measured with a tunable diode laser," I.E.E.E. J. Quant. Elect. QE-19, 755-764 (1983).

100. D. Harradine, B. Foy, L. Laux, M. Dubs, and J. I. Steinfeld, "Infrared double resonance of fluoroform-d with a tunable diode laser," J. Chem. Phys. 81, 4267-4280 (1984).

101. K. Knapp and R. K. Hanson, "Spatially resolved tunable diode-laser absorption measurements of CO using optical stark shifting," Appl. Opt. 22, 1980-1985 (1983).

102. J. A. O'Neill, J. Ye Cai, and G. W. Flynn, "Diode laser probe of CO_2 vibrational excitation produced by collisions with hot deuterium atoms from the 193 nm excimer laser photolysis of D_2S," J. Chem. Phys. 84, 50-58 (1986).

103. To the best of our knowledge this is the minimum reported absorbance. However, many of the papers on transient detection do not discuss sensitivity.

104. D. E. Jennings, "Absolute line strengths in ν_4, $^{12}CH_4$: A dual- beam diode laser spectrometer with sweep integration," Appl. Opt. 19, 2695-2700 (1980).

105. D. T. Cassidy and J. Reid, "High-sensitivity detection of trace gases using sweep integration and tunable diode lasers," Appl. Opt. 21, 2527-2530 (1982).

106. W. S. Nip, M. Drouin, P. A. Hackett, and C. Willis, "Multiphoton chemistry of perfluoropropene," J. Chem. Phys. 84, 932-935 (1980).

107. J. Stone, E. Thiele, and M. F. Goodman, "Collisional effects in the multiphoton dissociation of CF_2CFCl," J. Chem. Phys. 73, 2259-2270 (1980).

108. P. B. Davies, W. Lewis-Bevan, and D. K. Russell, "Infrared diode laser spectrum of the ν_1 band of CF_2 ($\tilde{x}^1A_1$)," J. Chem. Phys. 75, 5602-5608 (1981).

109. Modulation frequency is limited by the electronics in the laser control module (Laser Analytics Model LCM). Simple circuit modification is expected to allow modulation frequencies of > 1 MHz.

110. M. Gehrtz, W. Lenth, A. T. Young, and H. S. Johnston, "High-frequency-modulation spectroscopy with a lead-salt diode laser," Opt. Lett. 11, 132-134 (1986).

111. K. J. Siemsen and J. Reid, "Technique for obtaining cw CO_2 sequence laser lines using an incavity NH_3 cell," Appl. Opt. 17, 3523-3525 (1978).

112. K. Shimoda, "Limits of sensitivity of laser spectrometers," Appl. Phys. 1, 77-86 (1973).

113. Work at McMaster by J. J. Orlando, J. Reid, and D. R. Smith.